AN ANALYSIS OF

PULSE TRANSFORMERS

A thesis submitted for the degree of

Doctor of Philosophy

in Physics

to the

University of Waikato

New Zealand

by

Craig Brendon Harrison

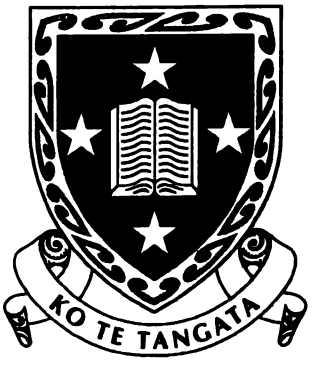

University of Waikato

1998

ABSTRACT

This thesis focuses on developing a comprehensive understanding of the behaviour of the output pulse transformer used in an electric fence energiser, a unique application which has received little attention in the literature.

Maxwell's Equations form the starting point for an investigation into the magnetisation of the magnetic core under high current pulse conditions. An equation is derived which describes the time dependent nature of the penetration of the magnetic field into the core material. The concept of a region of high permeability moving into the lamination as a result of rapid saturation is also developed.

Quantitative results are obtained for the area of this high permeability region, both from the pulse magnetisation equation and by analytical methods. The analytical approach is also used to derive expressions for the pulse current, output voltage and power, and inductance. The analytical model of the output transformer provides much insight into the transformer's behaviour, and into the influence upon performance of the various circuit elements.

The description of pulse magnetisation is a key factor in the development of both analytical and electrical circuit models of the output transformer.

The final part of the thesis considers the output transformer from the perspective of an electrical circuit model, which is developed as a direct representation of the physical transformer. The inductor-reluctance method is used to develop the model, and methods of calculating each parameter are derived, so that the final model may be obtained directly from the transformer's specification without the need for experimental measurements. The electrical circuit model is implemented using a SPICE simulator, and an analysis of the transformer highlights the major design parameters.

The description of pulse magnetisation, the analytical model and the electrical circuit model combine to provide a comprehensive description of the behaviour of the output transformer, and provide the tools required for design and further investigation of this application.

PREFACE

The transformer has played an essential role in electrotechnology since its inception. The application of an electric fence output pulse transformer has not been well researched, and this thesis addresses that gap in the literature.

Background information relating to the application, and relevant references are surveyed in Chapter One, with a comprehensive summary of electromagnetic and transformer theory presented in Chapter Two. In addition, an outline is given of the current state of electric fence theory and electric shock research, two topics which are highly relevant to an investigation of output transformers.

This thesis then develops a comprehensive framework for the theory and design of pulse transformers for electric fences. Three approaches are taken.

In Chapter Three, the effect of pulse magnetisation is presented. An expression describing the time varying nature of the penetration of the magnetic field into the core material is developed by solving the diffusion equation, which is derived from Maxwell's Equations. Saturation plays a major role in the performance of the output transformer, and is also investigated in this chapter.

An understanding of the magnetic behaviour of the core is a fundamental first step in understanding the operation of the transformer. In Chapter Four, a wider view of the application is taken by stepping back from the core to look at the entire transformer and discharge circuit. The output transformer is the major component of the electric fence energiser's capacitive discharge circuit. An analytical approach is taken to derive expressions for current, output voltage, power, inductance and saturation. These results provide a great deal of insight into the dependence of circuit behaviour upon the various elements.

The ultimate objective of this line of research is the practical application of the theory to design. The electrical circuit model developed in Chapter Five provides a crucial link between theory and practice. First, a comprehensive physical model is developed specifically for the output transformer, using the inductor-reluctance method. Then, techniques are presented by which all of the parameters required by the model may be calculated from the transformer's specification and geometry. Chapter Five continues with the implementation of this model in SPICE and an analysis of the critical parameters. This model further extends the understanding of the operation of the output transformer, and also provides a vital tool for trial, design and optimisation.

The thesis concludes with a discussion of the implications of the work. An outline of some practical results is provided, and recommendations are given regarding further work which would complement that undertaken for this thesis.

The following software was used in the course of this thesis:

PSpice 4.05 (MicroSim Corp.) for circuit simulation;
Mathcad 7 (Mathsoft) for numerical and symbolic calculation; and
Excel 7.0 (Microsoft Corp.) for graphing and calculation.

The preparation of this manuscript made use of:

Word 7.0 (Microsoft Corp.) for word processing;
Excel 7.0 for graphs; and
AutoCAD LT 3 (Autodesk Inc.) for diagrams.

The final copy was printed by an Hewlett Packard *LaserJet 6MP*.

ACKNOWLEDGEMENTS

I am continually inspired by the genius of Michael Faraday and James Clerk Maxwell, those giants of science who developed the fundamental theories of electromagnetism so many years ago. And as did Faraday and Maxwell, I would like to express my gratitude to God for creating such a fascinating universe, and for giving me the strength, perseverance and inspiration to understand such a small part of it through the completion of this research. The order and beauty evident in nature simply reinforces to me the fact that this universe was created with a purpose in mind.

I am grateful to Rudy Severns, who held the key to this work and gave it to me on 22nd April 1997 when he casually suggested that I look at Glasoe and Lebacqz's work on the diffusion equation. Evan Bydder's help over the last few months has been significant, and I am very grateful for all his assistance. John Walley was instrumental in allowing me to begin this research, and in the last six months has been tremendous support. John, thank you for your help and advice, especially regarding resource management.

I have needed the support of my family in the last six months and am so thankful to be part of such a fine one. Thank you Mum, Dad, Darren and Cherie, and Shane, Michelle and Alana for all that you have meant to me. Although the trip to Japan wasn't the celebratory conclusion to my doctorate that I had hoped, it was still a *sugoi* experience and I'd like to thank Glenn, Julian, Jordan and Haskel for helping take my mind off the thesis for a couple of weeks.

I would also like to express my appreciation to Ann Davis, for her advice which I followed despite my best intentions, and also to Garth Sutherland, whose initial reaction to my topic prompted me to look right back to the work of Faraday and Maxwell.

I am grateful for the opportunity to complete this work at Gallaghers, and want to say thanks especially to Martyn, Tony, Nathan and Stuart. I also appreciated Greg's efforts to create the pressure of a deadline, which was badly needed. Thanks also to those in R&D and

Production who have helped me keep my feet on the ground even if my head is in the clouds.

I was intrigued to read the following quote recently, which was written by an historian 80 years ago but seems to me to be extremely relevant today.

> *"As scientific men tell us continually, and as 'practical' men still refuse to learn, it is only when knowledge is sought for her own sake that she gives rich and unexpected gifts in any abundance to her servants. ... The world of today is still much more disposed to spend money on technical research than on pure science. ... We live today largely in the age of alchemists, for all our sneers at their memory. The 'business man' of today still thinks of research as a sort of alchemy."* [*Wells* 1920 pp. 480]

Transformers have sure been a challenging topic, one which often seems shrouded in mystery. In frustration at the beginning of my research, I wrote the following "Transformer Rules", which remain immutable in spite of our greatly increased understanding.

Rule 1: The transformer will behave opposite to what you expect

Rule 2: Transformer behaviour is uncertain

Rule 3: There ain't no free lunch

Rule 4: Everything depends on everything else

These sentiments are more eloquently expressed by James E. Green, who said

> *"In my work, I often meet other engineers who describe magnetics design as 'black magic'. My answer is that it is not really magic, but merely a higher form of science, where none of the laws of physics can be forgotten, much less disregarded."*

Craig Harrison

Ngaruawahia

5th December 1998

TABLE OF CONTENTS

Chapter Two **THEORY**

Chapter Four **ANALYTICAL MODEL**

Chapter Five ELECTRICAL CIRCUIT MODEL

Chapter Six **DISCUSSION**

Appendix One **CIRCUIT DUALITY**

Appendix Two **CALCULATION OF DYNAMIC CAPACITANCE**

LIST OF FIGURES

LIST OF TABLES

LIST OF SYMBOLS

Electricity and Magnetism

Symbol	*SI Unit*	*Description*
a	[m]	distance to centre of lamination
a	[A/m]	thermal energy parameter
A	[m^2]	area
A_c	[m^2]	core area
α		interdomain coupling parameter
$\boldsymbol{B}$	[T]	magnetic flux density
$\boldsymbol{B}_a$	[T]	applied magnetic field
B_r	[T]	residual flux density
B_s	[T]	saturation flux density
c		domain flexing parameter
c		speed of light, 2.998×10^8 m/s
C_s	[F]	storage capacitance
χ_m		magnetic susceptibility
d	[m]	conductor diameter
d	[m]	thickness of lamination
$\boldsymbol{D}$	[C/m^2]	electric induction
δ	[m]	magnetic field penetration depth
δ	[m]	skin depth
E	[V]	electromotive force, emf
E	[J]	energy
$\boldsymbol{E}$	[V/m]	electric field strength
ε_0		permittivity of free space, 8.85×10^{-12} F/m
f	[s^{-1}]	frequency
f_c	[s^{-1}]	critical frequency
f_L		inductance factor
F_m	[A]	magnetomotive force, mmf
G	[S]	conductance
$\boldsymbol{H}$	[A/m]	magnetic field strength
H_c	[A/m]	coercive field strength
I	[A]	current
I_m	[A]	magnetising current
$\boldsymbol{J}$	[A/m^2]	total electric current density
$\boldsymbol{J}_f$	[A/m^2]	conduction current density
K	[A/m]	domain anisotropy parameter
L	[H]	inductance
L_m	[H]	magnetising inductance
ℓ	[m]	magnetic flux path length
ℓ_g	[m]	air gap length

Symbol	*SI Unit*	*Description*
$\boldsymbol{M}$	[A/m]	magnetisation
M_s	[A/m]	saturation magnetisation
μ	[H/m]	permeability
μ_r		relative permeability
μ_0		permeability of free space, $4\pi \times 10^{-7}$ H/m
μ_Δ	[H/m]	incremental permeability
μ_i	[H/m]	initial permeability
μ_{max}	[H/m]	maximum permeability
n		turns ratio
N		number of turns
Φ	[Wb]	flux
$\boldsymbol{P}$	[C/m^2]	electric polarisation
$\mathcal{P}$	[H]	permeance
R	[Ω]	resistance
R_{ac}	[Ω]	ac resistance
R_{dc}	[Ω]	dc resistance
$\mathcal{R}$	[H^{-1}]	reluctance
ρ	[C/m^3]	total electric charge density
ρ_f	[C/m^3]	free charge density
ρ_p	[C/m^3]	polarisation charge density
σ	[S/m]	conductivity
t	[s]	time
τ	[s]	time constant
τ_m	[s]	magnetic time constant
U_m	[J]	magnetic energy
u	[m]	distance
V	[V]	induced voltage
V_0	[V]	initial capacitor voltage
v_d	[m/s]	rate of field penetration
y	[m]	distance
Z	[Ω]	impedance

Analytical Model

η		efficiency
H_a	[A/m]	applied field
H_k	[A/m]	knee point field strength
I_L	[A]	load current
I_p	[A]	primary current
ω	[s^{-1}]	characteristic frequency
N_p		number of turns of primary coil
N_s		number of turns of secondary coil
P_L	[W]	load power
q	[C]	charge
R_L	[Ω]	equivalent transformer series resistance
τ_a	[s]	analytical time constant
V_{out}	[V]	output voltage
w	[m]	width of lamination

Electrical Circuit Model

Symbol	*SI Unit*	*Description*
C_1	[F]	inter-coil capacitance
C_2	[F]	inter-coil capacitance
C_3	[F]	secondary coil capacitance
C_4	[F]	secondary coil capacitance
C_5	[F]	primary coil capacitance
E_{out}	[J]	output energy
I_{peak}	[A]	peak primary current
L_1	[H]	central flux path inductance
L_2	[H]	leakage flux path inductance
K_r		AC resistance co-efficient
L_3	[H]	outer flux path inductance
L_{g1}	[H]	air gap inductance
L_{g2}	[H]	air gap inductance
Ø	[m]	wire diameter
R_p	[Ω]	primary coil resistance
R_s	[Ω]	secondary coil resistance
R_c	[Ω]	equivalent core loss resistance
t_{pulse}	[A]	pulse width
V_{peak}	[V]	peak output voltage
V_{min}	[V]	minimum underswing voltage

Dynamic Capacitance

C_s	[F]	static volumetric capacitance
C_d	[F]	dynamic capacitance
$\vec{W}_s$	[J]	energy storage
W_d	[J]	energy dissipated per cycle
W_k	[J]	total transition energy

Chapter One BACKGROUND

In 1831 Michael Faraday demonstrated electromagnetic induction using the induction coil, and founded the age of electronics. The theoretical foundations of electricity and magnetism were established last century by Faraday (1791 - 1867), Hans Christian Oersted (1777 - 1851), André Marie Ampère (1775 - 1836), Heinrich Lenz (1804 - 1865) and James Clerk Maxwell (1831 - 1879), culminating in a set of equations known collectively as Maxwell's Equations.

The transformer has played an essential role in electrotechnology since its inception, with modern applications ranging from massive distribution systems to miniature surface mount designs. Yet apart from improvements in material science, today's designs contain essentially the same elements as the first practical transformer developed by Gaulard and Gibbs in 1883.

Considered here is an application, that of the output pulse transformer used in an electric fence energiser, whose unique requirements suggest that a thorough understanding of its operation is a necessary step in the search for the optimum design. These transformers have not been well researched previously, and this thesis seeks to address that gap in understanding.

1.1 INTRODUCTION

1.1.1 THE ART OF TRANSFORMER DESIGN

Due to the widespread application of the transformer, there exists a wealth of literature and experience surrounding its design and behaviour. As each new application has developed, literature and design rules specific to that application have developed in tandem. The literature is often so specific that transformers for different applications are often viewed as being different components. Examples of this are the induction coil, the inverter and the variac, which are essentially the same transformer despite being designed to meet very different requirements.

In spite of its widespread use, or perhaps because of it, engineers often appear to understand the design of a transformer for their specific application while being unfamiliar with the transformer's fundamental behaviour. This lack of understanding stems from a number of factors: the large number of non-ideal and non-linear effects inherent in transformer behaviour; an economic preference for off-the-shelf components; and the adequacy of simplifying assumptions, design rules and experience.

Electromagnetic theory is difficult to understand and apply, but thankfully for the electrical engineer, consideration to a fundamental level is in most applications not necessary. As each new application was developed, research and experience simplified the design process until elementary design procedures could be confidently used. This shielded the engineer from the difficulties of understanding electromagnetic theory, and opened the way for transformers to be easily designed and integrated into the new application. Unfortunately, the simplified theory is often assumed to be complete.

Today's literature echoes *Grossner* [1967 pp. 13-14], who says that transformers are designed by "*an amalgamation of circuit analysis, intuition, and trial and error. The component engineer would like to synthesise the final design by the direct application of general principles to the specifications before him, but in practice the design procedure is often influenced by previous proven designs. ... It is not inappropriate to view the total process as art as well as science.*"

This level of understanding is sufficient when the application is well known and has been widely researched, but may leave the engineer perplexed when a new application is presented. For any new application then, a thorough investigation is required of the fundamental behaviour of the transformer, so that the design procedure may be based upon sound theoretical principles.

1.1.2 INTRODUCTION TO ELECTRIC FENCING

The design of a transformer can never be considered in isolation from the remainder of the circuit. To fully appreciate the requirements of the electric fence output transformer (which shall be referred to in this thesis as simply the *output transformer*), an understanding of electric fencing and the electric fence energiser circuit is necessary. The following sections give a brief introduction to electric fencing, in order to provide a framework for the remainder of this thesis.[1]

1.1.2.1 History

Electric fencing has been in use for over 50 years, and is an accepted alternative to traditional non-electric fencing. It is widely used in agriculture due to its low cost, flexibility and portability, allowing paddocks to be easily and economically subdivided which leads to improved pasture management and farm productivity. Electric fencing has also been utilised in wildlife fencing and security applications.

Although electric fencing had been in widespread use in the USA since the 1930s, it wasn't until 1962 that the first effective design, capable of producing a safe high-current pulse, was patented by Philips at the Ruakura Agricultural Research Centre in Hamilton, New Zealand. This design used a capacitive discharge circuit, which had a lower output impedance than previous designs and was therefore more effective at increased fence loads. Ward and Woller further improved the design in 1963 by discharging the capacitor through a step-up

[1] For further information, refer to *McCutchan* [1980], who provides a detailed reference for electric fencing. The *Gallagher Power Fence Manual* [*Gallagher* 1996] is a comprehensive user's guide.

transformer, producing an output pulse with higher voltage for improved transmission along a fence line [*Gallagher* 1977].

Since 1963, the energiser's fundamental design has remained essentially the same, although considerable improvements have been made to reliability, control, safety and efficiency.

1.1.2.2 The Concept Of An Electric Fence

An electric fence energiser is designed to produce a brief pulse of high voltage electricity for distribution on a fence network. A high voltage is required to break through discontinuities in the circuit, such as poor wire connections or the hair and skin of animals touching the fence. The amount of energy in the pulse determines the size of the fence network that can be effectively powered while still maintaining an adequate voltage.

Electric fences rely on psychological, rather than physical, factors to form an effective barrier. The electric shock does directly stimulate a muscle and nerve reaction, but the primary reason that electric fences are effective is that, after receiving a few shocks, an animal becomes afraid to touch the fence.

Non-electric fences must be physically strong enough to withstand a challenge from an animal. An electric fence requires very little physical strength, because once animals have learnt to respect the fence, they will seldom challenge it for fear of receiving an electric shock.

1.1.2.3 Energiser Design

A simple electric fence energiser circuit is represented by the block diagram of Figure 1-1.

The *input circuitry* transfers electrical energy from the power source to the storage capacitor. If the source is AC (mains), the voltage is often increased with a charge pump before being rectified. DC (battery) sources usually use an inverter circuit to significantly increase the voltage level.

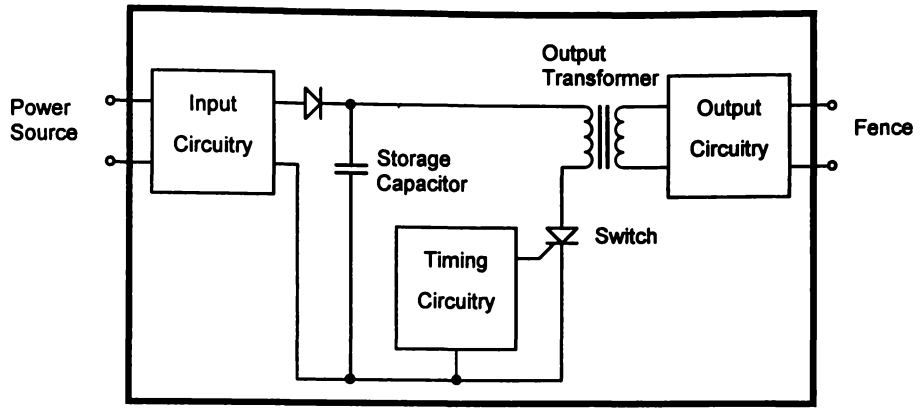

Figure 1-1 *Energiser Block Diagram*

The *storage capacitor* accumulates energy during the interval between output pulses. This energy is then transferred to the fence in one short, high energy pulse. The storage capacitor C_s is charged to an initial voltage V_0, resulting in a stored energy

$$E = \tfrac{1}{2} C_s V_0^2 \qquad \textit{Equation 1-1}$$

which is the effective (or potential) power of the energiser. Energisers range in stored energy from 50 mJ to 60 J.

The *timing circuitry* controls the switch (usually an SCR) and determines the pulse repetition rate. The pulse interval is typically one second, but may be increased on battery powered energisers to extend battery life.

The *output transformer* increases the voltage of the pulse produced by the capacitive discharge, often by a factor of about 10. It also provides some pulse shaping capability as well as electrical isolation between the fence and the power source - an important safety requirement for mains powered energisers.

Additional *output circuitry* may be required to further shape the pulse and limit the peak voltage, or to reduce EMI emission.

Many energiser circuits contain additional electronics to provide information about the fence conditions, to adapt the output power to suit fence conditions, to provide battery protection and battery backup, or to improve the reliability and performance of the energiser. Energiser design and output pulse characteristics are governed by strict Standards to ensure their safety.

1.1.2.4 Output Transformer Design

Although the underlying theory is poorly understood, the existing transformer designs used by most electric fence manufacturers perform satisfactorily. The size of the transformer core as a function of input power can vary widely, and the peak efficiency[2] ranges from 50 % to 90 %. Cost appears to be the most significant design criterion.

Materials used for the core include 0.5 mm silicon steel laminations, strip-wound C-cores, iron powder cores, ferrites, and even iron wires - none of which appear to greatly influence the transformer's performance. Even more notable is the fact that I-core designs exhibit performance comparable to full magnetic path E-I or C-cores, although cores with full magnetic paths appear to be more efficient for high energy pulses. The length of the air gap in full magnetic path cores has very little impact on the transformer's performance.

It would appear that air coupling is important in these designs, and the windings are arranged to minimise the distance between the primary and secondary coils. Layer winding is always used with the primary coil wound closest to the core.

High voltage isolation is a major factor in the design, as under open circuit conditions voltages of the order of 13 kV may be induced in the secondary coil. Safety Standards also specify strict requirements for isolation between primary and secondary. It is therefore common for output transformers to use separate bobbins for the primary and secondary coils, with the secondary bobbin being sectioned to reduce the maximum potential difference between adjacent wires. The coils are usually encapsulated with epoxy resin to provide both high voltage isolation and mechanical stability of the windings.

---

[2] *Peak efficiency* and *peak output energy* are terms commonly used in the electric fencing industry. As illustrated by the output performance graph of Figure 5-19, the output energy varies with the fence load. Peak efficiency and peak output energy refer to the efficiency and output energy respectively of the transformer at the maximum point on the energy-load curve.

1.1.2.5 Pulse Shape

Electric fence energisers produce a high-voltage short-duration pulse with a typical interval of one second, and a pulse shape optimised to travel effectively along the fence. The fence line is a very poor transmission medium, and may include multiple branches, poor connections, and significant leakage such as from grass touching live wires and providing a path to ground.

The load presented to the energiser has a significant impact on the shape of the output pulse. In practice, the effective fence load on the output terminals of the energiser can vary from an impedance of 60 Ω to 10 kΩ, and may include significant capacitance. The circuit design and amount of stored energy also impact the pulse shape. The shape of the pulse can therefore vary significantly between designs and operating conditions. Figure 1-2 shows one example of an output pulse.

EMI requirements, which are becoming increasingly important, suggest that high frequencies should be avoided. The frequency spectrum of the output pulse itself does not typically comprise significant harmonics in the radio-frequency range. Rather, switching transients in the circuit and arcing across faults on the fence are the usual sources of EMI.

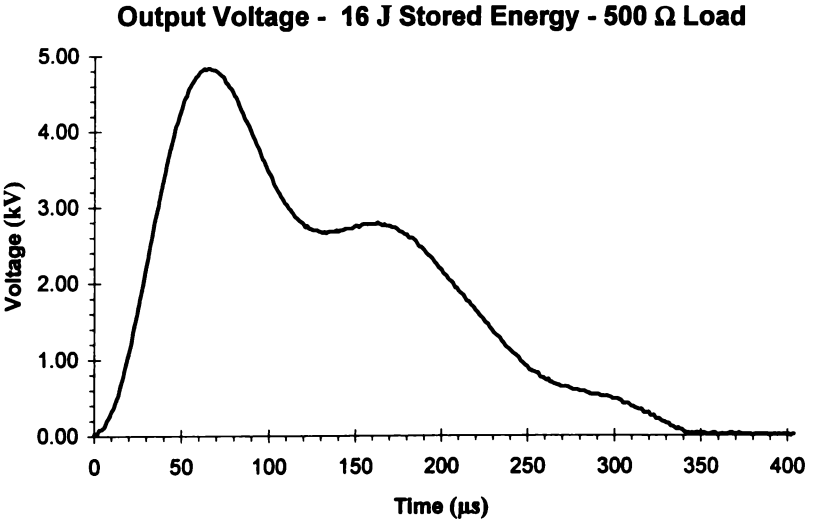

Figure 1-2 *Example Of An Output Voltage Pulse*

1.1.3 COMMERCIAL CONSIDERATIONS

Gallagher Group Ltd. is committed to researching and advancing the technology surrounding electric fencing, both in the agricultural and security markets. The output transformer is a major component of the energiser, in terms of cost, size, and impact on the performance. Gallagher have supported this research into the output transformer with a view to seeing improvements to energiser design through the practical application of the results.

1.1.3.1 Competition

As this work has been conducted in a commercial environment, there are corporate realities which have impacted this work.

Output transformer design has been undertaken at Auckland University under contract to Stafix, a New Zealand company which markets electric fencing equipment. It is unfortunate that due to the competition between Gallagher and Stafix, this topic could not be openly discussed with Auckland University. It does not appear however, that Auckland University has made any significant advance in the understanding and design of output transformers. Their design is well engineered, but appears to lack a thorough knowledge of the application, performance or Standards requirements.[3]

As is common with commercial projects, research into this application is rarely made public. It is therefore unclear whether similar research has been previously undertaken, although it is evident from an examination of other manufacturer's output transformer designs that no electric fencing company has made a significant improvement in this area.

---

[3] The objective of the design by Auckland University was to generate a pulse train of low harmonic content (marketed by Stafix as a Cyclic Wave™) using a resonant tank circuit [*Stafix* 1994]. This requires the design of a non-saturating output transformer, and uses a large iron powder core which remains unsaturated except at extreme loads. The result is a reasonably smooth output pulse, but efficiency of the circuit is poor and significant EMI emissions are still created by switching transitions, requiring further filtering to meet Standards requirements. The smooth pulse shape results primarily from the large inductance and capacitance in the primary discharge path, referred to as a pulse construction circuit by Stafix but identical in function to the components which Gallagher adds for EMI suppression. New Zealand Patent No. 250970/250037 was granted.

1.1.3.2 Research Benefits

The current research will result in a number of benefits, many of them intangible.

A thorough understanding of the transformer's behaviour in this application, and the ability to simulate its operation using an electrical circuit model, would provide the opportunity to optimise the design for any given criteria or to investigate alternative designs. Development times would also be reduced, as the design process becomes more clearly defined and the need for 'trial and error' prototyping decreases. It is expected that the greatest improvements would be made by seeking to lower the cost of the transformer. As well as improvements to existing designs, increased understanding of transformer behaviour may lead to new applications for transformers in electric fence circuits.

The presentation of this research in the form of a thesis will also be particularly useful to future researchers and design engineers.

1.2 LITERATURE REVIEW

A thorough review of the literature has resulted in few references being found which are directly relevant to this work. This highlights the uniqueness of the output transformer design and the need for further research.

There is, of course, a wealth of information regarding magnetics and transformers in general, and many specialised designs have been well reported in the literature. The recent advances in switch mode power supplies are reflected by an abundance of papers but few coherent and complete texts. These references are of some interest however, as a number of them address efforts to develop non-linear transformer models suitable for electrical circuit simulators.

A few references are available on topics which share some commonality with output transformers. Radar pulse transformer and high energy pulse transformer literature has

yielded the most useful information. Internal combustion engine ignition coils are a similar application, but unfortunately this technology has been developed within the industry and very little literature is in the public domain.

The literature reviewed below was of assistance in developing a general appreciation for electromagnetism and transformer design, and was helpful in the development and simulation of the transformer model. However, with the exception of the key references noted in Section 1.2.2, previous research has given very little guidance on the key issue of pulse magnetisation of the output transformer core.

Greater benefit was gained by visiting acknowledged experts [*Severns* 1997, *Collins* 1997 and *Krolski* 1997] to discuss issues specific to the output transformer, and these meetings were instrumental in the completion of this work.

Three systems of units are in common use in transformer literature: the SI (MKS) system, the CGS system (used in the USA for small transformers, permanent magnets, or small conventional electric machines) and the Imperial system (again in use in the USA). The USA is gradually conforming to the internationally accepted SI system, but it is important to be aware of the different units when reviewing literature, particularly old American texts. SI units are used exclusively in this thesis.

1.2.1 BACKGROUND LITERATURE

1.2.1.1 Electromagnetic Theory

Electromagnetism has been a rather stable science for the last century, so many texts are available which provide a good general theoretical background, ranging from Faraday's original *Experimental Researches In Electricity* [*Faraday* 1839] (if one doesn't like maths) and Maxwell's *A Treatise On Electricity And Magnetism* [*Maxwell* 1892] (if one does like

maths)[4] through to the latest texts. *Lorrain and Corson* [1970] has proven an extremely useful reference, and there has also been occasion to refer to *Reitz, Milford and Christy* [1979].

1.2.1.2 Transformer Design

Steady state and mains power applications have been thoroughly researched over the years, and numerous texts cover transformer design and theory. This literature provides a general introduction to transformers, an example being *Grossner* [1967] which has a useful section on pulse transformers.

Paradoxical though it may appear, the vast wealth of general transformer literature can be overwhelming and may sometimes make it difficult to find the right information for the problem at hand. Manufacturers' data books, design guides and application notes can therefore be among the best design resources available, as they focus on providing only the essential design information. Those found useful for this work included *Allied Signal* [1998], *Magnetics* [1991], *Micrometals* [1995] and *Philips* [1998]. Seminar and course notes such as *Klontz, Novotny and Severns* [1997] and *Severns* [1996] have also proven to be invaluable. Because of the unique requirements of output transformers, these sources provide background information only.

1.2.2 KEY REFERENCES

Of the literature reviewed, the following three references were found to have the greatest relevance to the current topic, and their contribution to this thesis is outlined in the following sections.

---

[4] Faraday did not use mathematical notation to describe his discoveries, and his ideas were not accepted by the scientific community until Maxwell expressed them in the mathematical terminology of the preceding scientific period. In the introduction to the 1st Edition of his Treatise, Maxwell wrote "*...before I began the study of electricity I resolved to read no mathematics on the subject till I had first read through Faraday's 'Experimental Researches on Electricity'.*" [*Maxwell* 1892 p. viii].

1.2.2.1 *Modelling And Design Of Energiser Pulse Transformers*

The only reference found which specifically investigates the output transformer of an electric fence energiser is the Masters thesis presented by Harrison in 1992, titled *Modelling And Design Of Energiser Pulse Transformers*. The primary objective of this research was to develop a working computer model of the transformer which could be used to investigate and improve the design.

The transformer's performance in this application was recognised as being influenced by the non-linearity of the magnetic core. To implement the model, *Harrison* used PSpice, a commercial version of the SPICE electrical circuit simulator which has a non-linear transformer model that is based on the Jiles-Atherton theory. Despite some limitations, the model achieved good results and was found useful in practical design work.

This model was used to identify the major loss component in the capacitive discharge circuit as being series resistance, a result that was confirmed experimentally. The model was also used to investigate saturation, which was shown to be a significant factor in the performance and efficiency of output transformers. The critical model parameters were identified as being series resistance, air gap length and magnetising inductance.

Harrison made a number of recommendations for further work, among them being: that a detailed investigation be made of the performance and characterisation of the magnetic core; that a thorough investigation be undertaken of core saturation and design methods for controlling this; and that the modelling techniques be extended to I-core transformers. These recommendations are covered by the current work.

1.2.2.2 *Pulse Generators*

During World War II, enormous progress was made in the USA and Great Britain on the theory and development of radar and related systems. Following the war, this information was published in a 28 volume series by the Radiation Laboratory of the Massachusetts Institute of Technology. Volume Five, published in 1948 and edited by Glasoe and Lebacqz, deals with *Pulse Generators* and includes a section written by Bostick concerning pulse transformers. The original requirement for radar systems was for 100 kW square

pulses with a duration of 1 μs and a frequency of 1 kHz, but *Bostick* goes well beyond this specification. This reference seems to be the only comprehensive work on this class of transformer - pulse transformer theory appears to have begun and ended with this war effort. *Glasoe and Lebacqz* [1948] has been the primary reference for the current work on output transformers.

Bostick begins his section with a brief treatment of general transformer theory, then moves on to equivalent circuits for pulse transformers, showing how the equivalent circuit parameters may be calculated and measured. The concepts of characteristic impedance and impedance matching are introduced, and relationships are established between the elements in the equivalent circuit and the optimum load impedance, pulse duration and efficiency. Also discussed is the effect of the pulse transformer parameters on the output pulse shape and frequency response.

The diffusion of the magnetic field into the core material is discussed and analysed. Bostick's contribution in this area will be noted later in this thesis when pulse magnetisation is considered in detail.

While giving a theoretical justification for all design criteria, Bostick notes that in order to be understood the theory must be simplified to the point where the accuracy is compromised. Transformer design therefore relies heavily on "*past experience, and extrapolation from previous successful designs*" [*Glasoe and Lebacqz* 1948 p. 610]. In particular, "*the measured values of* [leakage inductance, parasitic capacitance and magnetising inductance] *are usually more accurate than the calculated values because it is very difficult to control the coil dimensions with great accuracy and to have exact knowledge of the effective permeability of the core under the particular conditions of operation.*" [*ibid.* p. 553].

Radar pulse applications differ from electric fencing in that the pulses typically have a width of 1 μs and a primary current of 5 A peak, compared to electric fence pulses of the order of 300 μs and 300 A. This results in significantly different pulse magnetisation characteristics. While the approach presented by Bostick has been of immense value, his results have limited relevance due to these differences between the applications.

1.2.2.3 *High Speed Pulse Technology*

1965 saw the publication of an English translation of the first two volumes of Früngel's reference work, *High Speed Pulse Technology*, which provides a very thorough investigation of pulse phenomenon and the capacitor discharge technique. Most of his work is concerned with high power discharges of the order of megawatts and megaamps, with a focus on the circuit as a whole. Früngel relies heavily on experimental results, and provides little theoretical analysis of the transformer systems he describes.

In his treatment of high voltage pulse transformers, Früngel reprints with permission from the previously mentioned work by Bostick in *Glasoe and Lebacqz* [1948].

Früngel states that the objective of a pulse transformer is to exactly reproduce a square impulse introduced into its primary, and that the pulse transformer normally has a very small leakage inductance and a high efficiency, but relatively small pulse power. Früngel distinguishes between the pulse transformer, as discussed by Bostick, and what he terms the 'peak power' or 'shock' transformer, whose objective is to allow the production of a peak power greater than 2000 MW. The shape of the output pulse is produced in the transformer itself. According to Früngel, peak power transformers have a high leakage inductance, and achieve the high peak output voltage with a magnetic core material that is highly magnetisable but produces high losses during demagnetisation. Low quality, thick laminations are typically used for this purpose. There is some similarity between peak power transformers and energiser output transformers.

Früngel makes the following comments on page 212 regarding peak power transformers.

> *"A skin effect cannot occur, since growing fields, when originating from primeval condition, penetrate a conductor or a magnetic material completely. Skin effect or other surface phenomena develop only during some alternating action or during a change in the rate of growth of fields. Owing to these fundamental properties of swing-in phenomena during the instant of switching on, it is possible to use almost any arbitrary ferrous sheet material for the core in impulse transformer of this type, as it is certain to be penetrated by the field. Thin sheets will serve as well as thick sheets of 0.2mm. Only in heavier sheets of 0.35 or 0.5mm thickness can there be observed a drop in voltage."*

"The ferromagnetism in the iron core can spread only to a small extent during such a short impulse duration. One finds, therefore, a steep gradient of the magnetic field in cores of such impulse transformer at only a few centimeters' distance from the origin of the excitation, the surrounding primary winding. ... In such transformers it is therefore useless to employ closed magnetic cores, since during its short life the impulse proper is not able to utilize the lower magnetic reluctance created by a closed magnetic circuit. As long as during the short impulse duration there is sufficient core volume for magnetic field expansion or for orientation of sufficient magnetic domains, it is without consequence whether the magnetic circuit outside the coil field is closed or not. For rough approximation it can be said that the iron core should project at each end of the coil for about ¼ of the coil length."

These explanations certainly address the observed performance of peak power transformers. However, Früngel appears to have misinterpreted the diffusion effect caused by eddy currents, commonly referred to as magnetic skin effect. Due to the low value of permeability in air, the magnetic field is established instantly around the entire surface of the core and in the small air gaps between laminations. The phenomena described by Früngel are rather caused by the finite amount of time taken for the magnetic field to penetrate the core, and by saturation once the core has been penetrated. This thesis discusses these issues in depth.

Früngel gives a short description of the automotive ignition coil and the electric fence energiser, but in both cases focuses on the circuitry rather than the transformer. Two comments, on pages 258 and 260 respectively, are worth noting.

"For an optimum physiological effect the auxiliary capacitor and the main capacitor are so dimensioned that in cooperation with the transformer primary the circuit is tuned to a discharge frequency of about 250 [Hz] *... Experiments have shown that in all mammals of comparatively similar size, the same frequency has optimum effect because the sensory nervous systems of men and other mammals are almost identical."*

"In order to avoid radio interference caused by the long wire lines, which act like antennas it is advisable to design the transformer with proper arrangement of primary and secondary - for instance, by elimination of capacitive coupling - so that hard discharge pulses, which cannot be prevented in the primary, are carried over to the

secondary in such a manner that frequency portions above 10 [kHz] *are avoided. An arrangement conducive to that end is the separation of primary and secondary adjacent to each other so that a voltage pulse is induced in the secondary only by detour through the iron of the transformer core. A core of normal dynamo grade sheets, especially the low grades, cannot carry over interfering high frequencies owing to its high iron losses.*"

In 1976 a third volume was published in which Früngel gave an update on advances in pulse technology during the intervening years. He describes low-inductance air-cored pulse transformers whose primary applications include high-current pulses for plasma research, high-pulsed magnetic fields, and pulsed light sources. He presents no new information concerning high voltage pulse transformers.

1.2.3 ADDITIONAL REFERENCES

The following section provides an overview of additional references, which were of some relevance to the current topic but did not contribute directly to the primary work of this thesis.

1.2.3.1 Eddy Currents

The subject of eddy currents is poorly covered by contemporary electromagnetics textbooks, with the notable exceptions of *Smythe* [1950] and *Landau and Lifshitz* [1960]. Interest in this subject was revived by the discovery of high-temperature superconductors, as outlined by *Saslow* [1991, 1992] who found that he needed to refer to Maxwell's treatment of eddy currents [*Maxwell* 1892] before making progress in understanding this topic. When reading Maxwell's work, it is difficult to overcome the barrier presented by the pre-vector 19th Century notation. *Saslow* begins to address this issue by highlighting the application of Maxwell's theory of eddy currents in thin conducting sheets, and his use of the method of images, to problems in superconductivity.

1.2.3.2 Hysteresis

The currently accepted model of magnetic hysteresis ascribes the phenomenon to the irreversible, dissipative motion of Bloch walls separating magnetic domains. In 1986, Jiles and Atherton presented a paper describing a mathematical model of the hysteresis mechanism [*Jiles and Atherton* 1986]. In this model, the authors first derive the anhysteric curve based on domain wall bending and translation, and then include hysteresis by considering a frictional force caused by the pinning of domain walls on defect sites. This was the first quantitative model of hysteresis and has greatly assisted in the understanding of this effect. The authors have extended this theory in later work, for example *Garikepati, Chang and Jiles* [1988], and *Jiles* [1994].

The Jiles-Atherton theory is summarised in Chapter 2.1.2, and its application to the modelling of output transformers is discussed in Chapter 5.

Other mathematical descriptions of hysteresis have been proposed [*Hodgdon* 1988], including the popular Preisach model [*Mayergoyz* 1988, *Pescetti* 1989] in which the magnetic domains are each assumed to have their own characteristic hysteresis loop. *Chatterjee* [1995] presents a simple alternative to the more difficult models by using a mean-field approach.

1.2.3.3 Transformer Modelling

A number of methods have been developed to accurately model the transformer, and *Severns* [1992, 1996] provides a comprehensive overview of these techniques. Difficulties arise when attempting to include a non-linear magnetic core, so many references focus on this aspect of the transformer model.

Williams [1994] reviews several modelling methods and identifies the Jiles-Atherton model as being the most accurate, though having a number of errors in its formulation and suffering from a lack of correspondence between the required parameters and manufacturer's data. He also concludes that several of the Jiles-Atherton equations are not derived theoretically as it first appears, but are rather approximations based on observation.

Williams then develops an algorithm which implements the Jiles-Atherton model of non-linear ferromagnetic hysteresis, and incorporates this into a SPICE based circuit model. This model covers only the implementation of the non-linear core. Williams suggests that additional effects such as eddy current losses and other frequency domain effects could be added to the magnetic subsystem using lumped resistors, capacitors or inductors.

Pernía, Nuño and Lopera [1995] present a model based on Maxwell's Equations which is derived from the geometry of the core and windings. The model is synthesised from electric circuit components and is therefore suitable for simulation.

Collins [1990] investigates dynamic parasitic capacitance and presents a modelling approach that calculates the equivalent capacitance value. Collins' method is outlined in Appendix 2, and is used in Chapter 5 during the development of the electrical circuit model.

1.2.3.4 Simulation

Due to the widespread use of SPICE based electrical circuit simulators, a large number of references are available on this topic, most of which deal with basic circuit simulation. Papers have addressed more specialised topics including the modelling of hysteresis or non-linear magnetics, which has been of help when considering the implementation of the electrical circuit model described in this thesis.

Nehmadi et. al. [1990] discusses the simulation of a magnetic pulse compression circuit, including non-linear core modelling, which is implemented using the PSpice core model. The penetration of the core by the magnetic field is considered. *Prigozy* [1993, 1994] investigates the non-linear magnetic core model provided by PSpice, and *Pei and Lauritzen* [1986] suggest a model using two non-linear controlled sources which may be implemented on SPICE2.

Other papers have investigated SCR modelling [*Giacoletto* 1989, *Albou* 1993] and given advice on solving convergence problems [*Intusoft* 1996, *Castro* 1988].

1.2.3.5 Ignition Coils

Internal combustion engine ignition transformers share the requirement for a high voltage pulse with electric fencing, and have been used in hobby designs for electric fence projects [*Dawson* 1982, *Clarke* 1995]. Unfortunately, ignition coil design literature suffers from the same problem as that of output transformers, in that advances are developed primarily by manufacturers who are reluctant to publish their research.

Of the few references available, most are written for electronics hobbyists, for example the article by *Wevill* [1981] in *Practical Electronics.* In *Steuerbare Kondensator-Zündanlage*, *Maurer* [1975] describes an ignition circuit which uses a flyback converter to charge a storage capacitor which is then discharged through a step-up transformer. This is very similar to an electric fence circuit, but the article discusses only the circuitry and not the transformer design.

The references, and discussion with *Krolski* [1997], indicate that ignition coils are sufficiently different from output transformers for there to be little to be gained from investigating their design. Internal combustion engine ignitions require a faster pulse repetition rate (related to the engine rpm) and a lower pulse energy of the order of 100 mJ. The most common ignition circuit is based on an inductive discharge. This is unsuitable for electric fencing due to its inherently high output impedance which results in poor performance on heavily loaded fences [*Dawson* 1985].

1.2.3.6 Fence Theory

The electrical behaviour of electric fencing has been investigated in *Electric Fences: Modelling The Electrical Characteristics And Behaviour Of Electric Fence Systems* [*Hancock* 1991], which provides an excellent summary of the current research in this area. *Hancock* presents a unified approach to the little studied field of electric fencing, and investigates the following:

- the behavioural relationship between the energiser, fence and animal;
- the effects of pulsed electric shock, and its relationship to fence effectiveness;
- safety issues;
- the application of transmission line theory to electric fences;
- the characterisation and modelling of fences.

Of greatest relevance to the current work is Hancock's identification of the following factors which enhance the effective performance of a pulse on a fence-line:

1. high peak voltage;
2. smooth waveform with a large pulse width;
3. high energy.

A high peak voltage and energy improves the effectiveness of the shock at the end of a long fence-line. A smooth waveform and large pulse width imply that the pulse contains predominantly low frequency components, and will therefore minimise attenuation of the pulse during propagation along the fence.

Hancock is an excellent general background reference relevant to any aspect of electric fencing or design, and is referred to on numerous occasions in this thesis. Other general electric fencing references tend to focus on the practicalities of installing and operating electric fences, or on animal behavioural studies. The most notable of these is *McCutchan* [1980].

1.2.3.7 Shock Theory

A most informative reference on shock is *Wadsworth and Chanmugam* [1988], which contains some very useful information on the stimulation of nerve and muscle fibres by electric currents. This reference is written for physiotherapists, as high voltage generators are used in physiotherapy to stimulate nerves and muscles.

The biological action of nerve stimulation is discussed in detail, including conditions under which muscles cannot recover from involuntary contraction (that is, one cannot voluntarily release one's grip) - a topic of great interest in terms of electric fence safety. The effect of pulse duration and current level is discussed. Devices producing pulsed peak currents as high as 400 mA are used in physiotherapy, and are considered safe because of the short pulse duration of 100 μs.

Barnes [1989] presents an astounding paper from South Africa on the requirements for an effective lethal electric fence. Of note is that Barnes refers to the use of voltage impulses of less than 100 ms duration at a frequency of 1 s as the "non-lethal mode". The severity of shock and injury caused by an electric current flowing through the human body is presented both qualitatively and quantitatively. There is also some discussion of body impedance.

The thesis by *Hancock* [1991] presents research including some experimental data on the effect of electric fence pulses on humans, and also provides a useful summary of safety and Standards issues.

Electric fencing safety Standards are (with the exception of the UL Standards in the USA) based on the reports produced by the International Electrotechnical Commission, Technical Committee 64 Working Group 4 [*IEC 479* 1984, *Biegelmeier* 1987].

Results from these references are summarised in Chapter 2.4 which discusses shock theory.

1.3 OBJECTIVES

The wide range of output transformer styles existing in electric fence energisers is testament to the lack of a robust theory to guide the engineer towards an optimum design. While many of these transformers display satisfactory performance, the fact that such disparate designs can have similar performance would indicate that we are missing something.

The primary objective of this thesis is to achieve a comprehensive understanding of the behaviour of the transformer in this application, based on sound theoretical considerations. The motivation is that, by understanding why these transformers operate the way they do, it may be possible to take advantage of their unique requirements and design the optimum output transformer. Practical application of the theory is left to further work.

This thesis then is concerned with analysing the output transformer. Specific objectives involve three areas of analysis.

1. **Electromagnetic Treatment** At the most fundamental level, the behaviour of the output transformer is related to the interaction of the magnetic field, created by the discharge of the storage capacitor through the primary winding of the transformer, with the core material. It is clear from the success of I-core transformer designs that this behaviour is quite different to most transformer applications. Achieving a complete description of the electromagnetic behaviour is therefore the first objective.

2. **Analytical Model** An analytical study of the transformer will provide a wealth of information regarding the relationship between elements in the equivalent circuit of the transformer and its behaviour. The behaviour of the output transformer is also closely linked to the circuit providing the pulsed input, and can never be considered in isolation from this. The second objective is to undertake a thorough analytical study of the output transformer and capacitive discharge circuit.

3. **Electrical Circuit Model** The final objective is to develop a realistic and accurate electrical circuit model of the output transformer. This will provide information about the behaviour and desirable characteristics of the transformer, in addition to allowing the transformer to be simulated and optimised without the need for a physical prototype. This model will provide a strong link between theory and design.

This research is also seen as an opportunity to investigate the recommendations for further research suggested by previous work [*Harrison* 1992].

Chapter Two THEORY

Magnetism has been used for almost 2000 years, and today has found applications in almost every area of life. The foundations of electromagnetism were developed by Ampère, Faraday and Maxwell, culminating in Maxwell's Equations which define the relationship between electricity and magnetism. Faraday's discovery of electromagnetic induction in 1831 led to the development of the transformer, which has played an essential role in electrotechnology.

This chapter presents an overview of electromagnetic and transformer theory relevant to the electric fence application, in order to provide a background for the rest of this thesis. The primary references have been *Lorrain and Corson* [1970], *Reitz, Milford and Christy* [1979], *Klontz, Novotny and Severns* [1997], and *McGraw-Hill* [1992].

The two aspects of electric fencing theory which have a significant impact on the output transformer design are the electrical behaviour of fences and shock, and theory related to these topics is also discussed.

2.1 ELECTROMAGNETIC THEORY

2.1.1 MAXWELL'S EQUATIONS

The theory of magnetism was developed independently from that of electricity until Oersted showed that the two subjects were linked. This relationship between magnetism and electricity was developed further by Ampère, Faraday and Maxwell, but was not fully understood until Einstein proposed his theory of relativity.

Maxwell's Equations form the foundation on which electromagnetism is built. They apply to all electromagnetic phenomena in media which are at rest with respect to the co-ordinate system used, and are valid for non-homogeneous, non-linear and non-isotropic media - that is, they are completely general. They are partial differential equations involving space and time derivatives of the field vectors $\boldsymbol{E}$ and $\boldsymbol{B}$, the total charge density ρ, and the current density $\boldsymbol{J}$, which define the relationship between electricity and magnetism and allow the fields produced by sources of charge and current to be determined. These equations do not yield the values of $\boldsymbol{E}$ and $\boldsymbol{B}$ directly; they must be integrated with the appropriate boundary conditions taken into account.

Maxwell's Equations in differential form are

$$\nabla \cdot \boldsymbol{E} = \frac{\rho}{\varepsilon_0} \qquad \textit{Equation 2-1}$$

$$\nabla \cdot \boldsymbol{B} = 0 \qquad \textit{Equation 2-2}$$

$$\nabla \times \boldsymbol{E} = -\frac{\partial \boldsymbol{B}}{\partial t} \qquad \textit{Equation 2-3}$$

$$\nabla \times \boldsymbol{B} = \mu_0 \boldsymbol{J} + \frac{1}{c^2}\frac{\partial \boldsymbol{E}}{\partial t} \qquad \textit{Equation 2-4}$$

where

$\boldsymbol{E}$ = electric field strength [SI unit: V/m]
$\boldsymbol{B}$ = magnetic flux density [SI unit: T]

ρ = total electric charge density [SI unit: C/m^3]
$= \rho_f + \rho_p$
where ρ_f = free charge density
ρ_p = polarisation charge density[1]
$= -\nabla \cdot \boldsymbol{P}$
$\boldsymbol{P}$ = electric polarisation [SI unit: C/m^2]

$\boldsymbol{J}$ = total electric current density [SI unit: A/m^2]
$$= \boldsymbol{J}_f + \frac{\partial \boldsymbol{P}}{\partial t} + \nabla \times \boldsymbol{M}$$
where $\boldsymbol{J}_f$ = conduction current density[2]
$\frac{\partial \boldsymbol{P}}{\partial t}$ = polarisation current density
$\nabla \times \boldsymbol{M}$ = magnetisation current density[3]
$\boldsymbol{M}$ = magnetisation [SI unit: A/m]

$$c^2 = \frac{1}{\varepsilon_0 \mu_0}$$
c = speed of light, 2.998×10^8 m/s
ε_0 = permittivity of free space, 8.85×10^{-12} F/m
μ_0 = permeability of free space, $4\pi \times 10^{-7}$ H/m

Each of Maxwell's equations represent a mathematical expression of certain experimental observations. As such they cannot be proven, but as a result of extensive experimental work are now believed to apply to all macroscopic situations. Equation 2-1 is Gauss' law, which in turn derives from Coulomb's law; Equation 2-2 is usually said to represent the fact that single magnetic poles have never been observed; Equation 2-3 is the differential form of Faraday's law of electromagnetic induction; and Equation 2-4 represents an extension of Ampère's law. In Maxwell's time, the reason for these relationships was not understood, something which had to wait until the development of relativity and quantum mechanics.

---

[1] Also known as *bound charge density*.

[2] Also known as *transport current density* or *free charge current density*.

[3] Also known as *atomic current density*.

Equation 2-4 can be written[4] in the more common form of

$$\nabla \times \boldsymbol{H} = \boldsymbol{J}_f + \frac{\partial \boldsymbol{D}}{\partial t} \qquad \textit{Equation 2-5}$$

where $\frac{\partial \boldsymbol{D}}{\partial t}$ is known as the displacement current density[5] and $\boldsymbol{H}$ is the magnetic field strength. In order to solve magnetic field problems, it is essential to know the relationship between $\boldsymbol{B}$ and $\boldsymbol{H}$. It is convenient to define a magnetic susceptibility χ_m and a relative permeability μ_r such that

$$\boldsymbol{M} = \chi_m \boldsymbol{H} \qquad \textit{Equation 2-6}$$

where $\boldsymbol{M}$ is the magnetisation within the material that is contributed by the material, and $\boldsymbol{H}$ is the applied magnetic field strength. From Maxwell's Equations, the expression

$$\boldsymbol{B} = \mu_0(\boldsymbol{H} + \boldsymbol{M}) \qquad \textit{Equation 2-7}$$

may be derived, which when substituting for the magnetisation $\boldsymbol{M}$ from Equation 2-6 gives

$$\boldsymbol{B} = \mu_0(1 + \chi_m)\boldsymbol{H} = \mu_0\mu_r\boldsymbol{H} = \mu\boldsymbol{H} \qquad \textit{Equation 2-8}$$

where $\mu_r = 1 + \chi_m$ *Equation 2-9*

The quantity μ is called the permeability, and is usually obtained by experiment. Both χ_m and μ_r are dimensionless quantities. As the applied magnetic field strength $\boldsymbol{H}$ increases, the magnetisation of a material will approach a maximum value known as the saturation magnetisation $\boldsymbol{M}_s$, and the magnetic flux density $\boldsymbol{B}$ will only continue to increase because of the $\mu_0\boldsymbol{H}$ term.

---

[4] This uses the relationship between *electric field strength* $\boldsymbol{E}$ and *electric induction* $\boldsymbol{D}$ of $\boldsymbol{D} = \varepsilon\boldsymbol{E} = \varepsilon_0\boldsymbol{E} + \boldsymbol{P}$, which is analogous to the relationship between *magnetic field strength* $\boldsymbol{H}$ and *magnetic induction* $\boldsymbol{B}$, $\boldsymbol{B} = \mu\boldsymbol{H} = \mu_0(\boldsymbol{H} + \boldsymbol{M})$ given in Equation 2-7.

[5] The displacement current term, required for charge conservation, represents one of Maxwell's major contributions to electromagnetic theory. The reality of this current has only recently been demonstrated by direct measurement, as reported by *Bartlett and Corle* [1985] who used automotive ignition coils in their experimental apparatus to amplify the signals.

2.1.2 MAGNETISM

Magnetic effects can be regarded as a consequence of the motion of electric charges. All matter consists ultimately of atoms, with each atom containing electrons moving in orbit around the nucleus. These electron circuits, each of which is confined to a single atom, are called atomic currents. There are thus two kinds of current: a conventional current, which consists of charge transport (the motion of free electrons or ions); and atomic currents, which are pure circulatory currents. Both types of current may produce magnetic fields.

2.1.2.1 Classification Of Magnetic Materials

The magnetic properties of all materials cause them respond in some way to a magnetic field, with the response related to the material's value of magnetic susceptibility χ_m. If χ_m is small and positive, the material is called *paramagnetic* and the magnetic flux density is strengthened by the presence of the material. If χ_m is small and negative, the material is *diamagnetic* and the magnetic flux density is weakened by the presence of the material. Since $|\chi_m| << 1$ for both paramagnetic and diamagnetic materials, these materials show almost no response to the applied magnetic field.

There is a small class of materials however for which $\chi_m >> 1$. This behaviour arises from the spins of the electrons. If the spins of atoms or molecules align in a common direction, the material can exhibit a net magnetisation in the absence of an applied field, and the magnetic behaviour is known as *ferromagnetism*. Such a material usually has a profound effect on the magnetic flux density.

A material which has an anti-parallel arrangement of equal spins displays *anti-ferromagnetism*, and since the electron spins exactly cancel, anti-ferromagnetism is too weak to be of any practical use.

Ferrimagnetism occurs when the magnetic moments of neighbouring ions tend to align anti-parallel to each other, but there is still an appreciable resultant magnetisation as the moments are of different magnitudes.[6]

The relationships between electron spin and magnetism are illustrated in Figure 2-1.

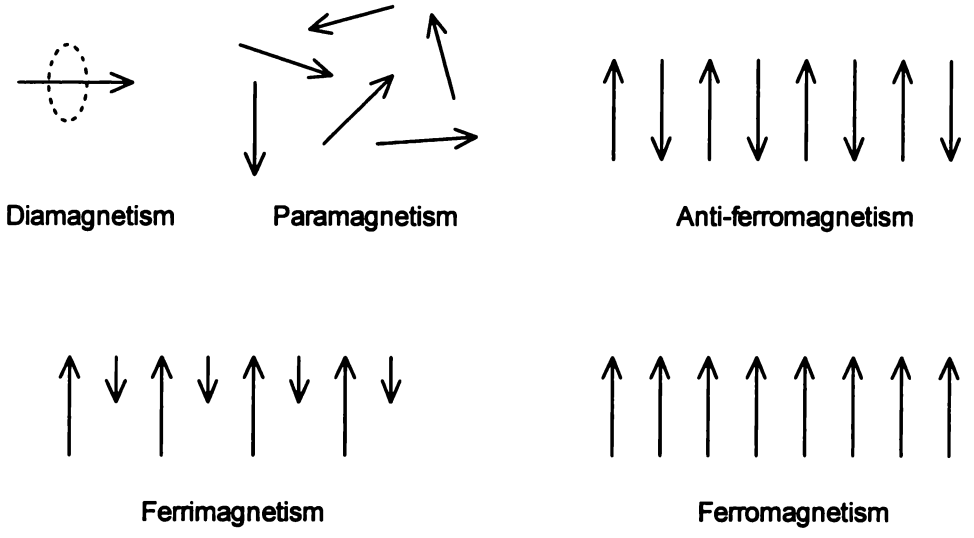

Figure 2-1 *Classification Of Magnetic Materials*

Although it is usual to refer only to ferromagnetism when discussing magnetic properties (as is the case in the following sections), the bulk properties of ferrimagnets resemble those of ferromagnets, and in fact, ferrimagnetism may be considered to be a subset of ferromagnetism.

2.1.2.2 Domain Theory

In 1907, the French physicist Weiss developed the central thought that explained the observed properties of ferromagnetic materials, and which still provides the basis of our theory of non-linear ferromagnetism. Weiss postulated that a ferromagnetic body must be

[6] Ferrimagnetism is also known as *Néel ferromagnetism*.

composed of small regions or domains, each of which is magnetised to saturation level with a direction of magnetisation which need not be parallel to other domains. Changes in the bulk magnetisation of a material arises from changes in size and orientation of these domains. This theory was extended by Landau and Lifshitz who in 1935 presented a thermodynamic theory of domains [*Landau and Lifshitz* 1960 p. 158].

Domain size varies widely depending on the composition, purity and state of strain of the material, and on energy relationships. The exchange forces which produce magnetisation are associated with crystallographic structure producing a directional dependence of magnetisation with respect to the crystal axis. This directional dependence is known as crystal anisotropy. The improved magnetic properties in the direction of the crystal axis are exploited in grain oriented steels.

The boundary region between two oppositely oriented domains is known as the Bloch wall. A 180° change in magnetisation will preferably occur over a large distance to minimise potential energy in the wall, but wall width will be restricted by the restraining influence of crystal anisotropy. An additional energy relationship involves the magnetostatic or field energy surrounding a magnetised volume. A magnetised volume tends to subdivide - it will be energetically possible for subdivision to occur until the decrease in magnetostatic energy is less than the potential energy associated with the Bloch wall foundation. At this point, the arrangement of the domains is that of minimum total potential energy. External fields produced to magnetise or demagnetise the material only disturb the balance of the potential energies involved, resulting in the familiar s-shaped magnetisation curve.

2.1.2.3 Magnetisation Curve

In the demagnetised condition where domains are randomly oriented and are not subject to a magnetising force, a bulk sample of material will appear unmagnetised - that is the magnetic flux density is zero. Although there is really no general magnetisation curve or loop, the most common shape is that shown in Figure 2-2, which may be termed *sigmoid.* The following account of the process of magnetisation relates primarily to magnetically soft materials, which have low coercivity and high permeability.

1. For low values of external field, domain boundary walls stretch in a reversible process.

2. As the magnetic field strength is increased, domain boundaries begin to move through the material in an irreversible process (described in Section 2.1.2.4). The more favourably oriented regions grow at the expense of their less favourably oriented neighbours, and a large increase in magnetic flux density occurs.

3. At still higher values of magnetic field strength, the magnetisation vectors are rotated against the forces of strain and crystal anisotropy into alignment with the direction of the applied field. All domains are ultimately aligned when the material reaches saturation. Increasing the magnetic field strength further will only increase the magnetic flux density to the extent that would occur in a non-ferromagnetic substance.

4. Removing the magnetic field causes some relaxation - the domains rotate back to the easy direction of magnetisation. This relaxation can be minimised by making the direction of easy magnetisation co-incident with the desired direction of magnetisation.

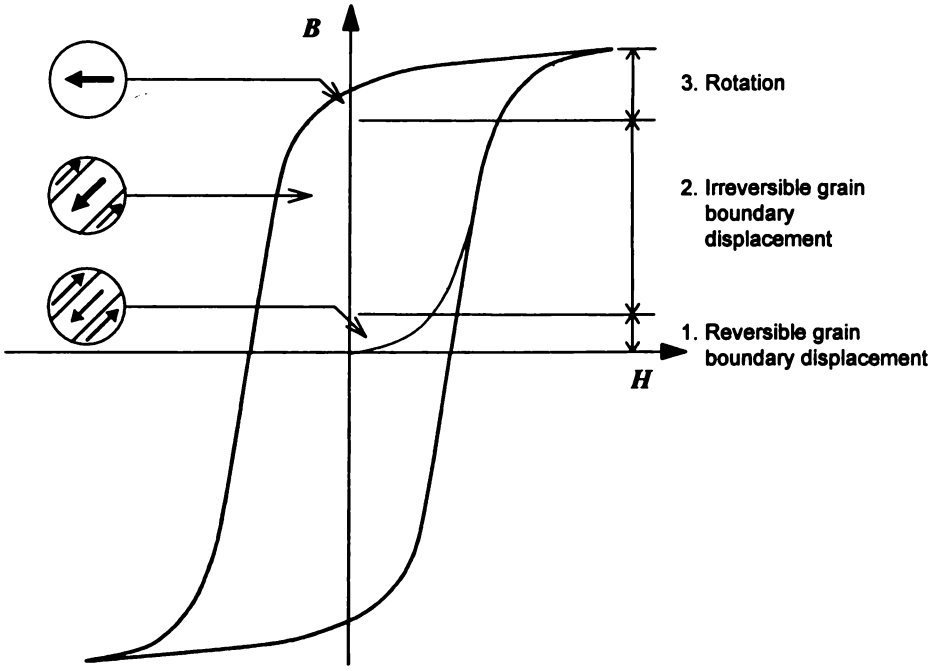

Figure 2-2 *Domain Orientation* [*Fink* 1975]

2.1.2.4 Ferromagnetic Hysteresis

The first comprehensive theory of the hysteresis mechanism was presented by *Jiles and Atherton* [1986]. It explains the observed phenomenon and models the hysteresis loop by considering impedances to domain wall motion due to pinning sites encountered by the domain walls as they move. The Jiles-Atherton theory is outlined in this section.

Anhysteric Magnetisation

In an isotropic material,[7] the energy per unit volume of a typical domain is given by

$$E = -\mu_0 \boldsymbol{m} \cdot \boldsymbol{H}_e \qquad \textit{Equation 2-10}$$

where E = energy per unit volume of typical domain
$\boldsymbol{m}$ = magnetic moment per unit volume of typical domain
$\boldsymbol{H}_e$ = effective magnetic field strength[8]

Coupling between the domains can be expressed as a coupling to the bulk magnetisation $\boldsymbol{M}$, and the effective magnetic field strength can be written as

$$\boldsymbol{H}_e = \boldsymbol{H} + \alpha \boldsymbol{M} \qquad \textit{Equation 2-11}$$

where α = interdomain coupling parameter

α is defined experimentally. The response of the magnetisation to the effective field can be expressed as

$$M_{an}(H_e) = M_s f(H_e) \qquad \textit{Equation 2-12}$$

where M_s = saturation magnetisation
M_{an} = anhysteric magnetisation

and f is an arbitrary function of the effective field which takes the value zero when H_e is zero, and the value one as H_e tends to infinity.

---

[7] The equations may be extended to include anisotropic material. See also *Hodgdon* [1988].

[8] H_e is the internal magnetic field strength experienced by the domain, as distinct from the applied magnetic field strength.

Equation 2-12 applies to an ideal solid with no impedance to changes in magnetisation caused by pinning sites, and is the anhysteric curve M_{an} along which domain walls achieve true equilibrium for the field H. The anhysteric curve may be obtained experimentally by superimposing a decaying AC signal onto a steady DC magnetic field, H.

The function chosen to model the anhysteric curve is a modified Langevin expression.

$$M_{an}(H_e) = M_s\left[\coth\left(\frac{H_e}{a}\right) - \frac{a}{H_e}\right] \qquad \textit{Equation 2-13}$$

where a = thermal energy parameter [SI units: A/m]

Hysteric Magnetisation

The Langevin equation describes the AC, or anhysteric, magnetisation curve. The DC, or initial, magnetisation curve lies below the AC curve, approaching it asymptotically at high fields.

Reversible wall displacement would occur in an ideal (unpinned) specimen with a potential that increases with the magnetisation. The domain boundary would come to rest when the work done by the field is balanced by the magnetisation energy of the sample. When the field is removed, the domain wall would return to the original location.

However, domain wall motion is impeded by pinning sites, causing irreversible changes in magnetisation and creating the hysteresis loop shown in Figure 2-2. These pinning sites are imperfections such as non-magnetic contaminants and voids in the crystal lattice of the magnetic material. In the Jiles-Atherton theory, all pinning sites are assumed to be the same, and to be uniformly distributed throughout the solid.

The total energy dissipated by this impedance when a domain wall is moved through a distance between domains is given by

$$E_{pin}(M) = K\int_0^M dM \qquad \textit{Equation 2-14}$$

where K = domain anisotropy parameter [SI units: A/m]

M = bulk magnetisation of solid

Hence for a uniform distribution of pinning sites, the total work done against pinning is proportional to the change in magnetisation

$$\int M dB_e = \int M_{an}(H_e) dB_e - K \int \frac{dM}{dB_e} dB_e$$

where B_e = effective magnetic flux density

$$\Rightarrow M = M_{an} - \delta K \frac{dM}{dB_e}$$

where δ = +1, for $\frac{dH}{dt} > 0$

= -1, for $\frac{dH}{dt} < 0$

$$\Leftrightarrow \frac{dM}{dH} = \frac{(M_{an} - M)}{\frac{\delta K}{\mu_0} - \alpha(M_{an} - M)}$$ ***Equation 2-15***

This shows that apart from the perturbation due to the coupling of magnetisation expressed through the co-efficient α, the rate of change of magnetisation M with field is proportional to the displacement from the anhysteric M_{an} - M.

A domain wall held by two pinning sites bends when subject to a magnetic field - initially a reversible change in magnetisation. Bending continues until the wall either touches a nearby pinning site to which it becomes attached, or breaks away and moves discontinuously and irreversibly until it encounters further pinning sites.

The amount of domain wall bending depends on the domain wall surface energy, the strength of the pinning sites, and the difference between the prevailing magnetisation $M(H)$ and the anhysteric magnetisation at the same field $M_{an}(H)$. The domain walls bend to reduce the difference between the prevailing magnetisation and the anhysteric magnetisation.

The force F experienced by a domain wall is due to the applied field minus a contribution due to the tendency of a ferromagnet towards a random orientation of its domain configuration.

$$F = (M_{an} - M)$$ ***Equation 2-16***

If the moments of the two domains are parallel and anti-parallel to the field

$$M_{rev} = 2\Delta V m$$
$$\approx c(M_{an} - M)$$

where ΔV = volume swept out by bulging domain wall

$c = \frac{\chi'_{0,norm}}{\chi'_{0,anhys}}$, the ratio of initial differential susceptibilities of the normal and anhysteric magnetisation curves, known as the domain flexing parameter

Magnetisation can therefore be calculated as the sum of the irreversible component M_{irr} given by Equation 2-15 and a reversible component M_{rev},

$$\frac{dM}{dH} = \frac{1}{1+c\frac{\delta K}{\mu_0} - \alpha(M_{an} - M)} \frac{M_{an} - M}{} + \frac{c}{1+c} \frac{dM_{an}}{dH} \qquad \textit{Equation 2-17}$$

which completely describes the hysteresis curve of a ferromagnetic material.

2.1.3 MAGNETIC MATERIALS

Although all materials are magnetic, the term *magnetic material* usually refers to those which can support a relatively large magnetisation. The materials which are most important to magnetic technology are ferromagnetic and ferrimagnetic materials.[9] Ferromagnetic materials are the elements iron, cobalt, nickel, and their alloys, some manganese compounds, and some rare earth elements. Ferrites are ceramic ferrimagnetic oxides with iron oxide as the main ingredient and usually with some nickel, zinc or manganese elements.

[9] A small class of organic compounds exhibits magnetic properties. See *Miller and Epstein* [1990].

The principal disadvantages of magnetic materials are the non-linearity in the ***B-H*** relationship, the losses associated with cyclic excursions of the hysteresis loop, and the losses and skin effect created by internal eddy currents resulting from finite conductivity. The properties of magnetic materials can be varied through the addition of alloys and are also strongly influenced by the manner in which the finished material is prepared, especially any heat treatment employed.

Figure 2-3 illustrates the characteristic ***B-H*** curve and some related parameters. It is clear that the permeability as defined by Equation 2-8 is never constant. In fact, depending on the value of ***H***, μ may vary from being extremely small to extremely large. For each application then, appropriate approximations must be made for the permeability from a consideration of the relevant region of the ***B-H*** diagram. A number of specific definitions for μ have emerged, three of which are depicted below, but actual calculations are often carried out by working directly from the graphs.

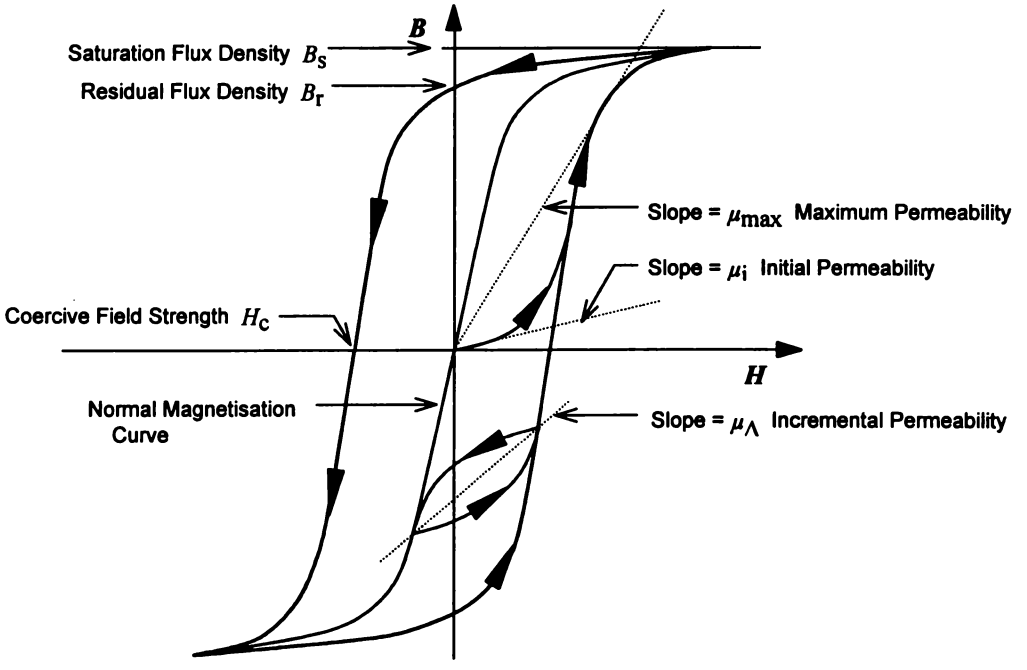

Figure 2-3 *General B-H Loop In Ferromagnetic Material*
[*Klontz, Novotny and Severns* 1997]

In spite of these disadvantages, the properties and even the non-idealities of magnetic materials have been exploited in many inventive ways, and a wide range of materials have

been developed with properties suited to specific applications. For example, the hysteresis loop is exploited by permanent magnets and recording devices.

Engineering magnetic materials are customarily divided into two categories: *soft* and *hard*. The names refer to the ease with which the level of magnetisation can be changed by an applied field, rather than the mechanical hardness. Soft magnetic materials can be easily magnetised and demagnetised - they have low values of coercive field strength and are used when the magnetisation must change with time, as in alternating current devices. Hard magnetic materials have high values of coercive field strength and resist changes in their magnetisation, making them suitable for permanent magnets.

Materials with magnetic properties between those of hard and soft materials find their principal application in magnetic recording, and may be termed *recording materials*.

Table 2-1 gives an indication of some of the properties of common magnetic materials.

Material	Composition	Saturation Flux Density, B_s (T)	Maximum Permeability, μ_r
Annealed Iron	100 % Fe	2.15	5 500
Silicon Steel	3 % Si, 97 % Fe	2.02	8 000
Permalloy	45 % Ni, 55 % Fe	1.60	50 000
Mumetal	5 % Cu, 2 % Cr, 77 % Ni, 16 % Fe	0.75	150 000
Permendur	50 % Co, 50 % Fe	2.40	6 000
Metglas	13.5 % B, 3.5 % Si, 2 % C, 81 % Fe	1.61	300 000
MnZn ferrite	$MnZnFe_2O_4$	0.45	5 500
NiZn ferrite	$NiZnFe_2O_4$	0.32	450
Iron Powder	Micrometals Type 26	1.38	230

Table 2-1 *Magnetic Material Properties*[10]

[10] Data from *American Institute of Physics Handbook* [*Gray* 1972], *Magnetics* [1991], *Micrometals* [1995], *Allied Signal* [1998] and *Philips* [1998].

2.1.3.1 Iron Alloys

The element with the highest saturation flux density at room temperature is iron, which is also low in cost and widely available. It is therefore natural that iron and iron-based alloys be the most commonly used soft magnetic materials. For direct current applications such as electromagnets for lifting scrap iron or for providing laboratory fields, solid iron parts may be used.

Devices to be operated at power frequencies are made of *laminations* punched from thin sheet. Laminations are used to reduce the magnitude of the circulating eddy currents induced by the changing magnetic flux. These eddy currents generate heat and reduce efficiency. The laminations are coated with insulating varnish to prevent eddy currents from flowing between laminations in a stack, and to prevent the stack from acting as a shorted turn which would result in very large eddy currents. Adjacent laminations will have a finite area between them, due to the varnish and warpage of the laminations. The permeability of this area is negligible compared to the magnetic material, and the effective cross sectional area of a laminated iron core is therefore reduced by a 'stacking factor'.

The most common alloying element in commercial iron is carbon, which is detrimental to soft magnetic properties, especially if a small coercive field strength is required. Magnetic iron therefore requires a low carbon content. The special low-carbon steel sheet for magnetic applications is known as *electrical steel.* It is often cold-rolled to increase strength and hardness during manufacturing and punching operations, and is then annealed to restore magnetic properties.

Improved magnetic properties may be obtained by adding alloying elements that increase the electrical resistivity of the steel and hence reduce eddy current losses. The usual choice is silicon which, while increasing resistivity, tends also to reduce the saturation flux density. The proportion of silicon typically ranges from 1 % to 3.25 %.

Silicon steel can be treated to produce a strong crystallographic texture, or preferred orientation, which gives the sheet strongly directional (anisotropic) properties. This *grain-oriented* steel is widely used for medium and small power transformer, with non-oriented grades of similar composition being used for large motors and generators. The sheet thickness for use at 50 to 60 Hz is generally around 0.5 mm. Ordinary electrical steel

(without silicon) is used for small motors and transformers, where efficiency is of less concern than cost.

In applications where a very high permeability is required, especially at frequencies higher than 60 Hz, the usual choice of core material is a nickel-iron alloy, often containing a small percentage of molybdenum to improve the mechanical and magnetic properties. These alloys have various commercial names but are generically known as *Permalloy*. Nickel alloys have low losses, but are very expensive and have a low saturation flux density and very small magnetic anisotropy. Nickel-iron alloys can be rolled to a thickness of less than 0.025 mm.

The cobalt alloys (such as *Permendur*) exhibit increased saturation flux density but suffer from high cost and losses. The usual composition includes about 50 % cobalt.

2.1.3.2 Amorphous Alloys

A relatively new class of materials for power frequencies is the amorphous metal alloys or metallic glasses, which comprise magnetic material in a non-crystalline state and are manufactured by a rapid solidification process. These alloys contain about 80 % magnetic elements such as iron, nickel or cobalt, with the balance comprising glasseous elements such as boron, silicon, phosphorous and carbon.

Amorphous alloys are non-crystalline and highly homogeneous, with high electrical resistivity and excellent soft magnetic properties. Their saturation flux density depends on the composition, with a maximum value of about two-thirds that of pure iron. The maximum thickness is about 0.025 mm, hence amorphous alloys are generally available only as tape wound cores. Amorphous alloys are more expensive than conventional sheet steels, but are useful where very low power losses are necessary, or where frequencies are up to several kilohertz. They also display extremely high peak permeabilities, for example Metglas 2714A which has a μ_{peak} of 10^6 [*Allied Signal* 1998].

2.1.3.3 Iron Powder

Powdered iron provides another important class of core materials, especially for inductors and RF applications. Powdered iron cores consist of magnetic particles mixed into an insulating binder, which creates the equivalent of a distributed air gap. The magnetic particles are typically molybdenum-nickel-iron (molypermalloy), nickel-iron or iron-aluminium-silicon. Powdered iron cores generally have a low but highly controlled relative permeability in the range of ten to a few hundred.

The binding material provides a high resistivity, hence powdered iron is suitable for high frequency applications up to the megahertz range. The saturation flux density is much greater than that of ferrites, and is more than half that of iron. Powdered iron cores can be easily produced in different shapes, and with their equivalent distributed air gap are suitable for conventional applications which require an air gap.

2.1.3.4 Ferrites

An important class of materials for higher frequency devices is the soft ferrites. Above 20 kHz, the eddy current losses in any continuous metallic material become prohibitive so that ferrites or iron powder cores must be used.

Ferrites are ceramic ferrimagnetic oxides, which are spinels of the general composition MFe_2O_4, and garnets $M_3Fe_5O_{12}$, where M represents a metal which is usually nickel, zinc or manganese. They offer low losses up to frequencies of 10 MHz, combined with high permeability and very high resistivity. Ferrites suffer from the disadvantages of having a low saturation flux density of about one-quarter that of iron, of being brittle, and of having a low thermal conductivity.

Ferrite parts are made by pressing the oxide powder into the desired shape and sintering at elevated temperature to bond the individual particles by solid-state diffusion. They are easily produced in a wide range of shapes, and a variety of grades exist to cover different frequency and power requirements. Ferrite is very often the only realistic choice for magnetic material for high frequency applications.

Because of their very high electrical resistivity, the losses in ferrites at typical operating frequencies are almost entirely due to hysteresis. As a result, the loss is linearly dependent on frequency and virtually independent of the waveform of the flux.

2.2 TRANSFORMER THEORY

2.2.1 FARADAY'S LAW

Faraday's Law governs the relationship between a voltage and the corresponding magnetic flux density. It is one of the Maxwell Equations, and is given in differential form in Equation 2-3. In its integral form, Faraday's Law is written

$$\oint_C \boldsymbol{E} \cdot d\ell = -\frac{\partial}{\partial t}\int_S \boldsymbol{B} \cdot \boldsymbol{da} \qquad \textit{Equation 2-18}$$

Let V be the induced voltage around the closed path C, for one turn of the transformer coil. Then for an N turn coil we have

$$V = -N\frac{\mathrm{d}}{\mathrm{d}t}\int_S \boldsymbol{B} \cdot \boldsymbol{da} \qquad \textit{Equation 2-19}$$

$$\Leftrightarrow \int V(t)\,\mathrm{d}t = -N\int_S \boldsymbol{B}(y,t) \cdot \boldsymbol{da} \qquad \textit{Equation 2-20}$$

where voltage V is a function of time and magnetic flux density $\boldsymbol{B}$ varies with time and position. In most practical situations, this can be simplified to the more familiar and useful form of

$$V = -N\frac{\mathrm{d}\Phi}{\mathrm{d}t} \qquad \textit{Equation 2-21}$$

where flux Φ is given by Equation 2-22. The voltage induced in the coil is therefore proportional to the rate of change of flux.

$$\Phi = BA \qquad \textit{Equation 2-22}$$

where area A is perpendicular to the magnetic flux density B. If the change in magnetic flux density is ΔB (usually known as the 'flux swing', or 'maximum working flux density'), Equation 2-21 can be written as

$$\int V\mathrm{d}t = -NA\Delta B \qquad \textit{Equation 2-23}$$

2.2.2 AMPERE'S LAW

Ampère's Law, another of the Maxwell Equations and given previously in Equation 2-4, describes the relationship between current and magnetic field strength. It is shown here in quasi-static integral form, that is the displacement current term is neglected.

$$\oint \boldsymbol{H} \cdot d\ell = I_t \qquad \textit{Equation 2-24}$$

I_t indicates the total current passing through a surface, so for a coil of N turns conducting a current I, $I_t = NI$. In order that line and surface integrals do not need to be evaluated to find the magnetic flux, we assume that the magnetic field H is constant in a given region, and is aligned in the direction of the path of integration. This assumption is usually valid for a uniform magnetic material, or over small distances in free space. Equation 2-24 then simplifies to the more useful form

$$H\ell = NI \qquad \textit{Equation 2-25}$$

where ℓ is the path length enclosing the current NI.

2.2.3 THE MAGNETIC CIRCUIT

When the flux due to a magnetic field is confined to a certain path, the concept of the *magnetic circuit* can be developed. From Equations 2-25 and 2-22, and remembering that $\boldsymbol{B} = \mu \boldsymbol{H}$ as given by Equation 2-8, we find that

$$\Phi \frac{\ell}{\mu A} = NI \qquad \textit{Equation 2-26}$$

where the quantity NI is known as the magnetomotive force (mmf) F_m, that is,

$$F_m = NI \qquad \textit{Equation 2-27}$$

The quantity $\frac{\ell}{\mu A}$ is a constant of the magnetic circuit of path ℓ, and is known as the reluctance, $\mathcal{R}$. Flux will tend to follow the lowest reluctance path in a circuit.

$$\mathcal{R} = \frac{\ell}{\mu A} \qquad \textit{Equation 2-28}$$

Reluctance is the reciprocal of permeance $\mathcal{P}$, that is,

$$\mathcal{R} = \frac{1}{\mathcal{P}} \qquad \textit{Equation 2-29}$$

Equation 2-26 is therefore a magnetic circuit analogue of Ohm's Law. Kirchhoff's laws also have corresponding magnetic circuit analogues. From Ampère's Law, we find that for a single loop magnetic circuit comprising many distinct series sections of reluctance,

$$F_m = \Phi \left(\mathcal{R}_1 + \mathcal{R}_2 + \ldots + \mathcal{R}_p \right) \qquad \textit{Equation 2-30}$$

or for a general magnetic circuit,

$$\sum_{i=1}^{q} F_{mi} = \sum_{i=1}^{p} \Phi \mathcal{R}_i \qquad \textit{Equation 2-31}$$

Similarly, if more than one flux path exists, Equation 2-2 states that the sum of the fluxes entering a magnetic node must be zero. Thus the magnetic analogue of Kirchhoff's current law is

$$\sum_{i=1}^{r} \Phi_i = 0 \qquad \textit{Equation 2-32}$$

Electric Quantity	SI Unit	Magnetic Quantity	SI Unit
Current I	[Ampère, A]	Magnetic flux Φ	[Weber, Wb]
Current density J	[A/m^2]	Magnetic flux density[11] B	[Tesla, T][12]
Conductivity σ	[S/m]	Permeability μ	[H/m]
Electromotive force[13] (emf) E	[Volt, V]	Magnetomotive force (mmf) F_m	[A][14]
Electric field strength E	[V/m]	Magnetic field strength[15] H	[A/m]
Conductance G	[Siemens, S]	Permeance[16] $\mathcal{P}$	[Henry, H]
Resistance R	[Ohm, Ω]	Reluctance[17] $\mathcal{R}$	[H^{-1}]

Table 2-2 *Circuit Analogues*

Table 2-2 presents the analogous quantities of magnetic and electric circuits. As electric circuit theory is well developed and understood, it is often helpful to think of magnetic circuits in terms of their electric circuit analogue. It is also possible to convert a magnetic

---

[11] Magnetic flux density is also known as *magnetic induction.*

[12] W/m^2 is also commonly used.

[13] The term emf strictly applies to a source of electrical energy, but is sometimes misused as being equivalent to potential difference or voltage.

[14] Ampere-turns [A·t] is often used as the mmf increases in proportion to the number of turns.

[15] Magnetic field strength is also known as *magnetising force.* An obsolete synonym is *magnetic intensity.* Although H is, by analogy with E, usually called the *magnetic field,* it must be remembered that the true mean field is really B. In this thesis, the term *magnetic field* is used in a general sense and does not distinguish between B and H.

[16] The preferred SI symbol for permeance is Λ, but this is seldom used in literature.

[17] It is unfortunate that the usual symbol for both electrical resistance and reluctance (magnetic resistance) is R. To avoid confusion, this thesis will use the symbol $\mathcal{R}$ for reluctance.

circuit to an electric circuit model, so that well-known electrical circuit analysis techniques may be applied.

By substituting Equation 2-26 into Equation 2-21, we have

$$V = -\mu \frac{N^2 A}{\ell} \frac{\mathrm{d}I}{\mathrm{d}t} \qquad \textit{Equation 2-33}$$

where the factor $\mu \frac{N^2 A}{\ell}$ is a geometric property of the magnetic circuit and is defined as the electrical quantity of inductance L, that is,

$$L = \mu \frac{N^2 A}{\ell} \qquad \textit{Equation 2-34}$$

$$\Rightarrow L = \frac{N^2}{\mathcal{R}} \qquad \textit{Equation 2-35}$$

Equations 2-33 and 2-21 therefore provide a direct link between the electric and magnetic circuits.

$$V = -N \frac{\mathrm{d}\Phi}{\mathrm{d}t} = -L \frac{\mathrm{d}I}{\mathrm{d}t} \qquad \textit{Equation 2-36}$$

or alternatively,

$$\Phi = \frac{LI}{N} \qquad \textit{Equation 2-37}$$

Inductance differs from quantities such as resistance in that it is not a physical property of a component, but is simply a factor defined for convenience. Inductance may also be used to define the energy U_{m} stored in a coil.

$$U_{\mathrm{m}} = \tfrac{1}{2} L I^2 \qquad \textit{Equation 2-38}$$

As discussed in Chapter 2.1.3, the relative permeability of most materials is almost unity, but magnetic materials provide the opportunity to guide or confine magnetic flux to a defined path.

Although magnetic circuits are analogous to electric circuits, the fact that flux is not always well confined to the magnetic material means that magnetic circuit problems are not as straightforward to analyse as the electric circuit analogy would suggest. The ratio of the permeability of iron to that of air may reach 10^6, but is typically of the order of 10^3, while the corresponding ratio of conductivities for electric circuits can be as high as 10^{20}.

The above equations assume that the magnetic circuit is well defined. When the path of the magnetic flux is not well defined (for example in a solenoid), the value of the inductance may be derived from field theory, flux plotting, experimentation, or solution of Maxwell's equations.

2.2.4 THE IDEAL TRANSFORMER

One of the most important magnetic circuit devices is the transformer, which enables a change in the level of voltage (and current) of an AC system with very little power loss, voltage drop or waveform distortion. Properly designed transformers are so nearly 'ideal', that in many applications a model which neglects the inevitable imperfections of the transformer may be adequate.

The basic structure of a two winding, shell type transformer is shown in Figure 2-4. It consists of a magnetic core with the two windings arranged so that, to as great an extent as possible, they link the same magnetic flux. In this shell type core, the mutual flux divides in two and returns through the outside legs of the core. The designations primary and secondary are arbitrary except that it is common to think of the winding connected to the power source as the primary winding.

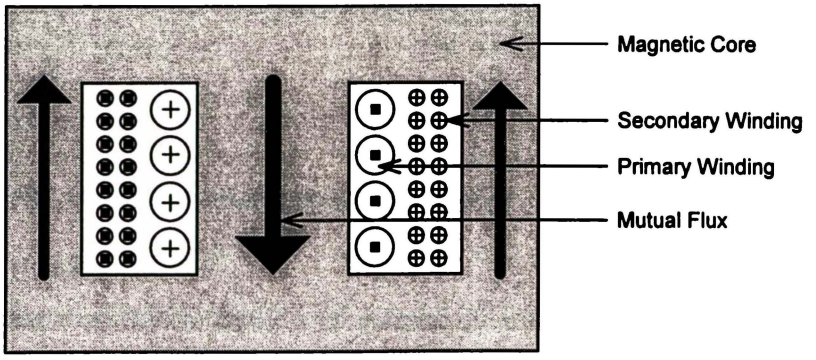

Figure 2-4 *Two Winding Shell Type Transformer*

[*Klontz, Novotny and Severns* 1997]

An ideal transformer assumes the following:

Assumption 1: that there is no coil resistance;

Assumption 2: that there is no leakage flux

(that is, all of the flux is confined to the core, and thus completely links both windings);

Assumption 3: that there is infinite permeability

(that is, the core does not require an mmf to support flux);

Assumption 4: that there are no core losses.

2.2.4.1 Operation

The physical representation, magnetic model and electrical circuit representation of an ideal two-winding transformer are shown in Figure 2-5. The primary is driven by a voltage source, and the secondary is terminated with a resistance. The magnetic model consists of an mmf source for each winding and a reluctance $\mathcal{R}_c = \frac{\ell_m}{\mu_c A_c}$ that models the properties of the core.

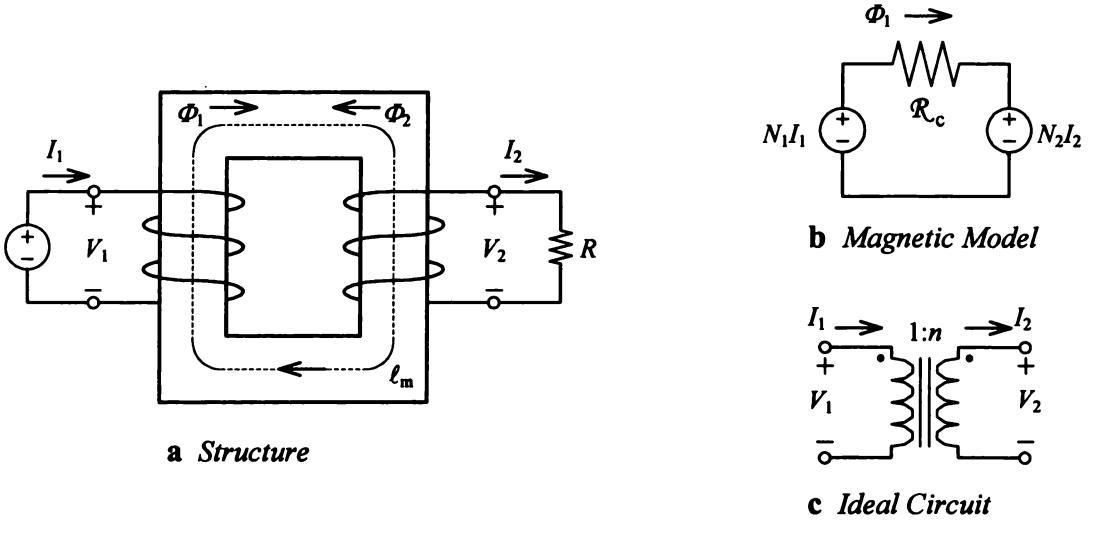

Figure 2-5 *Transformer Representation* [*Witulski* 1995]

When a voltage V_1 is applied to the primary for a length of time, a magnetic flux Φ_1 must be present in the core to satisfy Faraday's Law. The permeability μ_c of the core is high, which constrains the flux to the core, and by Assumption 2 all of the flux generated by the primary

winding also links the secondary winding. This time-varying flux Φ_1 induces a voltage V_2 in the secondary winding, according to Faraday's Law. Since the winding is terminated by a resistance R, current I_2 flows which by Ampère's Law must generate a magnetic field H_2, and hence by Equation 2-8, a flux density B_2 corresponding to a flux Φ_2, in a direction opposite to the flux Φ_1. This is shown in Figure 2-5a.

As I_2 induces the opposing flux Φ_2, I_1 increases by an equivalent amount to compensate, so that the total flux $\Phi = \Phi_1 - \Phi_2$ in the core remains constant. In the ideal transformer, the symmetry in the generation of the opposing flux suggests that Φ is equal to zero, although this does not follow directly from Assumption 3.

The opposing mmf source N_2I_2 must have a polarity opposite to N_1I_1 as shown in Figure 2-5b. The direction of the induced current is commonly expressed by Lenz's Law, which states that:

> *the direction of the induced current is always such that it produces a magnetic field that opposes the change in flux that produced it.*

Thus when Φ_1 increases, the induced current produces an opposing flux. If Φ_1 decreases, the induced current produces an aiding flux.

The voltage scaling relation of the transformer can be derived from Faraday's Law.

$$V_1 = -N_1 \frac{d\Phi}{dt}, \quad \text{and } V_2 = -N_2 \frac{d\Phi}{dt} \qquad \textit{Equation 2-39}$$

Since the same flux links both coils, the relationship between the primary and secondary voltage is

$$\frac{V_2}{V_1} = \frac{N_2}{N_1} = n \qquad \textit{Equation 2-40}$$

that is, the volts per turns is constant.

The current scaling relation can be found from Ampère's Law by summing the mmfs around the loop in the magnetic circuit model of Figure 2-5b:

$$N_1 I_1 - \Phi \mathcal{R}_c - N_2 I_2 = 0 \qquad \textit{Equation 2-41}$$

For an ideal transformer, Assumption 3 states that the core permeability is infinite, hence by Equation 2-28, $\mathcal{R}_c$ is zero. The current scaling relation is therefore

$$\frac{I_2}{I_1} = \frac{N_1}{N_2} = \frac{1}{n} \qquad \textit{Equation 2-42}$$

The voltage scaling ratio is a result of Faraday's Law, while the current scaling ratio is a result of Ampère's Law. Equations 2-40 and 2-42 illustrate conservation of energy, that is, the input power is equal to the output power. There is no energy storage in an ideal transformer.

Equations 2-40 and 2-42 can also be used to derive an impedance transformation relationship.

$$Z_1 = \frac{V_1}{I_1} = \frac{\frac{N_1}{N_2} V_2}{\frac{N_2}{N_1} I_2} = \left(\frac{N_1}{N_2}\right)^2 Z_2 \qquad \textit{Equation 2-43}$$

Impedances are thus transformed by the square of the turns ratio, when viewed on the opposite side of a transformer. This property is often used in situations where 'impedance matching' is desired, and is also the basis for analytically manipulating circuits containing transformers, by reflecting an equivalent component across the transformer in order to reduce circuit complexity.

2.2.4.2 Coil Polarity

The voltage polarity relationship of windings relative to each other is usually indicated by the 'dot notation'. The following rules are used to determine this relationship:

1. voltages induced in any two windings due to changes in mutual flux will have the same polarity at dot-marked terminals;

2. mmfs produced in the two windings will have additive polarity if positive currents flow into the dot-marked terminals;

3. the voltage induced in an open winding will be positive at the dot-marked terminal, if the current flowing into the dot-marked terminal of the other winding has a positive rate of change.

2.2.5 THE REAL TRANSFORMER

In many applications, a transformer's performance may be very nearly ideal. However, parasitic elements which cause the operation of the transformer to deviate from that of an ideal component are unavoidable, especially when the transformer operates near its limits. Non-ideal effects may also be tolerated for size, cost or other design related reasons. When any of the four assumptions made in Section 2.2.4 are not valid, their effect can be taken into consideration as discussed in the following sections.

2.2.5.1 Coil Resistance

While the resistive losses of the coils can be kept small by choosing a wire size appropriate to the coil current and frequency, resistance will always be present. The *IR* drop at full current is typically less than 2 % of the rated voltage, and is often significantly less than this in large transformers. Winding resistance may be incorporated into an electrical circuit model by simply connecting the appropriately valued resistor in series with the coil of the ideal transformer.

A direct current flowing in a uniform conductor will distribute itself uniformly over the cross-section of the conductor,[18] and the resistance of the coil is termed the DC resistance, R_{dc}. Alternating current has a tendency to concentrate at the surface of the conductor, which effectively increases the resistance to an AC value, R_{ac}. This effect becomes more pronounced as the frequency and conductor size increase, and is due to both copper skin effect and proximity effect [*Petkov* 1996]. Proximity effect is due to eddy currents induced in a conductor by the currents flowing in an adjacent conductor. The shape of the current waveform can have a significant impact on the AC resistance.

An alternating electric field decays exponentially with depth into the conductor. The skin depth δ, given by Equation 2-44, is defined as the distance at which the field has decayed to 1/e of the field at the surface. A critical frequency f_c is defined as the frequency at which the penetration is half the diameter of the conductor; for frequencies above f_c the resistance begins to increase as the effective area of the conductor decreases.

$$\delta = \sqrt{\frac{2}{\omega\sigma\mu}} \qquad \textit{Equation 2-44}$$

$$f_c = \frac{4}{\pi\sigma\mu d^2} \qquad \textit{Equation 2-45}$$

where d = diameter of the conductor

The skin depth and cut-off frequency for copper wire is

$$\delta = 66\times10^{-3}\frac{1}{\sqrt{f}} \qquad \textit{Equation 2-46}$$

$$f_c = 17\times10^{-3}\frac{1}{d^2} \qquad \textit{Equation 2-47}$$

[18] High currents through a plasma will tend to constrict themselves laterally by what is known as the *pinch effect*. The basic mechanism causing the pinch is the interaction of a current with its own magnetic field.

It is often convenient to combine all of the coil resistances into a single equivalent resistance placed on one side of the transformer, by using the impedance transformation relation, Equation 2-43. Reflecting to the side of winding one gives

$$R_{eq,1} = R_1 + \left(\frac{N_1}{N_2}\right)^2 R_2 \qquad \textit{Equation 2-48}$$

where all terms are defined in Figure 2-6.

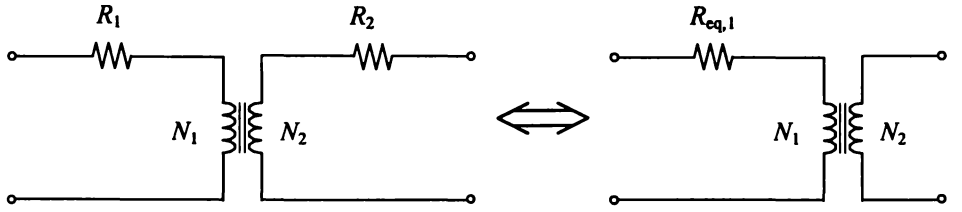

Figure 2-6 *Equivalent Winding Resistance*

2.2.5.2 Leakage Flux

Magnetic flux is never completely confined to the magnetic core material, so the assumption that all of the flux links every winding will never be completely true. Conceptually, the flux can be divided into mutual flux linking both windings, and leakage flux which links only one winding. The ideal transformer relations then apply to the mutual flux, with the leakage flux treated as a parasitic element. The voltage associated with the leakage flux reduces the effective input voltage, in a fashion similar to the *IR* drop.

This leakage flux is represented in the circuit by a series inductance on each side of the transformer [*Witulski* 1995]. As with coil resistance, it is convenient to combine all of the leakage inductance into an equivalent value on one side of the transformer.

Reflecting to the side of winding one gives

$$L_{eq,1} = L_1 + \left(\frac{N_1}{N_2}\right)^2 L_2 \qquad \textit{Equation 2-49}$$

where all terms are defined in Figure 2-7.

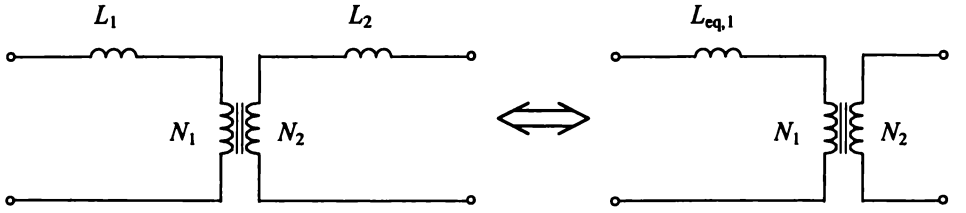

Figure 2-7 *Equivalent Leakage Flux*

2.2.5.3 Finite Core Permeability

If the transformer has finite permeability, $\mathcal{R}_c$ in Equation 2-41 is not equal to zero and we have

$$\Phi = \frac{N_1}{\mathcal{R}_c} I_1 - \frac{N_2}{\mathcal{R}_c} I_2 \qquad \textit{Equation 2-50}$$

By Faraday's Law then, the primary voltage is given by

$$\begin{aligned} V_1 &= -N_1 \frac{d\Phi}{dt} \\ &= -\frac{N_1^2}{R_c} \frac{d}{dt}\left(I_1 - \frac{N_2}{N_1} I_2\right) \end{aligned}$$

$$\therefore V_1 = -L_m \frac{dI_m}{dt} \qquad \textit{Equation 2-51}$$

where

$$L_m = \frac{N_1^2}{\mathcal{R}_c} \qquad \textit{Equation 2-52}$$

is known as the magnetising inductance, and I_m the magnetising current.[19] The voltage scaling law (Equation 2-40) is still valid, but with a finite permeability, the currents are no longer related by Equation 2-42. The magnetising current I_m models the energy required to 'magnetise' the core. Most transformers are designed for a low magnetising current by using a high permeability core with the minimum possible air gap.

2.2.5.4 Core Loss

The losses created within the magnetic material as a result of AC magnetic fields are of two types:

1. *Eddy Current Loss* - ohmic losses, created by currents circulating in the material as a result of Faraday Law induced voltages;

2. *Hysteresis Loss* - irreversible internal losses associated with the repeated cycling of the hysteresis loop.

These losses are difficult to accurately calculate and represent, and in practice are often estimated from measured core loss curves provided by the manufacturer. The usual representation comprises an equivalent core loss resistance R_c in parallel with the magnetising inductance L_m [*Glasoe and Lebacqz* 1948, *Klontz, Novotny and Severns* 1997]. This representation is strictly valid only for constant permeability and for eddy current losses, but is used as an approximation in more realistic situations where the permeability is variable, and where the core loss includes hysteresis loss.

Various references provide approximate formulae for calculating the core loss [*Engelmann* 1985, *Glasoe and Lebacqz* 1948, *Grossner* 1967], but these are very specific to individual applications and cannot be considered to be generally valid.

---

[19] I_m is sometimes referred to as the *exciting current.*

Eddy Current Loss

The eddy currents induced in magnetic material by an alternating external magnetic field result in an ohmic loss, which is proportional to the amount of current flowing and is dependent on the waveform. Eddy currents are discussed in more detail in Section 2.2.5.8.

Eddy currents may be controlled by subdividing the core into thin laminations. To be effective, the lamination thickness must be significantly smaller than the magnetic skin depth given by Equation 2-54. Above 20 kHz, the required lamination thickness is too small to be practical, so at these higher frequencies, powdered iron cores and ferrites are used because of their high internal resistance.

Hysteresis Loss

Hysteresis loss is a material dependent loss associated with the 'memory' possessed to some extent by all magnetic materials. As shown by the upper regions of the curve in Figure 2-3, the value of magnetic flux density $\boldsymbol{B}$ as $\boldsymbol{H}$ decreases is greater than as $\boldsymbol{H}$ increases; an effect which reverses in the lower regions of the curve. There is therefore a phase difference between voltage and current, and hence a power loss associated with the presence of hysteresis.

The hysteresis loss can be quantified by considering the electrical energy delivered to a coil in a magnetic circuit. By integrating this energy [*Glasoe and Lebacqz* 1948 pp. 626-629] it can be shown that there is an energy loss per unit volume equal to the area of the hysteresis loop, for each occasion the loop is traversed. The hysteresis loss is dissipated within the core material and is directly associated with the friction encountered by moving ferromagnetic domain walls, as discussed in Section 2.1.2.4.

Unlike eddy current loss, for a given $\boldsymbol{B}$-$\boldsymbol{H}$ loop amplitude the hysteresis loss is independent of the waveform, provided minor loops are not traversed.

2.2.5.5 Parasitic Capacitance

At high frequencies, the capacitances associated with the windings of a transformer can become significant and substantially modify the transformer's performance. Capacitance has an effect to some degree between any points of the transformer with a potential difference. Inter-layer and inter-winding capacitances usually dominate, although the structure and function of the transformer may cause the parasitic capacitance between other points to become significant. The equivalent model of Figure 2-8 shows a primary winding capacitance C_1, a secondary winding capacitance C_2 and an inter-winding capacitance C_{12}, which are the dominant parasitic capacitances for pulse transformers [*Glasoe and Lebacqz* 1948 pp. 507 - 508].

A lumped parameter equivalent model is useful for showing the effect of the capacitance on the transformer's performance. The electric field gradient is, however, distributed continuously, so the real situation is enormously complex and must be greatly simplified in order to be useful. In most applications, the simplifications have little detrimental effect on a model's accuracy.

2.2.5.6 Equivalent Circuit

Combining all of the non-ideal concepts discussed above yields the generally accepted transformer equivalent circuit (the classical π model) shown below.[20]

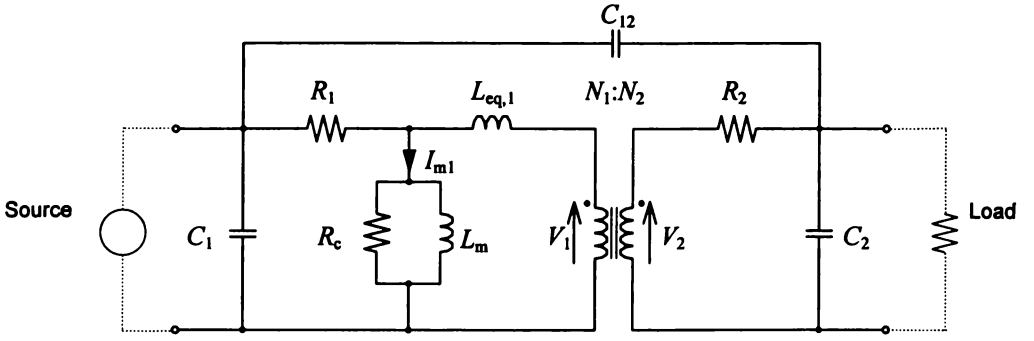

Figure 2-8 *Transformer Equivalent Circuit*

[*Klontz, Novotny and Severns* 1997]

2.2.5.7 Air Gaps

Many transformers have air gaps inherent in the construction of the core. Since the permeability of the core is typically several thousand times that of air, the reluctance of even a short gap is usually large compared to that of the rest of the circuit. The air gap can be added in series with the magnetic circuit as an additional reluctance with a permeability of μ_0. Alternatively, an effective permeability for the complete circuit can be calculated [*Harrison* 1992] by

$$\frac{1}{\mu_e} = \frac{1}{\mu_c} + \frac{\ell_g}{\ell_c \mu_0} \qquad \textit{Equation 2-53}$$

---

[20] This equivalent circuit uses general notation by designating the windings '1' and '2'. The terms primary and secondary are commonly used, but only derive meaning from the circuit to which the transformer is connected, in which case the coil connected to the source is termed the primary, and that connected to the load termed the secondary.
As the windings of an output transformer are usually referred to as primary and secondary, in cases where a circuit is related to an application in this thesis the subscripts 'p' for primary and 's' for secondary will be used.

where μ_e = effective core permeability

μ_c = permeability of core material

ℓ_c = magnetic path length of core material

ℓ_g = air gap length

In practice, flux spreads out when crossing this gap, as illustrated in Figure 2-9, making accurate analysis difficult. Approximate correction factors are sometimes used to estimate an increased effective gap area to account for this fringing [*Klontz, Novotny and Severns* 1997 §1.11]. These correction factors can give reasonable results provided the gap is small compared to the dimensions of the core faces.

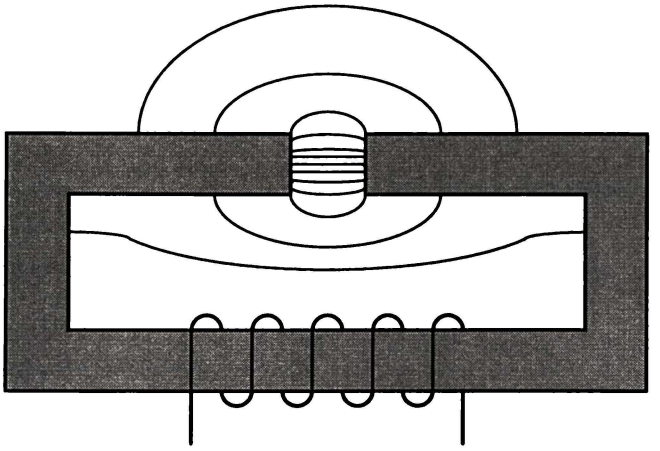

Figure 2-9 *Air Gap Fringing Flux* [*Klontz, Novotny and Severns* 1997]

2.2.5.8 Eddy Currents

An alternating external magnetic field will induce a variable electric field in the core material, as required by Faraday's Law. Localised differences in voltage combined with a finite material resistance will result in small circulating currents known as eddy currents. At high frequencies, these eddy currents may be great enough to limit the depth to which the flux penetrates. This phenomenon is known as *eddy current shielding* or *magnetic skin effect*, and is analogous to copper skin effect as will be seen by comparing the relevant equations.

Magnetic skin effect occurs at much lower frequencies than does copper skin effect, and even at mains frequencies needs to be controlled either by reducing the depth to which the flux must penetrate (for example, by using thin laminations), or by increasing the resistivity of the core (such as by choosing iron powder or ferrites cores).

For alternating fields, the magnitude of the field decays exponentially with distance penetrated into the core. The skin depth δ is defined as the distance at which the field has decayed to 1/e of the external field, and is given by Equation 2-54. There is a critical frequency f_c, at which the penetration is half the thickness of the core or lamination, given by

$$\delta = \sqrt{\frac{2}{\omega\sigma\mu}} \qquad \textit{Equation 2-54}$$

$$f_c = \frac{4}{\pi\sigma\mu d^2} \qquad \textit{Equation 2-55}$$

where d = thickness of the lamination

For transient fields, the eddy currents induced in the core limit the penetration depth as a function of time. For very short times, the effective frequency is very high therefore the penetration depth is very small. As time increases, the field is able to penetrate further into the core. This effectively means that the magnetic field requires a finite amount of time to fully penetrate and magnetise the core. This *pulse magnetisation* is discussed in detail in Chapter 3.

2.2.6 CORE SIZE

In a practical design situation, Faraday's Law is applied to solve for the number of turns. As shown by Equation 2-23, the area of the transformer core is required in order to calculate the number of turns. The difficulty then is in choosing the core size and geometry, and this decision is usually based on design experience.

The optimum core loss to copper loss ratio is a function of the magnetic material. For most ferrites, this ratio is around 0.8 [*Petkov* 1996], while for ferromagnetic material it is

typically 1 (that is, the greatest efficiency will be achieved when core loss and copper loss are equal [*Shepherd, Morton and Spence* 1970]). The core volume is commonly found by relating the throughput power to the maximum allowable temperature rise. For common applications, graphs and formulae exist for current density, core loss, thermal design, and the many application specific constants that are required.

Equation 2-56 is a typical transformer design equation [*Severns* 1996]. The large number of empirical factors illustrates how this type of design formula is useful only where the application has been widely researched and engineers have gained a wealth of design experience.

$$\text{Core Volume} = K_v \left[\frac{P_a}{K_f K_{cu} K_j f B_m} \right]^x \qquad \textit{Equation 2-56}$$

where P_a = 2VA = $E_1 I_1 + E_2 I_2$ = apparent power

B_m = maximum flux density

K_v = core shape factor

K_f = waveform factor

K_{cu} = copper utilisation factor

K_j = temperature rise factor

x = core shape factor (different to K_v)

2.2.7 AC Excitation

When the excitation in a magnetic system is a sinusoidal alternating current, two important effects occur which are absent in DC systems:

1. there is an induced voltage given by Faraday's Law (Equation 2-18) in all circuits linked by the magnetic flux;

2. losses occur within the material of the magnetic core.

The Faraday Law induced voltages are the *raison d'être* of most magnetic systems, as they are the basis of operation for all AC devices including transformers, motors and generators. They are also the cause of eddy currents, a major loss component, and one of the challenges

of magnetic design is to retain the desired Faraday Law induced voltages while suppressing the undesired parasitic voltage and associated loss producing eddy currents.

Faraday's Law in integral form is

$$\oint_C \boldsymbol{E} \cdot \boldsymbol{dl} = -\frac{\partial}{\partial t}\int_S \boldsymbol{B} \cdot \boldsymbol{da} \qquad \textit{Equation 2-57}$$

In AC transformer design, $\oint_C \boldsymbol{E} \cdot \boldsymbol{dl}$ is usually replaced by V_{rms}, the rms voltage applied to the coil, and $\int_S \boldsymbol{B} \cdot \boldsymbol{da}$ by Φ_{rms}, the rms value of the mutual flux. The negative sign is meaningless in AC systems, and with taking into account multiple turns, we have the simplified form of Faraday's Law given in Equation 2-21.

$$V_{rms} = N\frac{d\Phi_{rms}}{dt} \qquad \textit{Equation 2-58}$$

This provides a direct relationship between the total coil voltage and the flux through the coil. The concept of a direct relationship between voltage and flux in AC magnetic systems is an important basic principle used in design. The flux level can be established by selecting voltage, turns, and frequency. The necessary current will follow from the flux and magnetic circuit reluctance.

In the case of sinusoidal flux variation, $\Phi_{rms} = \Phi_{peak}\sin\omega t$, and the resulting sinusoidal voltage from Equation 2-58 is $V_{rms} = \omega N\Phi_{peak}\cos\omega t$. In terms of rms voltage

$$V_{rms} = \frac{\omega N\Phi_{peak}}{\sqrt{2}}$$
$$= \frac{2\pi}{\sqrt{2}} fN\Phi_{peak}$$

$$\Rightarrow V_{rms} = 4.44fN\Phi_{peak} \qquad \textit{Equation 2-59}$$

In most magnetic systems, the objective is to constrain the flux to a well defined path, hence the flux can be readily obtained from the transformer's geometry by finding the core area

and assigning a peak flux density. If A_c is the core area and B_m the chosen peak flux density, then $\Phi_{peak} = B_m A_c$ and Faraday's Law becomes

$$V_{rms} = 4.44 f N A_c B_m \qquad \textit{Equation 2-60}$$

This is an important design equation for sinusoidal AC systems. For a known core area, this equation allows the selection of the turns required for a specific maximum flux density B_m.

2.2.8 AUTOWOUND CONFIGURATION

Transformers are often used to conductively decouple (that is, provide electrical isolation in) a circuit. If this is not a requirement, an autowound arrangement can be used in which the primary and secondary are connected and have part of the coil in common. This results in a size reduction, especially when the required change in voltage level is small, because a portion of the power is conductively transferred.

2.3 FENCE THEORY

The optimum design of fence energisers requires a full understanding of the behaviour of the fence [*Brockelsby et. al.* 1977]. This presents an interesting challenge as the variation in fence conditions is almost endless - ranging from short, well-insulated fences such as those on security installations, to poorly maintained farm fences with multiple branches, vegetation leakage and poor connections.

A number of factors need to be considered when investigating the optimum output pulse: the fence characteristics; the propagation of the pulse; the effectiveness of the shock; and electric fencing safety requirements. An animal would need to receive an energy of at least 100 mJ for the fence to be considered an effective barrier, and a minimum voltage of 3 kV is required for the pulse to travel across poor connections and break down the contact resistance of an animal touching the fence [*Hancock* 1991].

Because of the wide range of operating conditions, there is no single ideal design for a fence pulse, but the following three guidelines will best satisfy the effective shock criteria everywhere along the fence [*Hancock* 1991]:

1. the pulse should have the highest possible peak voltage, consistent with safety and isolation considerations;

2. the pulse should comprise the lowest possible frequencies;

3. the pulse should have the highest possible energy, consistent with safety considerations.

In practice, the minimum voltage criteria will usually fail before the minimum energy criteria. For a pulse of fixed energy it is therefore preferable to design first for the maximum practical voltage, before considering the frequency spectrum or the pulse shape.

2.4 SHOCK THEORY

The magnitude of the current, rather than the voltage, determines the severity of an electric shock. Previous research into the effects of electric shock on humans and animals has concentrated on AC and DC current. *Barnes* [1989] presents Table 2-3 showing the effect of electric current on a man.

Current, I (mA)			Effect
AC - 50 Hz	DC	AC - 10 kHz	
0 - 1	0 - 5	0 - 9	No sensation
1 - 8	6 - 55	10 - 55	Mild shock
9 - 15	60 - 80	60 - 80	Painful shock
16 - 20	80 - 100		Some loss of muscular control
20 - 45	100 - 350		Severe shock and loss of muscular control
50 - 100	400 - 800		Possible heart failure (ventricular fibrillation)
> 100	> 800		Usually fatal

Table 2-3 *Effects Of Electric Current* [*Barnes* 1989]

Hancock [1991] extends this work to pulsed currents, and concludes that for an electric fence pulse to be regarded as effective, a shock energy of 100 mJ is required. However, there has been insufficient research into this subject to clearly understand fence pulse effectiveness.

The resistance of a current path through the body has a significant impact on the shock energy, and research has been carried out by *Biegelmeier* [1987], *Hultgren* [1989] and *Hancock* [1991] to determine the impedance of humans and animals. Contact resistance, which may vary widely, greatly influences this figure. For example, a dog with large soft paws sniffing a fence wire with a wet nose will present considerably less contact resistance than a sheep with overgrown toenails scratching its thick woollen rump against the fence. The type of electrical stimulation, and the current path through the body, also influences the impedance.

Contact resistance may initially be high, but may be reduced by two modes. The dielectric resistance between the fence and the animal may be broken down by high voltage, or a capacitive short circuit may be created at high frequencies. Both of these modes are present in the normal high-voltage short-duration energiser pulse.

Once the contact resistance is broken down, the internal resistance of a body is relatively low. The work by *Hancock* [1991], which focused on electric fence pulses, gives a figure of 885 Ω (with a standard deviation of 105 Ω) for human hand-to-hand impedance in contact with electric fence wires. As fence, contact, and ground conditions can vary enormously, this figure is valid only under the conditions specified. For a full discussion of body impedance and results under various conditions, refer to *Hancock* [1991].

Electric currents cause two distinct physiological effects: stimulation of the nerve endings (often felt as a tingling sensation), which may induce a muscle contraction; and stimulation of the muscle fibres, which directly causes an involuntary muscle contraction. *Hancock* [1991] chooses the level for an effective shock as being that at which involuntary muscle contraction begins.

The degree of response depends on the strength and duration of the exciting stimulus. A nerve fibre stimulated by an pulsed current of 0.02 ms to 1 ms duration will immediately reach the critical excitatory level and induce a muscle contraction. The muscle fibre

requires much higher intensities at this duration to be directly stimulated. Recovery of a nerve or muscle fibre normally takes 10 ms, during which time the fibre cannot be stimulated [*Wadsworth and Chanmugam* 1988].

Fence pulses often include considerable underswing, which does not contribute to the shock energy as the muscles have had insufficient time to recover from the primary voltage peak.

Strict safety Standards apply to electric fence energisers, to ensure that the likelihood of injury caused directly by an electric fence is very small. Ventricular fibrillation is the primary concern, and is the principal criteria by which the Standards limit energy and output pulse width. If the pulse repetition rate is less than the recovery period of a nerve or muscle fibre, a contracted muscle will not release, and so Standards also require that the pulse repetition rate is sufficiently low to allow ample time to "let go".

Chapter Three PULSE MAGNETISATION

In the first half of this century, the growth of electronics in areas such as power distribution, communications, and radar led to great advances in the understanding and design of transformers. Pulse transformers were investigated for their applications in radar and the production of high magnetic fields, and even today the volumes published by *Glasoe and Lebacqz* [1948] and *Früngel* [1965, 1976] provide the best theoretical understanding of transformer behaviour in these applications.

This theory was based on the requirements of pulse transformers used in WWII radar equipment, and the designs produced were so successful that in the last 50 years there has been little effort and, in fact, little need to advance this theory. The electric fence output transformer is a new application for which the original assumptions made when developing radar transformers are, in many cases, not valid. A design may be found to work acceptably, but an incomplete theoretical basis makes it difficult to improve or change the design.

This chapter seeks to address a gap in the understanding of *pulse magnetisation* - the time dependent penetration of the magnetic field into the core - which is a significant factor in the operation of output transformers. Starting from Maxwell's Equations, the theory is developed along similar lines to Bostick's work on radar pulse transformers [*Glasoe and Lebacqz* 1948], but is derived specifically for the electric fencing application. Any necessary simplifying assumptions will be recognised and fully discussed, and chosen to be appropriate for this application.

3.1 SIMPLIFYING ASSUMPTIONS

The simplifying assumptions which are required for the derivation of an equation for $\boldsymbol{B}(y,t)$ will be stated explicitly, so that the conditions under which this theory is valid are clear from the outset.[1] The output transformer commonly comprises a full E-I core of 0.5 mm silicon steel laminations.[2] The laminations are oriented as shown in Figure 3-1.

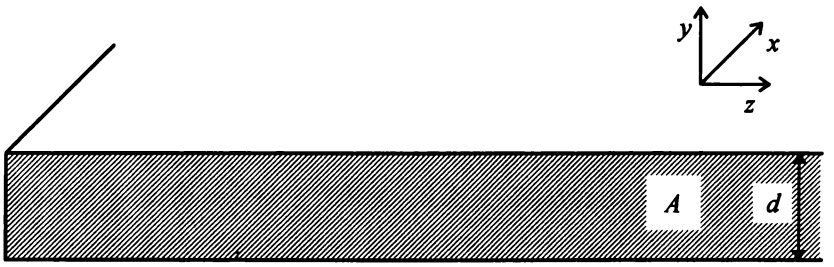

Figure 3-1 *Co-Ordinate Axes Of Lamination*

Assumption 1: Area A is equal to the net cross sectional area of the magnetic core perpendicular to the magnetic flux density $\boldsymbol{B}$.

- The core occupies all of the area enclosed by the coil (that is, the area required by bobbins and insulation can be neglected).
  Section 3.1.3 provides a justification for this assumption.
- Effective permeability μ_e is large enough to constrain all of the magnetic flux to the core.
  Although current designs frequently exhibit saturation under typical operating conditions, the relative permeability under what is commonly referred to as saturation can still be of the order of 1000. Thus, although the permeability may be low, it is still assumed to be significantly greater than that of air.[3]

---

[1] These assumptions are common for transformer design. *Glasoe and Lebacqz* [1948 pp. 617 - 618] make all of these assumptions in their analysis of pulse magnetisation.

[2] Figure 5-1 provides full specifications for this transformer.

[3] The point of saturation is far from precise for most materials (as is clearly shown by Figure 5-1d). Accordingly, when specific cores are examined in this thesis, the assumption of saturation occurring at a particular magnetic field strength $\boldsymbol{H}_s$ is avoided wherever possible.

Assumption 2: Magnetic flux density, $\boldsymbol{B} = B_z(y,t)$.

- The magnetic flux density $\boldsymbol{B}$ impressed at the surface of the core does not vary along its length, and is everywhere parallel to the centre-line of the lamination.
- The magnetic field does not vary in the x or z directions.
- Current flowing in the coil produces a magnetic field in the z direction only.

This assumption follows from the geometry of the transformer, and is illustrated in Figure 3-2.

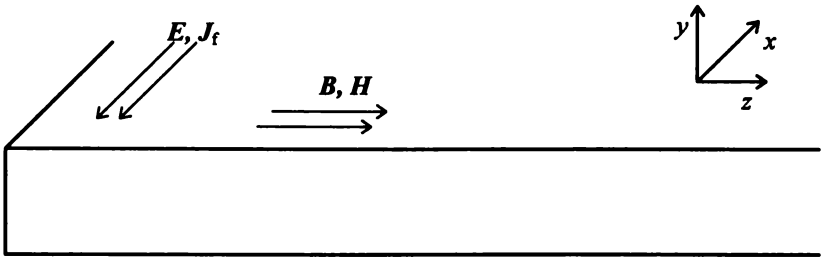

Figure 3-2 *Field Directions In Laminations*

Assumption 3: The width of the lamination (in the x direction) is much greater than the thickness d (in the y direction).

This assumption follows from the geometry of the laminations.

Assumption 4: The entire core can be represented as if it were comprised of a single long flat strip of iron.

- A stack of laminations exhibits the same behaviour as a single lamination.

Equation 3-13 shows that there is no time delay associated with establishing a magnetic field in air, since $\mu\sigma \sim 0$. For this reason, we can assume that the magnetic field created by the coil appears immediately at the surface of all laminations, regardless of whether the core consists of a single lamination or a stack of many laminations.

Assumption 5: Permeability μ_c of the core material is constant.

This assumption restricts the range of magnetic flux density through which the core is to be operated, and is commonly used in transformer design to allow the inductance to be calculated.

Assumption 6: Conduction currents are much larger than displacement currents.

- $\frac{\partial D}{\partial t}$ is therefore insignificant and may be neglected.

3.1.1 DISPLACEMENT CURRENT

Assumption 6 is valid for conductors as demonstrated by the following reasoning.[4] From Maxwell's Equations for non-homogeneous, non-linear and non-isotropic media

$$\nabla \times \boldsymbol{H} = \boldsymbol{J}_f + \frac{\partial \boldsymbol{D}}{\partial t} \qquad \textit{Equation 3-1}$$

where $\frac{\partial \boldsymbol{D}}{\partial t}$ = displacement current density

$\boldsymbol{J}_f$ = conduction current density

In a linear and isotropic medium, we can write that $\boldsymbol{D} = \varepsilon \boldsymbol{E}$ which gives

$$\nabla \times \boldsymbol{H} = \boldsymbol{J}_f + \varepsilon \frac{\partial \boldsymbol{E}}{\partial t} \qquad \textit{Equation 3-2}$$

In a conductor obeying Ohm's Law, $\boldsymbol{J}_f = \sigma \boldsymbol{E}$ and Equation 3-2 can be written as

$$\nabla \times \boldsymbol{H} = \boldsymbol{J}_f + \frac{\varepsilon}{\sigma} \frac{\partial \boldsymbol{J}_f}{\partial t}$$

$$\approx \boldsymbol{J}_f \left(1 + \frac{\varepsilon}{\sigma \tau}\right) \qquad \textit{Equation 3-3}$$

for changes over a time τ. The smallest time scale for a change of current in the electric fence output pulse application is estimated to be 10^{-6} seconds. The conductivity of a good

[4] See also *Lorrain and Corson* [1970 p. 439].

conductor is of the order of 10^7 S/m, and relative permittivity is approximately 1. Therefore, $\frac{\varepsilon}{\sigma\tau} \approx \frac{10^{-11}}{10^7 \cdot 10^{-6}} = 10^{-12}$, which is insignificant in comparison with 1.[5] Hence Equation 3-3, neglecting the displacement current, can be written as

$$\nabla \times H \approx J_f \qquad \textit{Equation 3-4}$$

3.1.2 MAGNETIC FIELD STRENGTH, *H*

Since from Assumption 2 it follows that the magnetic field strength H is parallel to the lamination, and considering that the magnetic field strength is continuous across a boundary, we can write that $\frac{B_{ext}}{\mu_{r,ext}} = \mu_0 H_{ext} = \mu_0 H_{int} = \frac{B_{int}}{\mu_{r,int}}$, where the subscript 'ext' refers to the magnetic field external to the core, and the subscript 'int' refers to the magnetic field internal to the core. The value of relative permeability varies discontinuously between the magnetic core and air, so the value of the magnetic flux density B must also be discontinuous across this boundary.[6]

The derivation given here evaluates the magnetic flux density within the lamination, in relation to the external magnetic flux density at the boundary of the core material. The magnetic field strength appears instantly at the boundary as a result of the current flowing in the transformer coil from the capacitive discharge.[7]

---

[5] For a typical MnZi ferrite, $\frac{\varepsilon}{\sigma\tau} \approx 3.5$ and Assumption 6 is therefore invalid. Ferrite materials instead require a solution to the *Wave Equation*. This investigation of pulse magnetisation is therefore only applicable to ferromagnetic materials. Ferrite cores are not used in the high power output pulse transformers investigated in this thesis.

[6] This is illustrated in Figure 3-7.

[7] In *Glasoe and Lebacqz* [1948], the average magnetic field strength across the lamination is assumed to increase linearly with time. This implies that a constant voltage is applied to the coil. The assumption made in this thesis, that the magnetic field strength is constrained at the boundary to the external value, would seem to better match a capacitive discharge pulse application than that used in *Glasoe and Lebacqz* [1948].

3.1.3 EFFECTIVE CORE AREA

When voltage is applied to a coil, a magnetic field is essentially created instantly at the surface of the laminations and diffuses inwards with time. In this thesis, we assume that the magnetic field is quickly driven into the lamination, so that the magnetic flux is constrained to the core and dominates Faraday's Equation. The validity of this assumption can be shown by considering a simplified situation.

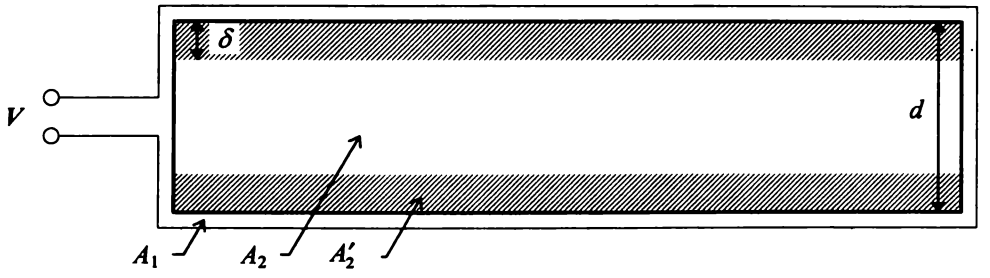

A_1 = area enclosed by coil outside laminations (coil area less lamination area)
A_2 = area of laminations (of width d)
A_2' = effective core area (of width 2δ)

Figure 3-3 *Simplified Transformer Core*

By assuming a constant coil voltage V and a magnetic flux density $\boldsymbol{B}$, Faraday's Law (Equation 2-18) becomes

$$V = -\frac{\mathrm{d}}{\mathrm{d}t}\int \boldsymbol{B}\mathrm{d}A$$

$$\approx -\frac{\mathrm{d}}{\mathrm{d}t}\boldsymbol{B}_1 A_1 - \frac{\mathrm{d}}{\mathrm{d}t}\boldsymbol{B}_2 A_2' \qquad \textit{Equation 3-5}$$

Initially, and for a short time after V is applied, $A_2' \approx 0$, and thus the core is not effective. Hence

$$V = -\frac{\mathrm{d}}{\mathrm{d}t}\boldsymbol{B}_1 A_1 \qquad \text{where } \boldsymbol{B} = \mu_0 \boldsymbol{H} \text{ as } \mu_r \text{ is effectively 1}$$

$$= -\mu_0 A_1 \frac{\mathrm{d}\boldsymbol{H}}{\mathrm{d}t}$$

But $H = \frac{I}{\ell}$ where ℓ = magnetic flux path length

$\approx$ distance around the core (by Assumption 1)

$$\Rightarrow V = -\frac{\mu_0 A_1}{\ell}\frac{dI}{dt}$$ ***Equation 3-6***

Integrating yields

$$Vt = -\frac{\mu_0 A_1}{\ell} I$$

$$\Rightarrow I = -kt \qquad \text{where } k = \frac{V\ell}{\mu_0 A_1}$$ ***Equation 3-7***

In a typical application, we would have

$$V = 600 \text{ V}$$

$$\ell = 0.1 \text{ m}$$

$$A_1 = 6.25 \times 10^{-4} \text{ m}^2$$

$$\Rightarrow k = 7.6 \times 10^{10}$$

Using these figures, current I rises to 76 A after only 1 ns, and this rapidly rising current will produce a strong magnetic field in A_1 which will force the field to diffuse into A_2 in a short amount of time. As the laminations have a permeability of the order of 5000 times greater than air, the magnetic field does not need to penetrate far into the core before the field in the lamination begins to dominate Faraday's Law (Equation 3-5).

3.2 MAGNETIC FIELD PENETRATION

We now consider the penetration of the magnetic field into a lamination. The directions of the electric and magnetic fields, outlined in Assumption 2, are defined as shown in Figure 3-4.

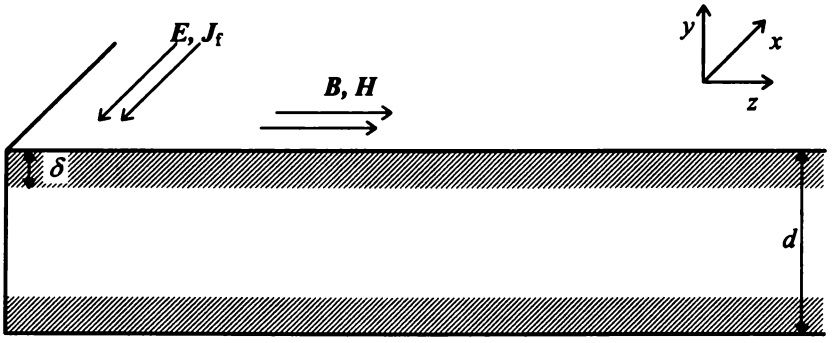

Figure 3-4 *Field Directions And Penetration Depth In Laminations*

3.2.1 DIFFUSION EQUATION

Starting from the most general form of Maxwell's Equations

$$\nabla \times \boldsymbol{E} = -\frac{\partial \boldsymbol{B}}{\partial t} \qquad \textit{Equation 2-3}$$

$$\nabla \times \boldsymbol{H} = \boldsymbol{J}_f + \frac{\partial \boldsymbol{D}}{\partial t} \qquad \textit{Equation 2-5}$$

which by Assumption 6 becomes

$$\nabla \times \boldsymbol{H} = \boldsymbol{J}_f \qquad \textit{Equation 3-4}$$

In a linear and isotropic medium such as the lamination, we can write that $\boldsymbol{B} = \mu \boldsymbol{H}$, and so Equation 3-4 becomes

$$\nabla \times \boldsymbol{B} = \mu \boldsymbol{J}_f \qquad \textit{Equation 3-8}$$

where μ = permeability of lamination.

The electric field E drives current J_f through the lamination in the direction shown in Figure 3-4. For conductors obeying Ohm's Law, $J_f = \sigma E$ where σ is the electrical conductivity.[8] In the lamination then, Equation 2-3 can be written as

$$\nabla \times J_f = -\sigma \frac{\partial B}{\partial t} \qquad \textit{Equation 3-9}$$

Taking the curl of Equation 3-8 and substituting into Equation 3-9 gives

$$\begin{aligned} \nabla \times (\nabla \times B) &= \mu \nabla \times J_f \\ &= -\mu\sigma \frac{\partial B}{\partial t} \end{aligned} \qquad \textit{Equation 3-10}$$

Making use of the vector identity $\nabla \times (\nabla \times A) = \nabla(\nabla \cdot A) - \nabla^2 A$, this can be written

$$\nabla(\nabla \cdot B) - \nabla^2 B = -\mu\sigma \frac{\partial B}{\partial t} \qquad \textit{Equation 3-11}$$

From Maxwell's Equations, $\nabla \cdot B = 0$, that is the magnetic field is non-divergent as shown in Figure 3-4. We also have

$$\begin{aligned} \nabla^2 B &= \nabla^2 B_x i + \nabla^2 B_y j + \nabla^2 B_z k \\ &= \nabla^2 B_z k \qquad \text{since } B_x = B_y = 0 \text{ by Assumption 2} \\ &= \left(\frac{\partial^2 B_z}{\partial x^2} + \frac{\partial^2 B_z}{\partial y^2} + \frac{\partial^2 B_z}{\partial z^2} \right) k \\ &= \frac{\partial^2 B_z}{\partial y^2} k \qquad \text{since, by Assumption 2, } B_z \text{ is a function of } y \text{ only} \end{aligned}$$

Hence Equation 3-11 can be simplified to the following *Diffusion Equation.*

$$\frac{\partial^2 B_z}{\partial y^2} = \mu\sigma \frac{\partial B_z}{\partial t} \qquad \textit{Equation 3-12}$$

---

[8] The iron core material typically used for transformer laminations has a conductivity $\sigma \approx 10^7$ S/m.

3.2.2 APPROXIMATE SOLUTION

An approximate short-time solution can be found for the penetration of the magnetic field into the lamination, to a depth δ in time τ_δ. Referring to Figure 3-4 and assuming that $\boldsymbol{B}$ is a function of d and t, we can estimate[9]

$$\frac{\partial^2 B_z}{\partial y^2} \approx \frac{\mathrm{d}}{\mathrm{d}y}\frac{\mathrm{d}B}{\mathrm{d}y}$$
$$\approx \frac{B}{\delta^2}$$

$$\frac{\partial B_z}{\partial t} \approx \frac{\mathrm{d}B}{\mathrm{d}t}$$
$$\approx \frac{B}{\tau_\delta}$$

Equation 3-12 then simplifies to

$$\frac{B}{\delta^2} = \frac{\mu\sigma B}{\tau_\delta}$$
$$\Leftrightarrow \tau_\delta = \mu\sigma\delta^2 \qquad \textit{Equation 3-13}$$

Equation 3-13 can be used to find the rate at which the field penetrates the laminations

$$v_\mathrm{d} = \frac{y}{t} \approx \frac{\delta}{\tau_\delta} = \frac{1}{\mu\sigma\delta} \qquad \textit{Equation 3-14}$$

or to relate the penetration depth to time

$$\delta = \sqrt{\frac{\tau_\delta}{\mu\sigma}} \qquad \textit{Equation 3-15}$$

---

[9] We first assume that $\boldsymbol{B}$ is a function of y only, in which case the partial derivative is equal to the general derivative, $\frac{\partial B}{\partial y} = \frac{\mathrm{d}B}{\mathrm{d}y}$. Next we assume that $\boldsymbol{B}$ is a function of t only, and so $\frac{\partial B}{\partial t} = \frac{\mathrm{d}B}{\mathrm{d}t}$.

Typical values for silicon steel laminations are $\sigma = 2.2 \times 10^6$ S/m, and $\mu \sim 0.006$ H/m ($\mu_r \sim 5000$). The depth of penetration as a function of time is therefore given by Equation 3-16 and is graphed in Figure 3-5.

$$\delta \approx 8.7 \times 10^{-3} \sqrt{\tau_\delta} \qquad \textit{Equation 3-16}$$

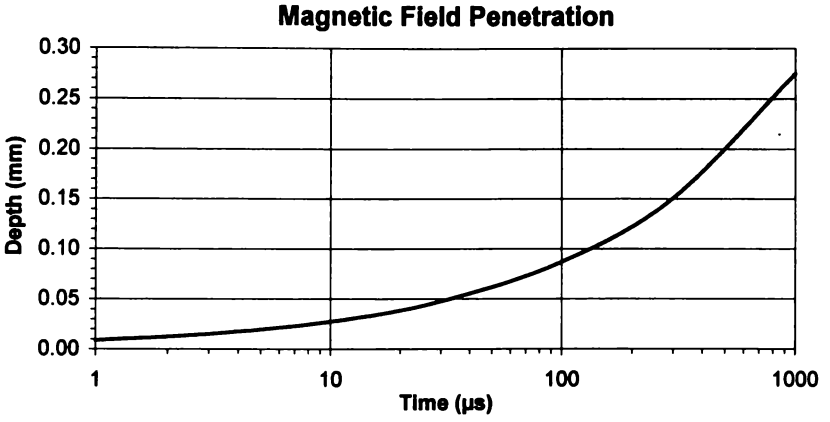

Figure 3-5 *Approximate Solution To The Diffusion Equation*

The pulse width of the example output pulse shown in Figure 1-2 is 350 µs. In this time, as shown by Figure 3-5 the magnetic field will penetrate to a depth of approximately 0.16 mm from the edge of the lamination. This penetration will occur from both edges of the lamination, therefore the field has effectively penetrated 0.32 mm.

Output transformers are commonly designed with 0.50 mm laminations, so this approximate solution indicates that the magnetic field is in effect only able to utilise 64 % of the core by the end of the pulse. Obviously the core is even less effective during the initial part of the pulse.

In Section 3.1.3 we demonstrated that the magnetic core dominates Faraday's Law in Equation 3-5, as required by Assumption 1. From Equation 3-16, the field will penetrate to a depth of 27.5 µm after 1 ns. Since we assumed that the core has an effective permeability of 5000 times that of air, then 27.5 µm of core is as effective as 1.3 mm of air (or bobbin material). The transformer geometry shown in Figure 5-1 specifies a gap between the primary coil and laminations of 1 mm, so we can be confident that the core very quickly dominates Faraday's Law, and that Assumption 1 is valid.

3.2.3 EXACT SOLUTION

We now seek an exact solution to the diffusion equation,

$$\frac{\partial^2 B_z}{\partial y^2} = \mu\sigma\frac{\partial B_z}{\partial t} \qquad \textit{Equation 3-12}$$

Let us consider again Figure 3-4, and include a representation of the magnetic field penetration into the lamination.

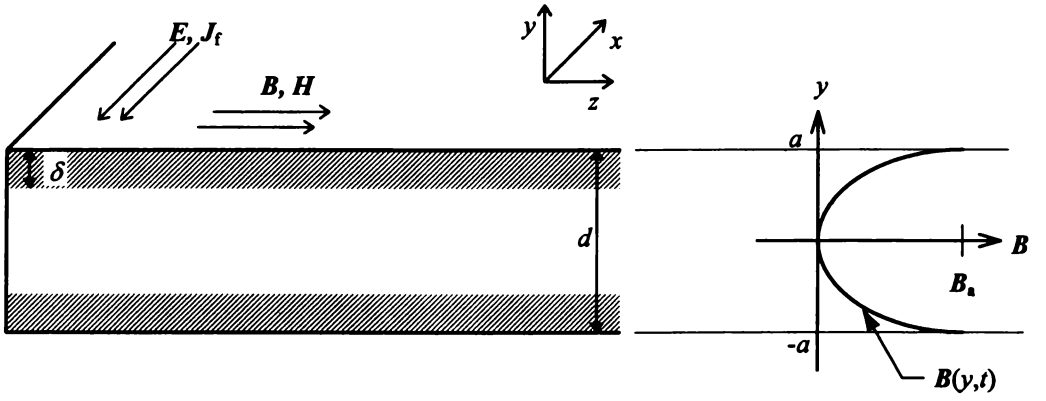

Figure 3-6 *Field Penetration Into Lamination*

To solve Equation 3-12, we will consider the trial solution

$$B_z(y,t) = Y(y)T(t) + \mathrm{C} \qquad \textit{Equation 3-17}$$

3.2.3.1 Boundary Conditions

The magnetic flux density outside the laminations is given as $B_{ext} = \mu_0 H_{ext}$ (in a direction tangential to the surface of the lamination), and is effectively created instantly by the capacitor discharging into the coil. At the edge of the lamination $y = \pm a$, the magnetic field strength H inside the lamination is equal to that outside, $H_a = H_{ext}$. In other words, there are

no discontinuities in the magnetic field strength [*Landau and Lifshitz* 1960 p. 115].[10] The magnetic flux density $\boldsymbol{B}$ increases however by a factor of μ_r, $\boldsymbol{B}_a = \mu_r \boldsymbol{B}_{ext}$, which is a discontinuous change between air and the magnetic core. The difference in profile between $\boldsymbol{B}$ and $\boldsymbol{H}$ is illustrated in Figure 3-7.

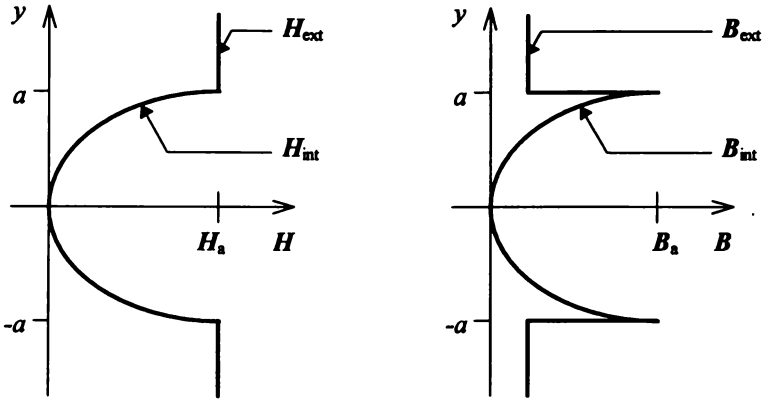

Figure 3-7 *Comparison Of B And H Profiles*

Although the magnetic field is created instantly at the surface of the lamination, it takes time to penetrate the core. At the beginning of the pulse, say $t = 0$, the full magnetic field $\boldsymbol{B}_a = \frac{\mu I}{\ell}$ is present at the edge of the lamination, but there is no magnetic field inside. With time however, the magnetic field penetrates the entire lamination and eventually reaches a value equal to that at the surface.

In considering this diffusion, the boundary conditions required for a solution are as follows:

Boundary Condition 1: $\boldsymbol{B}(a) = \boldsymbol{B}(-a) = \boldsymbol{B}_a \left(= \mu_0 \mu_r \boldsymbol{H}_a\right)$ at $y = \pm a$, for all t;

Boundary Condition 2: $\boldsymbol{B}(y) = 0$ for $-a < y < a$, at $t = 0$;

Boundary Condition 3: $\boldsymbol{B}(y) = \boldsymbol{B}_a$ for all y, as $t \to \infty$.

[10] The *tangential* component of magnetic field strength $\boldsymbol{H}$ is continuous across a boundary. The *normal* component of magnetic flux density $\boldsymbol{B}$ is continuous across a boundary. As shown in Figure 3-6, the magnetic field is tangential to the boundary.

3.2.3.2 Trial Solution

The trial solution, where Y is a function of y only and T is a function of t only, is

$$B_z(y,t) = Y(y)T(t) + \mathrm{C} \qquad \textit{Equation 3-17}$$

Differentiating[11] gives

$$\frac{\partial B_z}{\partial y} = Y'(y)T(t) \qquad \text{and} \quad \frac{\partial^2 B_z}{\partial y^2} = Y''(y)T(t)$$

Also, $\dfrac{\partial B_z}{\partial t} = Y(y)\dot{T}(t)$

Equation 3-12 can therefore be written as

$$Y''T = \mu\sigma Y\dot{T}$$

$$\Leftrightarrow \quad \frac{Y''}{Y} = \mu\sigma\frac{\dot{T}}{T} \qquad \textit{Equation 3-18}$$

But as we have chosen Y to be a function of distance y alone, and T to be a function of time t only, then both sides of Equation 3-18 must be equal to a constant which is independent of both y and t. Let this constant be k. We can therefore write

$$\frac{Y''}{Y} = \mu\sigma\frac{\dot{T}}{T} = -k^2$$

$$\Leftrightarrow Y'' + k^2 Y = 0 \qquad \textit{Equation 3-19}$$

$$\text{where} \quad k^2 = -\mu\sigma\frac{\dot{T}}{T} \qquad \textit{Equation 3-20}$$

---

[11] We write $\dfrac{\partial Y(y)}{\partial y}$ as Y', and $\dfrac{\partial T(t)}{\partial t}$ as $\dot{T}$.

Equation 3-19 is an harmonic equation, thus solutions will be of the form

$$Y = \mathrm{K}e^{sy} \qquad \textit{Equation 3-21}$$

$$\Rightarrow \frac{\partial Y}{\partial y} = Y' = s\mathrm{K}e^{sy}$$

$$\Rightarrow \frac{\partial^2 Y}{\partial y^2} = Y'' = s^2\mathrm{K}e^{sy}$$

Substituting into Equation 3-19 gives

$$s^2\mathrm{K}e^{sy} + k^2\mathrm{K}e^{sy} = 0$$

$$\Leftrightarrow \left(s^2 + k^2\right)e^{sy} = 0 \qquad \textit{Equation 3-22}$$

Hence either $s^2 + k^2 = 0$, or $e^{sy} = 0$. However, $e^{sy} = 0$ cannot be allowed as this leads to ln(0) which is undefined, thus $s^2 + k^2$ must equal zero.

$$\Rightarrow s = \pm \mathrm{j}k \qquad \text{where } \mathrm{j}^2 = -1 \qquad \textit{Equation 3-23}$$

Substituting Equation 3-23 back into Equation 3-21 gives the general solution

$$Y = \mathrm{K}_1 e^{jky} + \mathrm{K}_2 e^{-jky}$$

which can be re-written as

$$Y = \mathrm{P}'\cos(ky) + \mathrm{Q}'\sin(ky) \qquad \textit{Equation 3-24}$$

Now considering $T(t)$ which is a function of time only, and rearranging Equation 3-20 to

$$\frac{\dot{T}}{T} = -\frac{k^2}{\mu\sigma} \qquad \textit{Equation 3-25}$$

we have

$$\int \frac{1}{T} dT = \int \frac{-k^2}{\mu\sigma} dt$$

$$\Rightarrow \ln T = -\frac{k^2}{\mu\sigma} t + \ln T_0, \qquad \text{where } \ln T_0 \text{ is a constant}$$

$$\Rightarrow T = T_0 e^{-\frac{k^2 t}{\mu\sigma}} \qquad \textit{Equation 3-26}$$

3.2.3.3 Particular Solution

By substituting Equation 3-24 and Equation 3-26 into the trial solution Equation 3-17, we have a solution to the Diffusion Equation (Equation 3-12) of

$$B = YT + C$$

$$= (P' \cos ky + Q' \sin ky) T_0 e^{-\frac{k^2 t}{\mu\sigma}} + C \qquad \textit{Equation 3-27}$$

Redefining the constants to $P = P'T_0$ and $Q = Q'T_0$ gives

$$B = (P \cos ky + Q \sin ky) e^{-\frac{k^2 t}{\mu\sigma}} + C \qquad \textit{Equation 3-28}$$

The constants are evaluated by considering the boundary conditions. Using Boundary Condition 3: $B(y) = B_a$ as $t \to \infty$

$$\Rightarrow B_a = (P \cos ky + Q \sin ky) e^{-\infty} + C$$
$$= C$$

$$\therefore B = (P \cos ky + Q \sin ky) e^{-\frac{k^2 t}{\mu\sigma}} + B_a \qquad \textit{Equation 3-29}$$

Now using Boundary Condition 2 and choosing $y = 0$: $\boldsymbol{B} = 0$ for $y = 0, t = 0$

$$\Rightarrow 0 = (\mathrm{P}\cos 0 + \mathrm{Q}\sin 0)\mathrm{e}^{0} + B_{\mathrm{a}}$$
$$\Leftrightarrow \mathrm{P} = -B_{\mathrm{a}}$$

$$\therefore B = \left(-B_{\mathrm{a}}\cos ky + \mathrm{Q}\sin ky\right)\mathrm{e}^{-\frac{k^2 t}{\mu\sigma}} + B_{\mathrm{a}} \qquad \textit{Equation 3-30}$$

Next we use Boundary Condition 1: $\boldsymbol{B}(a) = \boldsymbol{B}(-a)$

$$\Rightarrow \left(-B_{\mathrm{a}}\cos ka + \mathrm{Q}\sin ka\right)\mathrm{e}^{-\frac{k^2 t}{\mu\sigma}} + B_{\mathrm{a}} = \left(-B_{\mathrm{a}}\cos(-ka) + \mathrm{Q}\sin(-ka)\right)\mathrm{e}^{-\frac{k^2 t}{\mu\sigma}} + B_{\mathrm{a}}$$
$$\Leftrightarrow \quad -B_{\mathrm{a}}\cos ka + \mathrm{Q}\sin ka = -B_{\mathrm{a}}\cos(ka) - \mathrm{Q}\sin(ka)$$
$$\Leftrightarrow \quad 2\mathrm{Q}\sin ka = 0$$

$$\Leftrightarrow \quad \mathrm{Q}\sin ka = 0 \qquad \textit{Equation 3-31}$$

$\therefore$ either $\mathrm{Q} = 0$, or $\sin ka = 0$.

Now from Boundary Condition 1 and choosing $t = 0$ we also have: $\boldsymbol{B}(a) = \boldsymbol{B}_{\mathrm{a}}$ at $t = 0$

$$\Rightarrow B_{\mathrm{a}} = \left(-B_{\mathrm{a}}\cos ka + \mathrm{Q}\sin ka\right)\mathrm{e}^{0} + B_{\mathrm{a}}$$
$$\Leftrightarrow B_{\mathrm{a}}\cos ka = \mathrm{Q}\sin ka \qquad \textit{Equation 3-32}$$

But from Equation 3-31, $\mathrm{Q}\sin ka = 0$ and so Equation 3-32 becomes

$$B_{\mathrm{a}}\cos ka = 0$$
$$\Leftrightarrow \cos ka = 0 \quad \text{since } B_{\mathrm{a}} \neq 0$$

$$\Rightarrow k = \frac{n\pi}{2a} \quad \text{where } n = \pm 1, \pm 3, \pm 5\ldots \qquad \textit{Equation 3-33}$$

Now Equation 3-33 also implies that $\sin ka \neq 0$, and so we must have $Q = 0$ from Equation 3-31.

$$\therefore\ B = -B_a \cos(ky) e^{-\frac{k^2 t}{\mu\sigma}} + B_a \qquad \textit{Equation 3-34}$$

$$\text{where} \qquad k = \frac{n\pi}{2a}$$

We may write this in a more convenient form

$$B_{z,n}(y,t) = B_a\left[1 - e^{-\frac{n^2 t}{\tau_m}} \cos\left(\frac{n\pi}{2a} y\right)\right] \qquad \textit{Equation 3-35}^{12}$$

$$\text{where } n = \pm 1, \pm 3, \pm 5\ldots$$

$$\text{and} \quad \tau_m = \mu\sigma\left(\frac{2a}{\pi}\right)^2 \qquad \textit{Equation 3-36}$$

Equation 3-35 is therefore a particular solution to the Diffusion Equation.

3.2.3.4 General Solution

Equation 3-35 was derived using Boundary Condition 2 by setting $y = 0$, but as illustrated by Figure 3-8 this does not fully satisfy the boundary condition over the range $-a < y < a$.

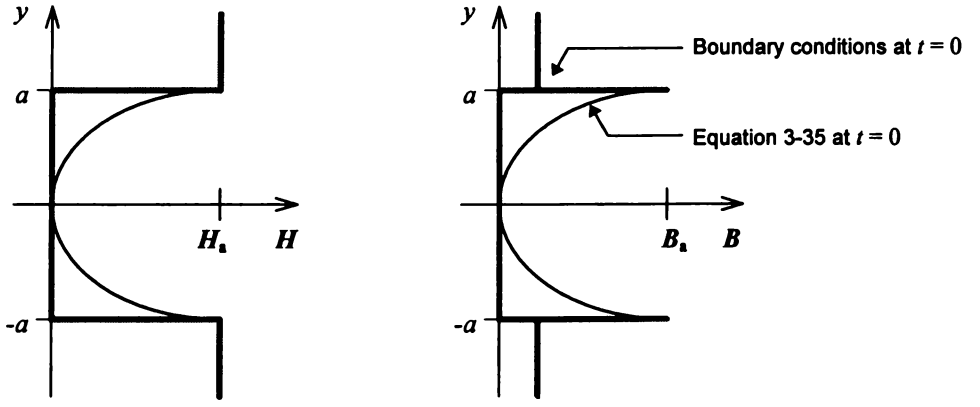

Figure 3-8 *Comparison Of Equation 3-35 With Boundary Conditions*

[12] Note that $2a = d$, the lamination thickness.

A Fourier series can used to represent the required function of the boundary condition at $t = 0$. The Fourier series representing a square pulse train is [*Lawden* 1959 p. 255]

$$F(t) = \lambda\left[1 + 2\sum_{n=1}^{\infty} \frac{\sin(n\lambda\pi)}{n\lambda\pi}\cos(n\omega t)\right] \qquad \textit{Equation 3-37}$$

If we choose the pulse width to be $\frac{\lambda\pi}{\omega} = a$, and the period to be $\frac{2\pi}{\omega} = 4a$, and noting that the pulse train needs to be inverted so that for $F(y) = 0$, B = constant K and for $F(y) = 1$, $B = 0$, then an appropriate Fourier Series can be written as

$$B = \frac{\mathrm{K}}{2}\lambda\left[1 - 2\sum_{n=1}^{\infty} \frac{\sin\left(\frac{n\pi}{2}\right)}{\frac{n\pi}{2}}\cos\left(\frac{n\pi}{2a}y\right)\right] \qquad \textit{Equation 3-38}$$

which written to fourth order is

$$B = \frac{\mathrm{K}}{2}\left[1 - \frac{4}{\pi}\cos\left(\frac{\pi}{2a}y\right) + \frac{4}{3\pi}\cos\left(\frac{3\pi}{2a}y\right) - \frac{4}{5\pi}\cos\left(\frac{5\pi}{2a}y\right) + \frac{4}{7\pi}\cos\left(\frac{7\pi}{2a}y\right)\right]$$

Equation 3-39

Since Equation 3-35 is a particular solution to the problem, the general solution can be written as a sum of particular solutions, thus

$$B_n = \beta_0\left[1 - \sum_{n=1}^{\infty} \beta_n \mathrm{e}^{-\frac{(2n-1)^2 t}{\tau_m}} \cos\left(\frac{(2n-1)\pi}{2a}y\right)\right] \qquad \textit{Equation 3-40}$$

which is valid for all time. Choosing $t = 0$ then, the first four terms are

$$B = \beta_0\left[1 - \beta_1\cos\left(\frac{\pi}{2a}y\right) - \beta_2\cos\left(\frac{3\pi}{2a}y\right) - \beta_3\cos\left(\frac{5\pi}{2a}y\right) - \beta_4\cos\left(\frac{7\pi}{2a}y\right)\right]$$

Equation 3-41

Equations 3-39 and 3-41 are both solutions at $t = 0$, and we can therefore equate the co-efficients to give:

$$\beta_0 = \frac{K}{2} = B_a \text{ by Boundary Condition 1}$$

$$\beta_1 = \frac{4}{\pi} \qquad \beta_2 = -\frac{4}{3\pi}$$

$$\beta_3 = \frac{4}{5\pi} \qquad \beta_4 = -\frac{4}{7\pi}$$

Hence the general solution which satisfies all of the boundary conditions, written to fourth order accuracy, is

$$B_z(y,t) = B_a\left[1 - \frac{4}{\pi}e^{-\frac{t}{\tau_m}}\cos\left(\frac{\pi}{2a}y\right) + \frac{4}{3\pi}e^{-\frac{9t}{\tau_m}}\cos\left(\frac{3\pi}{2a}y\right) - \frac{4}{5\pi}e^{-\frac{25t}{\tau_m}}\cos\left(\frac{5\pi}{2a}y\right) + \frac{4}{7\pi}e^{-\frac{49t}{\tau_m}}\cos\left(\frac{7\pi}{2a}y\right)\right] \qquad \textit{Equation 3-42}$$

or in general

$$B_z(y,t) = B_a\left[1 + \sum_{n=1}^{\infty}(-1)^n \frac{4}{(2n-1)\pi}e^{-\frac{(2n-1)^2 t}{\tau_m}}\cos\left(\frac{(2n-1)\pi}{2a}y\right)\right] \qquad \textit{Equation 3-43}$$

This solution provides a great amount of detail regarding the distribution of the magnetic field in the lamination, and can be solved to find the magnetic field for any given position and time.

The solution can include as many higher order terms as are required for accuracy. Due to the squared exponential term, the magnitude of the harmonics decreases rapidly with time. For $t > 50$ μs, a solution to first order is likely to provide acceptable accuracy. For $t < 10$ μs, fourth order harmonics are required to give a reasonable match to the boundary conditions. Figure 3-9 illustrates the profile of the magnetic field to 5th order accuracy as it penetrates the lamination.

This figure clearly shows the effect of pulse magnetisation, as the field gradually moves into the lamination. It supports in greater detail the approximate result found in Section 3.2.2,

This figure clearly shows the effect of pulse magnetisation, as the field gradually moves into the lamination. It supports in greater detail the approximate result found in Section 3.2.2, again showing the ineffectiveness of the core, especially during the initial stages of the pulse.

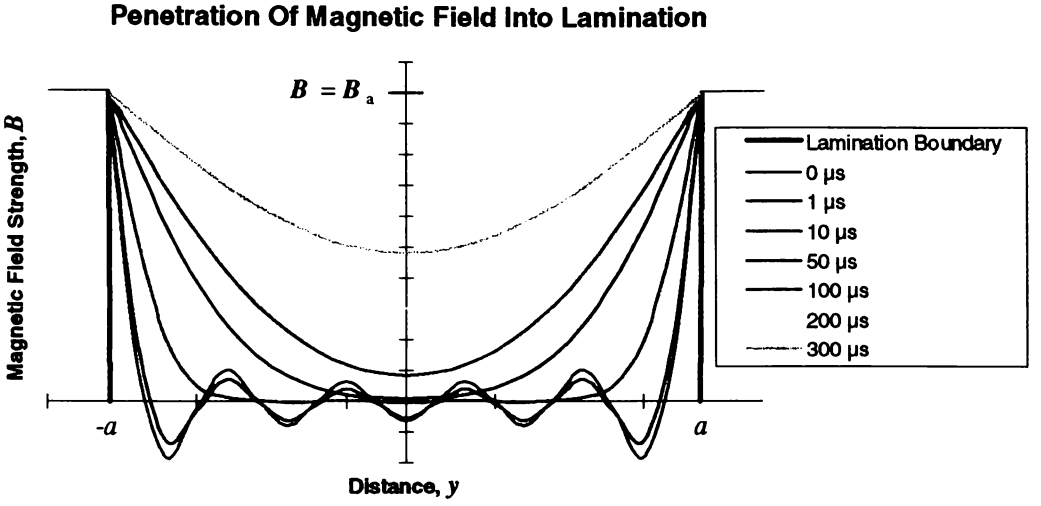

Figure 3-9 *General Solution To The Diffusion Equation (First Five Terms)*

3.2.4 Field At Centre Of Lamination

The field at the centre of the lamination, $y = 0$, can be found as a function of time and compared to that found by the approximate solution of Section 3.2.2. It can be seen that the particular solution given by Equation 3-35 satisfies the boundary conditions at $y = 0$. This equation may be simplified by considering only the first order term, which does not result in a significant loss of accuracy above 50 μs.

At $y = 0$ and returning only the term corresponding to $n = 1$, Equation 3-35 becomes

$$B \approx B_a\left[1 - e^{-\frac{t}{\tau_m}}\cos(0)\right]$$

$$= B_a\left(1 - e^{-\frac{t}{\tau_m}}\right) \qquad \textit{Equation 3-44}$$

$$\text{where } \tau_m = \mu\sigma\left(\frac{2a}{\pi}\right)^2 \qquad \textit{Equation 3-36}$$

In the case of a typical output transformer, the following values are applicable.

$$\mu \approx 0.006 \text{ H/m}$$

$$\sigma = 2.2 \times 10^6 \text{ S/m}$$

$$2a = d = 0.5 \times 10^{-3} \text{ m}$$

$$\Rightarrow \tau_m \approx 3.34 \times 10^{-4} \qquad \textit{Equation 3-45}$$

To illustrate this solution, let us normalise the equation to B_a. Then $B = 1 - e^{-2991t}$, and the following graph shows how the magnetic field at the centre of the lamination increases over time until it converges to B_a, the level of the field at the edge of the lamination. After 1 ms, the field at the centre is approximately equal to that of the exterior.

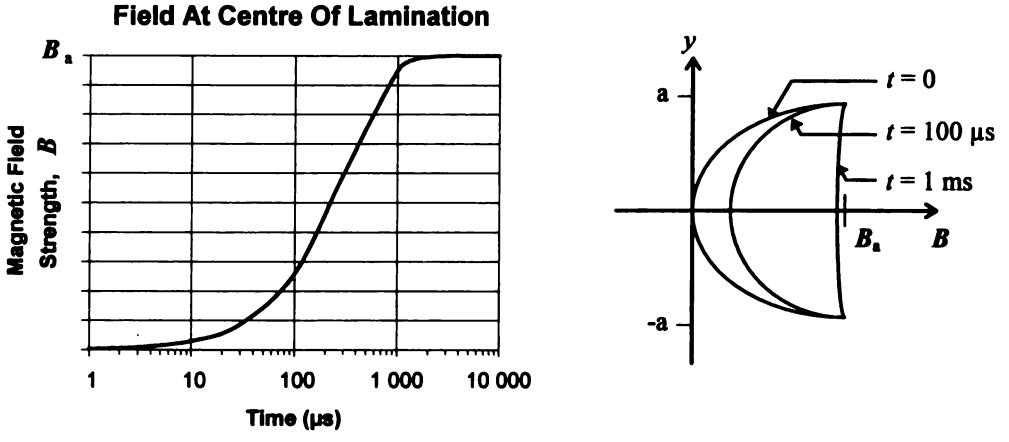

Figure 3-10 *Particular Solution To The Diffusion Equation*

In comparing Figure 3-10 to Figure 3-5, we can see that the approximate solution shows reasonable agreement with the particular solution. In both cases, the field at the centre of the lamination reaches about 30 % of the value at the boundary after 100 µs, and is close to 100 % after 1 ms.

3.3 SATURATION

Let us assume that the magnetic material inside the core is unmagnetised at the beginning of the pulse.[13] As the wavefront of the magnetic field penetrates the core and begins to magnetise the material, the permeability at any point within the core controls the magnetic field produced at that point. However, as is illustrated by Figure 5-1d, this permeability varies with the magnetic field strength, and if H continues to increase, the permeability reaches a peak then begins to decline, eventually returning to a value of μ_0 (the permeability of air) when the core is fully saturated.

The common understanding of saturation is that the magnetic material suddenly loses all permeability if it is extended past its saturation point. Figure 5-1d demonstrates however that in reality the permeability reduces gradually. For silicon steel, saturation is specified as $B_s = 2.0$ T, at which point the relative permeability is 22 - that is, the magnetic material is still 22 times more attractive to flux than air.

Saturation does however cause an avalanche effect due to the inter-dependence of current and inductance. Inductance is proportional to permeability (by Equation 2-34), and current is inversely proportional to inductance (by Equation 2-37). Hence when permeability begins to drop, current begins to rise. Now the magnetic field strength is directly dependent on the current (Equation 2-25), so increasing current results in increasing H and thus decreasing μ. This results in a further increase in current and the cycle repeats. As this happens almost instantaneously, the effect can be catastrophic for an unlimited current source, as may be the case for a mains transformer.

In addition to considering the penetration of the magnetic field into the lamination, it is therefore important to take a closer look at the subsequent saturation of the magnetic material.

---

[13] This assumption is generally valid for output transformers as they usually have a large inherent air gap and therefore a low residual flux density.

3.3.1 HIGH PERMEABILITY BAND

Under pulse conditions, the lamination can be modelled as comprising a central section which is devoid of magnetic field, a moving region which is fully magnetised, and a surface section which is saturated [*Glasoe and Lebacqz* 1948 p. 633]. There is, in effect, a *band of high permeability* which travels into the core at the speed of penetration of the magnetic field. Although the area of this band may be small in comparison to the total core area, due to the large relative permeability of the magnetised core material the average permeability of the entire core is still high. The core is not considered to be saturated until the region of saturation following this high-μ band has reached the very centre of the lamination.

The high permeability of magnetic materials is the basis for the operation of magnetic devices. The material in this area of high permeability typically has a permeability many thousand times that of the surrounding material. It thus dominates the dynamic behaviour of the magnetic properties of the material, and the area of the high-μ band is therefore the effective area of the core.

3.3.2 EFFECTIVE CORE AREA

Due to the cyclic interaction of permeability and current, saturation is a difficult problem to analyse and requires a numerical approach for an accurate solution. In addition, a full knowledge of the permeability vs. magnetic field characteristic of the material needs to be known, and this is difficult to obtain for proprietary core materials. However, by making judicious use of a few approximations, an analytical approach may be taken which provides some understanding of the process of saturation, and yields information that is of benefit during design.

The transformer and core described in Chapter 5 will be assumed where values are required, although this approach can easily be applied to other transformers and cores.

3.3.2.1 Permeability Curve

The permeability curve is approximated by the step function shown in Figure 3-11. From the manufacturer's data curve shown in Figure 5-1d, permeability has dropped to approximately half of its maximum value at a magnetic field strength of 300 A/m. This value is therefore chosen for the step point in the approximate permeability curve, and a μ_r value of 5000 is assumed, which is an average figure used previously for calculations.

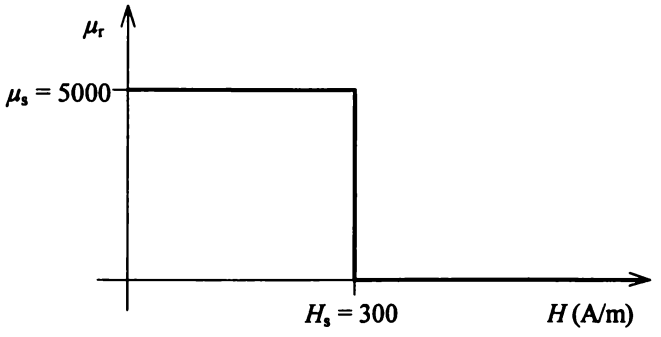

Figure 3-11 *Step Function Approximation For Permeability*

3.3.2.2 Average Over Distance

An average of the magnetic flux density is found with respect to distance. As the times associated with saturation are very small, higher order terms will be required to provide acceptable accuracy. The general form of Equation 3-43 will therefore be used.

The equation is first normalised equivalent to setting $B_s = 1$, which will be indicated by the subscript f. The normalised average field $\overline{B}_f$ therefore gives a figure for the average value of the magnetic field in the lamination as a fraction of the external (or applied) magnetic field, assuming the field to be constant.

The average is found across the entire lamination of width $2a$.

$$\left(\overline{B}_f\right)_y = \frac{1}{2a}\int_{-a}^{a} B(y)\,dy$$

$$= \frac{1}{a}\int_{0}^{a} B(y)\,dy \qquad \textit{Equation 3-46}$$

since the field distribution is symmetrical. Applying this to Equation 3-43 gives

$$\overline{B}_f(t) = \frac{1}{a}\int_0^a \left[1 + \sum_n (-1)^n \frac{4}{(2n-1)\pi} e^{-\frac{(2n-1)^2 t}{\tau_m}} \cos\left(\frac{(2n-1)\pi}{2a} y\right)\right] dy$$

Now $$\int_0^a dy = [y]_0^a = a$$

and $$\int_0^a \cos\left(\frac{(2n-1)\pi}{2a} y\right) = \left[\frac{2a}{(2n-1)\pi}\sin\left(\frac{(2n-1)\pi}{2a} y\right)\right]_0^a$$

$$= \frac{2a}{(2n-1)\pi}\left[\sin\left(\frac{(2n-1)\pi}{2}\right) - \sin(0)\right]$$

$$= (-1)^{n+1}\frac{2a}{(2n-1)\pi}$$

since $\sin\left(\frac{(2n-1)\pi}{2}\right) = (-1)^{n+1}$ and $\sin(0) = 0$

$$\Rightarrow \overline{B}_f(t) = \frac{1}{a}\left[a + \sum_n (-1)^n \frac{4}{(2n-1)\pi} e^{-\frac{(2n-1)^2 t}{\tau_m}} \cdot (-1)^{n+1} \frac{2a}{(2n-1)\pi}\right]$$

$$= 1 - \sum_n \frac{8}{(2n-1)^2\pi^2} e^{-\frac{(2n-1)^2 t}{\tau_m}} \qquad \textit{Equation 3-47}$$

as $(-1)^n \cdot (-1)^{n+1} = -1$.

3.3.2.3 Average Over Time

We similarly integrate Equation 3-47 to find the average over a time period t_p.

$$\left(\overline{B}_f\right)_t = \frac{1}{t_p}\int_0^{t_p} \overline{B}_f(t)\,dt$$

$$= \frac{1}{t_p}\int_0^{t_p}\left[1 - \sum_n \frac{8}{(2n-1)^2\pi^2} e^{-\frac{(2n-1)^2 t}{\tau_m}}\right]dt$$

Now $$\int_0^{t_p} dt = [t]_0^{t_p} = t_p$$

and $$\int_0^{t_p} e^{-\frac{(2n-1)^2 t}{\tau}}\,dt = \left[-\frac{\tau_m}{(2n-1)^2} e^{-\frac{(2n-1)^2 t}{\tau_m}}\right]_0^{t_p}$$

$$= -\frac{\tau_m}{(2n-1)^2}\left(e^{-\frac{(2n-1)^2 t_p}{\tau_m}} + e^0\right)$$

$$= \frac{\tau_m}{(2n-1)^2}\left(1 - e^{-\frac{(2n-1)^2 t_p}{\tau_m}}\right)$$

$$\Rightarrow \overline{B}_f = \frac{1}{t_p}\left[t_p - \sum_n \frac{8}{(2n-1)^2\pi^2}\cdot\frac{\tau_m}{(2n-1)^2}\left(1 - e^{-\frac{(2n-1)^2 t_p}{\tau_m}}\right)\right]$$

$$= 1 - \sum_n \frac{8\tau_m}{(2n-1)^4\pi^2 t_p}\left(1 - e^{-\frac{(2n-1)^2 t_p}{\tau_m}}\right) \qquad \textit{Equation 3-48}$$

where $\tau_m = \mu\sigma\left(\frac{2a}{\pi}\right)^2$

and t_p = time period.

3.3.2.4 Pulse Inductance

An approximation for the effective inductance of the core under pulse conditions may be found using Equation 3-48 and the approximation of the permeability graph in Figure 3-11.

Equation 3-48 describes the average magnetic flux density across the entire lamination for a time period t_p, normalised with respect to the magnetic flux density B_a created at the edge of the lamination by the current flowing in the coil. Rather than considering $\overline{B}_f$ to be the fraction of the total field B_a present across the entire lamination, we can think of this as an *equivalent peak value* - the fraction of the total area which is fully magnetised to a level B_a. This factor will be termed the *inductance factor*, f_L, that is

$$f_L = \overline{B}_f \qquad \textit{Equation 3-49}$$

Equation 3-48 by itself assumes that once the magnetic field has penetrated to a point, that point remains in a state of high permeability for the remainder of the pulse. As explained in Section 3.3.1, a more realistic assumption is that there is a band of high permeability travelling into the centre of the lamination, as the initial magnetisation is followed by saturation. We need to therefore calculate the time taken for saturation to occur at a point in the core once it has been magnetised.

For this we must refer to Figure 3-3 which is reproduced below.

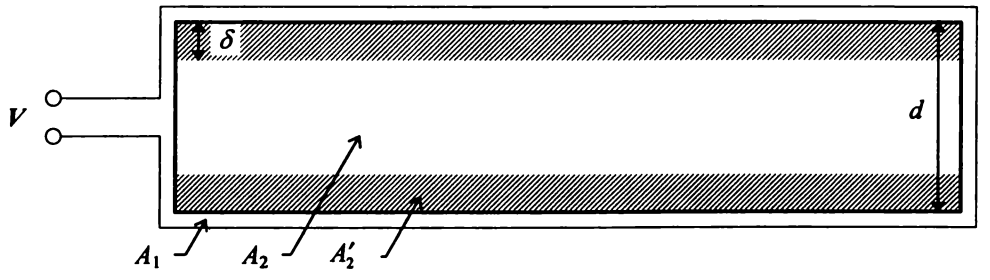

A_1 = area enclosed by coil outside laminations (coil area less lamination area)
A_2 = area of laminations (of width d)
A_2' = effective core area (of width 2δ)
$= f_L A_2$

Figure 3-3 *Simplified Transformer Core*

$$V \approx -\frac{\mathrm{d}}{\mathrm{d}t}\boldsymbol{B}_1 A_1 - \frac{\mathrm{d}}{\mathrm{d}t}\boldsymbol{B}_2 A_2' \qquad \textit{Equation 3-5}$$

As noted in Section 3.1.3, since the permeability of the lamination is approximately 5000 times that of air, $\boldsymbol{B}_2$ will become much greater than $\boldsymbol{B}_1$ immediately the magnetic field begins to penetrate the lamination. Despite A_2' being small we have shown that $\boldsymbol{B}_2 A_2' >> \boldsymbol{B}_1 A_1$. Equation 3-5 then becomes

$$\begin{aligned} V &\approx -\frac{\mathrm{d}}{\mathrm{d}t}\boldsymbol{B}_2 A_2' \\ &= -\mu A_2' \frac{\mathrm{d}\boldsymbol{H}}{\mathrm{d}t} \end{aligned} \qquad \textit{Equation 3-50}$$

where μ is assumed to be independent of time for this model. We need only consider the magnitude of the field in this situation. Integrating yields

$$Vt = \mu A_2' H$$

$$\Leftrightarrow t = \frac{\mu A_2'}{V} H \qquad \textit{Equation 3-51}$$

If H is chosen as the magnetic field strength at saturation H_s, then t will be the time taken for saturation to be reached. This is the interval between the time a point in the core is initially magnetised until the time it enters saturation, and can be substituted into Equation 3-48 to find the fraction of the total core area which comprises the high permeability band. Equations 3-51 and 3-48 may therefore be solved to find the inductance factor f_L which, when used in conjunction with Equation 2-34, will give a result for the effective inductance of the core under pulse conditions.

3.3.3 EXAMPLE OF INDUCTANCE FACTOR

To illustrate the concept of the *inductance factor* derived in the previous section, we will calculate the effective inductance of the transformer described in Figure 5-1.

For an initial time period, the inductance is assumed constant so that current flow can be calculated.[14] The initial time period is chosen to be 0.5 μs, which is long enough for the magnetic field to begin to penetrate the core thereby creating some inductance to limit the current, but is not long enough to impact upon the pulse shape.

We need to first estimate A_2', the initial area of the core, as a function of time. The permeability curve is approximated by Figure 3-11.

$$A_2' = f_L A_2 \qquad \textit{Equation 3-52}$$

$$f_L = \left[1 - \sum_n \frac{8\tau_m}{(2n-1)^4 \pi^2 t_p}\left(1 - e^{-\frac{(2n-1)^2 t_p}{\tau_m}}\right)\right] \qquad \textit{Equation 3-53}$$

Over such a short time period, higher order harmonics play a significant role as illustrated by Figure 3-9. The accuracy of the result calculated to n^{th} order is indicated by the contribution of the n^{th} harmonic term of the result. Evaluating the result to higher order terms obviously provides greater accuracy, and less difference between successive terms as illustrated by Table 3-1.

For this application, τ_m may be evaluated as follows:

$$\tau_m = \mu_s \sigma \left(\frac{2a}{\pi}\right)^2 \qquad \textit{Equation 3-36}$$

where $\mu_s = 0.006$ H/m

$\sigma = 2.2 \times 10^6$ S/m

$2a = d = 0.5 \times 10^{-3}$ m

$$\Rightarrow \tau_m = 3.34 \times 10^{-4} \qquad \textit{Equation 3-54}$$

---

[14] In an electrical circuit simulator, this starting value is known as the bias point.

Setting $t_p = 0.5$ μs and $\tau_m = 3.34 \times 10^{-4}$ in Equation 3-53 gives the following result.

Inductance Factor, f_L	Order	Correction	Error
0.1900	1st	8.10E-01	81.0 %
0.1006	2nd	8.95E-02	47.1 %
0.0688	3rd	3.18E-02	31.6 %
0.0528	4th	1.60E-02	23.2 %
0.0434	5th	9.42E-03	17.8 %
0.0373	6th	6.13E-03	14.1 %
0.0330	7th	4.24E-03	11.4 %
0.0300	8th	3.06E-03	9.3 %
0.0277	9th	2.28E-03	7.6 %
0.0259	10th	1.73E-03	6.3 %
0.0246	11th	1.35E-03	5.2 %
0.0235	12th	1.06E-03	4.3 %
0.0227	13th	8.42E-04	3.6 %
0.0220	14th	6.77E-04	3.0 %
0.0215	15th	5.48E-04	2.5 %
0.0210	16th	4.47E-04	2.1 %
0.0207	17th	3.67E-04	1.7 %
0.0204	18th	3.03E-04	1.5 %
0.0201	19th	2.52E-04	1.2 %
0.0199	20th	2.10E-04	1.0 %

Table 3-1 *Inductance Factor For Initial Time Period*

To 20th order then, the inductance factor is 0.02 with an error of 1.0 %, and Equation 3-52 becomes

$$A_2' = 20 \times 10^{-3} A_2 \qquad \textit{Equation 3-55}$$

This result takes into account the diffusion of the magnetic field, but not the saturation of the core. By substituting Equation 3-55 into Equation 3-51, we may now solve for the time to saturation t_s, where H_s is chosen as the magnetic field strength required for saturation as given in Figure 3-11.

$$t_s = \frac{\mu_s A_2'}{V} H_s$$

where $\mu_s = 0.006$ H/m

$A_2' = 20 \times 10^{-3} A_2$

$A_2 = 6.15 \times 10^{-4}$ m^2

$V = 600$ V

$H_s = 300$ A/m

$\Rightarrow t_s = 37$ ns ***Equation 3-56***

A point in the magnetic material therefore saturates only 37 ns after it is magnetised.

The area of the core covered by the band of high permeability can therefore be found by substituting t_s = 37 ns into Equation 3-53. This calculates the area swept out by the advancing wavefront between the time that the core is magnetised until the time that it saturates.

As this time period is very small, harmonics continue to be significant to very high orders. The 50th order term contributes only 0.8 % to the result, but the cumulative effect of the 51st to 120th terms is such that their combined contribution is 17 %, a significant proportion of the final result. The equation converges after the 120th term to an inductance factor of $f_L = 5 \times 10^{-3}$.

The effective inductance of the core can then be calculated from Equation 2-34.

$$L = \mu_s \frac{N^2 A_e}{\ell}$$ ***Equation 2-34***

where $\mu_s = 0.006$ H/m

$N = 50$

$A_e =$ effective area of core, $f_L \times A$

$f_L = 5 \times 10^{-3}$

$A = 6.15 \times 10^{-4}$ m^2

$\ell = 153 \times 10^{-3}$ m

$\Rightarrow L = 301$ µH

The inductance factor indicates how small the effective inductance of the core actually is under pulse conditions. The real situation is enormously complex, and this value should be treated as a rough estimate only and verified by measurement at every opportunity. However, in situations where the transformer has not been built, for example when modelling a new design, the process outlined in this example can be useful for providing an estimate where a value for inductance is required.

Chapter Four ANALYTICAL MODEL

The objective of any analytical investigation is to derive relationships between circuit elements and behaviour. These analytical equations are very helpful in understanding the circuit's behaviour, and lead to design criteria and an understanding of the limits of operation of the device. While numerical methods may display greater accuracy, they are unable to provide the overview of circuit behaviour afforded by an analytical model.

The emphasis in this chapter is on developing a sound analytical description of the output transformer. Due to the complexity of transformer operation, in particular the interdependence of inductance and current, a large number of assumptions are required in order to achieve a workable solution. However, the resultant model is shown to match the behaviour of a real transformer and provide much useful design information.

The comments made by Bostick at the end of his analytical study of pulse transformers are very appropriate.

> "*A complete and accurate solution of the problem can be achieved only by laborious graphical methods that fail to give the average investigator the comprehensive view provided by analytical solutions. It is the author's belief that this foregoing theory, rough and brief as it is, is of definite value in being able to show in an analytical manner the dependence of the circuit behaviour on the various elements.*" [*Glasoe and Lebacqz* 1948 p. 589].

4.1 CURRENT

An electric fence pulse is created by the sudden discharge of a storage capacitor C_s charged to an initial voltage V_0. Once current begins to flow through the primary winding of the transformer, magnetic fields are created which electromagnetically couple the primary and secondary coils.

The primary current determines the value of the magnetising field $H(I)$, which controls the value of the permeability $\mu(H)$, which in turn establishes the inductance $L(\mu) = \frac{N\Phi}{I}$.

The actual mechanism underlying this behaviour is extremely complex, as has been discussed previously, and is again evident from the fact that the impedance of the inductance, $Z(L)$ heavily influences the flow of current. Hence the discharge current both determines and is determined by the inductance. A number of simplifying assumptions must therefore be made to allow any meaningful analysis of the circuit.

4.1.1 SIMPLIFYING ASSUMPTIONS

The general transformer equivalent circuit of Figure 2-8 will be simplified to suit this application as follows:

1. The parasitic capacitances C_1, C_{12} and C_2 have less significance at the relatively low frequencies inherent in the fence pulse, and will be ignored;[1]

2. The secondary winding resistance R_s is assumed to be negligible in comparison with the load resistance, and will be disregarded;[2]

---

[1] When the spectral characteristic of a fence pulse is analysed, the peak amplitude typically occurs around 1 kHz with the spectrum falling away quickly at higher frequencies (see for example Figure 5-20). The proportion of the spectrum above 20 kHz is small [*Hancock* 1991].

[2] This assumption is only valid if $R_{load} >> R_s$, say $R_{load} = 250\ \Omega$. As noted in Assumption 4, a typical value of 500 Ω will be assumed for the fence load when required during this analytical investigation, in which case Assumption 2 is valid. In cases where R_s is significant, it can be reflected to the primary side of the transformer and combined with R_p as given by Equation 2-48.

3. The leakage inductance L_{eq} will be ignored. The relative permeability of the core can reasonably be expected to be much greater than that of air ($\mu_r >> 1$), even when the core is saturated,[3] which implies that $L_{eq,1}$ will have a smaller value than the magnetising inductance L_m;[4]

4. The resistance representing the fence load will be reflected to the primary side of the transformer (using Equation 2-43) to give an equivalent load resistance of $R_{l,eq} = \left(\frac{N_p}{N_s}\right)^2 R_{load}$. A typical value of 500 Ω will be assumed for the fence load when required, although in practice the value of the load can vary widely;

5. Core loss resistance R_c and reflected load resistance $R_{l,eq}$ will be combined as a single equivalent series resistance,[5] $R_L = \frac{R_{l,eq} R_c}{R_{l,eq} + R_c} = \frac{\left(\frac{N_p}{N_s}\right)^2 R_{load} R_c}{\left(\frac{N_p}{N_s}\right)^2 R_{load} + R_c}$.

4.1.2 Simplified Equivalent Circuit

Based on these assumptions, a simplified equivalent circuit which is applicable to the output transformer is drawn in Figure 4-1. The ideal transformer[6] draws no current and performs an exact voltage transformation by the turns ratio $n = \frac{N_s}{N_p}$. For the sake of simplicity then, this ideal transformer will be disregarded in the following analysis, and the resultant output voltage will simply need to be scaled by a factor of n to find the correct magnitude.

---

[3] Refer to the discussion in Chapter 3.3, and to Figure 5-1d.

[4] This assumption is valid for all times greater than the immediate onset of the pulse, before which the magnetic field has had insufficient time to penetrate the core, and therefore $\mu \approx \mu_0$.

[5] For $R_{load} < 2500$ Ω, the effect of R_c is insignificant and may be ignored.

[6] The ideal transformer is discussed in Chapter 2.2.4.

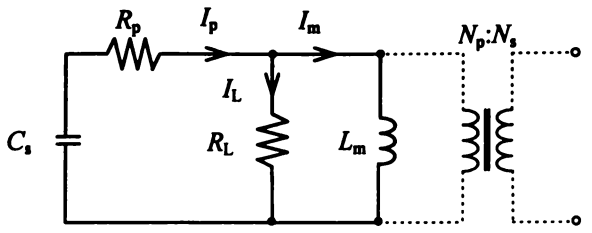

Figure 4-1 *Output Transformer Equivalent Circuit*

The total current I_p flowing from the capacitor consists of the *magnetising current* I_m which is required to transfer the energy across the transformer, and the *load current* I_L which opposes the magnetising current, thereby causing an increase in primary current in order to maintain the original level of the magnetising current.

4.1.3 MAGNETISING CURRENT EQUATION

We will now derive an equation which describes the magnetising current I_m, starting with Kirchhoff's voltage law around the circuit.

$$V_{C_s} = V_{R_p} + V_{R_L}$$ ***Equation 4-1***

$$\Leftrightarrow \frac{q}{C_s} = R_p I_p + R_L I_L$$

$$\therefore \frac{\dot{q}}{C_s} = R_p \dot{I}_p + R_L \dot{I}_L$$ ***Equation 4-2***

The variables can all be written in terms of I_m. For the parallel branch we can write

$$V_{R_L} = V_{L_m}$$

$$\Leftrightarrow I_L R_L = L_m \dot{I}_m$$

$$\Rightarrow I_L = \frac{L_m}{R_L} \dot{I}_m$$ ***Equation 4-3***

$$\therefore \dot{I}_L = \frac{L_m}{R_L} \ddot{I}_m$$ ***Equation 4-4***

Kirchhoff's current law yields

$$I_p = I_L + I_m \qquad \textit{Equation 4-5}$$

and substituting for I_L from Equation 4-3 results in

$$I_p = \frac{L_m}{R_L}\dot{I}_m + I_m \qquad \textit{Equation 4-6}$$

$$\therefore \dot{I}_p = \frac{L_m}{R_L}\ddot{I}_m + \dot{I}_m \qquad \textit{Equation 4-7}$$

Since $\dot{q} = -I_p$, substituting for I_p in Equation 4-6 gives

$$\dot{q} = -\frac{L_m}{R_L}\dot{I}_m - I_m \qquad \textit{Equation 4-8}$$

Substituting Equations 4-8, 4-7 and 4-4 into Equation 4-2 results in

$$\frac{1}{C_s}\left(\frac{-L_m}{R_L}\dot{I}_m - I_m\right) = R_p\left(\frac{L_m}{R_L}\ddot{I}_m + \dot{I}_m\right) + R_L\left(\frac{L_m}{R_L}\ddot{I}_m\right)$$

$$\Leftrightarrow \left(\left(\frac{R_p}{R_L}+1\right)L_m C_s\right)\ddot{I}_m + \left(\frac{L_m}{R_L} + R_p C_s\right)\dot{I}_m + I_m = 0$$

$$\Leftrightarrow kL_m C_s \ddot{I}_m + \left(\frac{L_m}{R_L} + R_p C_s\right)\dot{I}_m + I_m = 0 \qquad \textit{Equation 4-9}$$

$$\text{where}^7\ k = \frac{R_p}{R_L} + 1$$

This is an homogeneous 2nd order ordinary differential equation, and its solution will require three boundary conditions. The following conditions are applicable:

Boundary Condition 1: $I_m = 0$ at $t = 0$;

Boundary Condition 2: $q = C_s V_0$ at $t = 0$;

Boundary Condition 3: $q = 0$ at $t = \infty$.

---

[7] If $R_{load} > 500\ \Omega$, $k \approx 1$.

4.1.4 SOLUTION TO MAGNETISING CURRENT EQUATION

Using the trial form $I_m = A_1 e^{\lambda t}$, the auxiliary equation of Equation 4-9 can be written as

$$\lambda^2 A_1 e^{\lambda t} k L_m C_s + \lambda A_1 e^{\lambda t}\left(\frac{L_m}{R_L} + R_p C_s\right) + A_1 e^{\lambda t} = 0$$

$$\Leftrightarrow \lambda^2 k L_m C_s + \lambda\left(\frac{L_m}{R_L} + R_p C_s\right) + 1 = 0$$

The roots of λ are given by

$$\lambda = \frac{-\left(\frac{L_m}{R_L} + R_p C_s\right) \pm \sqrt{\left(\frac{L_m}{R_L} + R_p C_s\right)^2 - 4kL_m C_s}}{2kL_m C_s}$$

$$= -\left(\frac{L_m}{R_L}\frac{1}{2kL_m C_s} + \frac{R_p C_s}{2kL_m C_s}\right) \pm \sqrt{\left(\frac{L_m}{R_L}\frac{1}{2kL_m C_s} + \frac{R_p C_s}{2kL_m C_s}\right)^2 - \frac{4kL_m C_s}{4k^2 L_m^2 C_s^2}}$$

$$= -\left(\frac{1}{2kR_L C_s} + \frac{R_p}{2kL_m}\right) \pm \sqrt{\left(\frac{1}{2kR_L C_s} + \frac{R_p}{2kL_m}\right)^2 - \frac{1}{kL_m C_s}} \qquad \textit{Equation 4-10}$$

We define the following time constants for the current pulse

$$\tau_a = \frac{2kL_m R_L C_s}{L_m + R_p R_L C_s} \qquad \textit{Equation 4-11}^{8}$$

$$\omega = \frac{1}{\sqrt{kL_m C_s}} \qquad \textit{Equation 4-12}$$

$$\Rightarrow \lambda = -\frac{1}{\tau_a} \pm \sqrt{\frac{1}{\tau_a^2} - \omega^2} \qquad \textit{Equation 4-13}$$

---

[8] The subscript 'a' will be used to denote the time constant τ_a defined during the derivation of the analytical model. This notation is used to avoid confusion with the magnetic field time constant τ_m, which was defined during the investigation into pulse magnetisation.

Using typical values for the discharge circuit, the deterministic will be negative for $L_m < 10$ mH. In reality, the primary inductance is expected to be much less than this[9] and we can therefore write

$$\lambda = \frac{-1}{\tau_a} \pm j\omega \qquad \textit{Equation 4-14}$$

with the trial solution becoming

$$I_m = A_1 e^{\left(\frac{-1}{\tau_a} \pm j\omega\right)t} \qquad \textit{Equation 4-15}$$

This may be simplified to the general solution

$$I_m = e^{\frac{-t}{\tau_a}}\left(A_2 \sin \omega t + A_3 \cos \omega t\right) \qquad \textit{Equation 4-16}$$

The constants A_2 and A_3 are now evaluated by applying the boundary conditions.

Boundary Condition 1: $I_m = 0$ at $t = 0$

$$\Rightarrow 0 = e^0\left(A_2 \cdot 0 + A_3 \cdot 1\right)$$

$$\Leftrightarrow A_3 = 0 \qquad \textit{Equation 4-17}$$

and so Equation 4-16 becomes

$$I_m = A_2 e^{\frac{-t}{\tau_a}} \sin \omega t \qquad \textit{Equation 4-18}$$

[9] With a negative determinant, the current is an under-damped oscillating waveform. If the effective primary inductance is increased to the order of millihenries, and the fence load is very heavy, say less than 100 ohms, then the current pulse will change from oscillatory to damped.

Boundary Condition 2: $q = C_s V_0$ at $t = 0$

Boundary Condition 3: $q = 0$ at $t = \infty$

From Equation 4-8 we have

$$\dot{q} = -\frac{L_m}{R_L}\dot{I}_m - I_m$$

$$\Rightarrow q = -\frac{L_m}{R_L} I_m - \int I_m dt \qquad \textit{Equation 4-19}$$

Substituting for I_m from Equation 4-18 gives

$$q = -\frac{L_m A_2}{R_L} e^{\frac{-t}{\tau_a}} \sin \omega t - A_2 \int e^{\frac{-t}{\tau_a}} \sin \omega t \, dt$$

$$= -\frac{L_m A_2}{R_L} e^{\frac{-t}{\tau_a}} \sin \omega t + \frac{A_2 e^{\frac{-t}{\tau_a}}}{\frac{1}{\tau_a^2} + \omega^2}\left(\omega \cos \omega t + \frac{1}{\tau_a} \sin \omega t\right) + A_4$$

$$= -\frac{L_m A_2}{R_L} e^{\frac{-t}{\tau_a}} \sin \omega t + \frac{A_2 e^{\frac{-t}{\tau_a}}}{1 + \frac{1}{\omega^2 \tau_a^2}}\left(\frac{1}{\omega} \cos \omega t + \frac{1}{\omega^2 \tau_a} \sin \omega t\right) + A_4$$

Equation 4-20

By Boundary Condition 3, at $t = \infty$ Equation 4-20 becomes

$$0 = -\frac{L_m A_2}{R_L} \cdot 0 \sin \omega t + \frac{A_2 \cdot 0}{1 + \frac{1}{\omega^2 \tau_a^2}}\left(\frac{1}{\omega} \cos \omega t + \frac{1}{\omega^2 \tau_a} \sin \omega t\right) + A_4$$

$$\Rightarrow A_4 = 0 \qquad \textit{Equation 4-21}$$

$$\therefore q = -\frac{L_m A_2}{R_L} e^{\frac{-t}{\tau_a}} \sin \omega t + \frac{A_2 e^{\frac{-t}{\tau_a}}}{1 + \frac{1}{\omega^2 \tau_a^2}}\left(\frac{1}{\omega} \cos \omega t + \frac{1}{\omega^2 \tau_a} \sin \omega t\right) \qquad \textit{Equation 4-22}$$

By Boundary Condition 2, at $t = 0$ Equation 4-22 becomes

$$C_s V_0 = -\frac{L_m A_2}{R_L} \cdot 1 \cdot 0 + \frac{A_2 \cdot 1}{1 + \frac{1}{\omega^2 \tau_a^2}} \left(\frac{1}{\omega} \cdot 1 + \frac{1}{\omega^2 \tau_a} \cdot 0 \right)$$

$$\Rightarrow A_2 = \omega C_s V_0 \left(1 + \frac{1}{\omega^2 \tau_a^2} \right) \qquad \textit{Equation 4-23}$$

The time constants ω and τ_a are dependant upon the following: L_m, which is variable during the course of the pulse; R_L, which can be any value in the range of 0.1 Ω to 160 Ω for the same transformer, and may vary during use; and R_p and C_s, which vary considerably between designs. It is therefore difficult to even estimate the values of the time constants, but we will assume that $\omega\tau_a >> 1$. In situations where this condition does not hold, the factor $1 + \frac{1}{\omega^2 \tau_a^2}$ will need to be included in the result.

For $\omega\tau_a >> 1$ then, $A_2 \approx \omega C_s V_0$ and Equation 4-18 becomes

$$I_m = \omega C_s V_0 e^{\frac{-t}{\tau_a}} \sin \omega t \qquad \textit{Equation 4-24}$$

4.1.5 Primary Current Equation

We can now solve for the current I_p which flows from the capacitor through the primary winding of the transformer. From Equation 4-3 we have

$$I_L = \frac{L_m}{R_L} \dot{I}_m \qquad \textit{Equation 4-3}$$

where I_m is given by Equation 4-24.

Hence

$$I_L = \frac{L_m}{R_L}\frac{d}{dt}\left(\omega C_s V_0 e^{\frac{-t}{\tau_a}} \sin \omega t\right)$$

$$= \frac{L_m}{R_L}\omega C_s V_0\left(\frac{-1}{\tau_a} e^{\frac{-t}{\tau_a}} \sin \omega t + \omega e^{\frac{-t}{\tau_a}} \cos \omega t\right)$$

$$= \frac{\omega^2 L_m C_s V_0}{R_L} e^{\frac{-t}{\tau_a}}\left(\cos \omega t - \frac{1}{\omega \tau_a} \sin \omega t\right)$$

Since $\omega^2 = \frac{1}{kL_m C_s}$, we can write

$$I_L = \frac{V_0}{kR_L} e^{\frac{-t}{\tau_a}}\left(\cos \omega t - \frac{1}{\omega \tau_a} \sin \omega t\right) \qquad \textit{Equation 4-25}$$

For $\omega\tau_a >> 0$ we can write

$$I_L \approx \frac{V_0}{kR_L} e^{\frac{-t}{\tau_a}} \cos \omega t \qquad \textit{Equation 4-26}$$

The primary current can then be found by substituting Equations 4-26 and 4-24 into Equation 4-5

$$I_p = I_L + I_m \qquad \textit{Equation 4-5}$$

$$= \frac{V_0}{kR_L} e^{\frac{-t}{\tau_a}} \cos \omega t + \omega C_s V_0 e^{\frac{-t}{\tau_a}} \sin \omega t$$

$$\Rightarrow I_p = \frac{V_0}{kR_L} e^{\frac{-t}{\tau_a}}\left(\cos \omega t + \omega C_s R_L k \sin \omega t\right) \qquad \textit{Equation 4-27}$$

4.2 OUTPUT VOLTAGE

Referring to Figure 4-1, the reflected output voltage V_L given by the voltage across R_L is equivalent to the voltage across L_m. As the load has been reflected to the primary side of the transformer, the correct magnitude of the output voltage will be $V_{out} = \frac{N_s}{N_p} V_L$. The reflected output voltage may therefore be found from

$$V_L = R_L I_L \qquad \textit{Equation 4-28}$$

where I_L is given by Equation 4-26. Hence

$$V_L = \frac{V_0}{k} e^{\frac{-t}{\tau_a}} \cos \omega t \qquad \textit{Equation 4-29}$$

The output voltage on the secondary side of the transformer is therefore given by

$$V_{out} = \frac{N_s}{N_p} \frac{V_0}{k} e^{\frac{-t}{\tau_a}} \cos \omega t \qquad \textit{Equation 4-30}$$

The primary current pulse given by Equation 4-27, the magnetising current of Equation 4-24, and the output voltage pulse of Equation 4-30 are illustrated in Figure 4-2. The exact form of each curve depends on the various circuit element values as well as the time constants τ_a and ω, which in turn depend on the transformer, load, and saturation characteristic of the core. The general waveforms shown below correspond well to those commonly seen on real electric fence energisers.

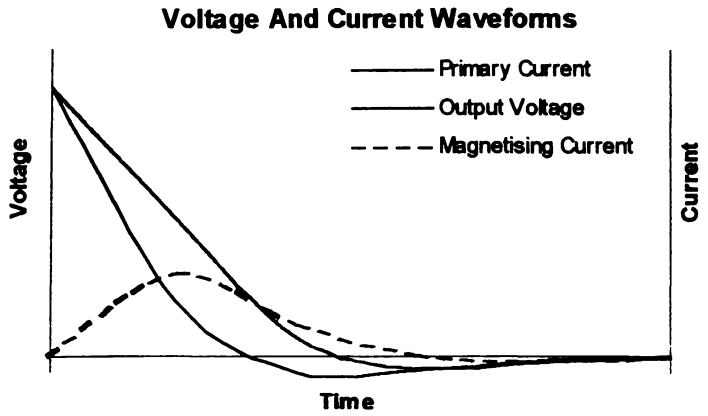

Figure 4-2 *Current And Voltage Waveforms*

4.3 OUTPUT POWER

4.3.1 LOAD POWER EQUATION

In Chapter 2.4, it was noted that voltage underswing did not contribute to the shock experienced by an animal touching an electric fence. The effective power delivered to the load is therefore the power up to the time t_0 when the voltage first falls to zero. Setting Equation 4-29 to zero gives

$$\begin{aligned} 0 &= \frac{V_0}{k} e^{\frac{-t_0}{\tau_a}} \cos \omega t_0 \\ &= \cos \omega t_0 \end{aligned}$$

$$\therefore \omega t_0 = \frac{\pi}{2}$$

$$\Leftrightarrow t_0 = \frac{\pi}{2\omega} \qquad \textit{Equation 4-31}$$

Power delivered to the load is given by integrating the square of the voltage, divided by reflected load resistance, from 0 to t_0.

$$\begin{aligned} P_L &= \int_0^{\frac{\pi}{2\omega}} \frac{V_L^2}{R_L} dt \\ &= \frac{V_0^2}{k^2 R_L} \int_0^{\frac{\pi}{2\omega}} e^{\frac{-2t}{\tau_a}} \cos^2 \omega t \, dt \\ &= \frac{V_0^2}{k^2 R_L} \int_0^{\frac{\pi}{2\omega}} e^{\frac{-2t}{\tau_a}} \left(\frac{1 + \cos 2\omega t}{2} \right) dt \end{aligned}$$

$$\Rightarrow P_L = \frac{V_0^2}{2k^2 R_L} \left[\int_0^{\frac{\pi}{2\omega}} e^{\frac{-2t}{\tau_a}} dt + \int_0^{\frac{\pi}{2\omega}} e^{\frac{-2t}{\tau_a}} \cos 2\omega t \, dt \right] \qquad \textit{Equation 4-32}$$

First Integral Term

$$\int_0^{\frac{\pi}{2\omega}} e^{\frac{-2t}{\tau_a}}\,dt = \frac{-\tau_a}{2} e^{\frac{-\pi}{\omega\tau_a}} - \frac{\tau_a}{2}$$

$$\approx -\frac{\tau_a}{2} \qquad \text{where } \omega\tau_a >> 1$$

Second Integral Term

$$\Rightarrow \int_0^{\frac{\pi}{2\omega}} e^{\frac{-2t}{\tau_a}} \cos 2\omega t\,dt = \left[\frac{e^{\frac{-2t}{\tau_a}}}{\frac{4}{\tau_a^2} + 4\omega^2} \left(\frac{-2}{\tau_a} \cos 2\omega t + 2\omega \sin 2\omega t \right) \right]_0^{\frac{\pi}{2\omega}}$$

$$= \left[\frac{e^{\frac{-\pi}{\omega\tau_a}}}{\frac{4}{\tau_a^2} + 4\omega^2} \left(\frac{-2}{\tau_a} \cos \pi + 2\omega \sin \pi \right) \right.$$

$$\left. - \frac{e^0}{\frac{4}{\tau_a^2} + 4\omega^2} \left(\frac{-2}{\tau_a} \cos 0 + 2\omega \sin 0 \right) \right]$$

$$= \frac{e^{\frac{-\pi}{\omega\tau_a}}}{\frac{4}{\tau_a^2} + 4\omega^2} \left(\frac{2}{\tau_a} \right) - \frac{1}{\frac{4}{\tau_a^2} + 4\omega^2} \left(\frac{-2}{\tau_a} \right)$$

$$= \frac{2}{4\omega^2\tau_a \left(1 + \frac{1}{\omega^2\tau_a^2} \right)} \left(e^{\frac{-\pi}{\omega\tau_a}} + 1 \right)$$

$$\approx \frac{1}{\omega^2\tau_a} \qquad \text{where } \omega\tau_a >> 1$$

Therefore Equation 4-32 is evaluated as

$$P_L = \frac{V_0^2}{2k^2 R_L}\left(\frac{-\tau_a}{2} + \frac{1}{\omega^2 \tau_a}\right)$$

$$= \frac{V_0^2 \tau_a}{4k^2 R_L}\left(\frac{2}{\omega^2 \tau_a^2} - 1\right) \qquad \text{but for } \omega\tau_a >> 1$$

$$\Rightarrow P_L \approx \frac{V_0^2 \tau_a}{4k^2 R_L} \qquad \textit{Equation 4-33}^{10}$$

$$\text{where } \tau_a = \frac{2kL_m R_L C_s}{L_m + R_p R_L C_s} \qquad \textit{Equation 4-34}$$

The power delivered to the load is a function of the magnetising inductance L_m through the inclusion of the time constant τ_a. As a result of the effects of pulse magnetisation, L_m varies during the course of the pulse. We can investigate the limits of this behaviour by considering L_m to be either large or small, and can be assured that the true response lies somewhere between these extremes.

4.3.2 Large L_m Behaviour

We first consider the situation where L_m is large, for which we find that τ_a may be simplified to

$$\tau_a = 2kR_L C_s \qquad \textit{Equation 4-35}$$

and the load power to

$$P_L = \frac{\frac{1}{2} C_s V_0^2}{k} \qquad \textit{Equation 4-36}$$

$$\text{where } k = \frac{R_p}{R_L} + 1$$

[10] The negative sign which appears in the equation has been ignored as we are interested only in the magnitude of the power.

Referring to Figure 4-1 we can see that this equation is intuitively obvious - if the magnetising inductance is large so that the magnetising current is negligible, then nearly all of the energy stored by the capacitor (Equation 1-1, $E = \frac{1}{2} C_s V_0^2$) will be delivered to the circuit resistance over the period for which $V_L > 0$. Remembering that R_L is a combination of load and core loss resistance, Equation 4-36 requires that the core loss and primary winding resistance be small for maximum power to be delivered to the load.

4.3.3 SMALL L_m BEHAVIOUR

We now consider L_m to be small in comparison to R_p, R_L and C_s, in which case we can simplify τ_a to

$$\tau_a = \frac{2kL_m}{R_p} \qquad \textit{Equation 4-37}$$

In this case, the load power is given by

$$P_L = \frac{V_0^2}{2k} \frac{L_m}{R_L R_p} \qquad \textit{Equation 4-38}$$

It is expected that, in practice, the magnetising inductance will be small due to the small effective core area available during the pulse.

4.3.4 EFFICIENCY

If the magnetising inductance L_m is small, Equation 4-38 can be used to find an expression for the efficiency η of the transformer. Since

$$\eta = \frac{P_{out}}{P_{in}} \qquad \textit{Equation 4-39}$$

and for the pulse application, the input power is equal to the energy E stored in the capacitor, we can write

$$\eta = \frac{P_L}{E} = \frac{V_0^2}{2k}\frac{L_m}{R_L R_p}\cdot\frac{2}{C_s V_0^2}$$

$$\Rightarrow \eta = \frac{L_m C_s}{R_p\left(R_p + R_L\right)} \qquad \textit{Equation 4-40}$$

Equation 4-40 clearly shows that increasing the effective inductance will improve the efficiency. It also identifies the primary winding resistance R_p as being significant, which is also predicted by the electrical circuit model in Chapter 5.4.3 and has previously been found experimentally [*Harrison* 1992].

These results confirm that the analytical solutions display the correct trends, and therefore that they can be trusted to provide insight into the behaviour of the output transformer, even though the application needs to be greatly simplified for the analysis.

4.4 INDUCTANCE

We now turn our attention towards the inductance of the transformer, which requires a consideration of the permeability of the magnetic core material and the pulse magnetisation discussed in Chapter 3.

Before finding an expression for inductance, we must first redefine the co-ordinate axes and develop an approximation for the permeability which reflects the saturation of the core.

4.4.1 TRANSFORMATION OF *Y*-AXIS

In Chapter 3, the orientation of the axes and position of the lamination were defined as shown in Figure 3-6. This resulted in Equation 3-43 which describes the growth of the magnetic field inside the core material.

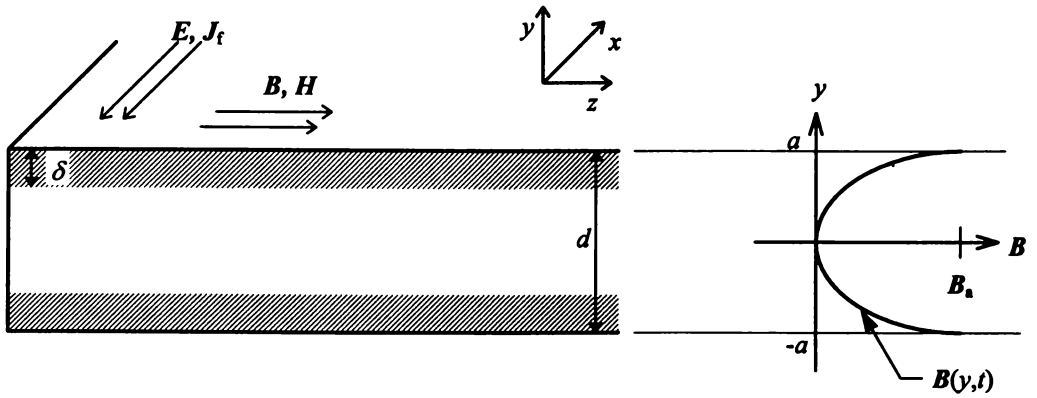

Figure 3-6 *Field Penetration Into Lamination*

$$B_z(y,t) = B_a\left[1+\sum_{n=1}^{\infty}(-1)^n\frac{4}{(2n-1)\pi}e^{-\frac{(2n-1)^2 t}{\tau_m}}\cos\left(\frac{(2n-1)\pi}{2a}y\right)\right]$$

Equation 3-43

In the present analytical investigation it will be an advantage to use an asymmetrical function. This will allow us to consider only the region where y is small, giving the opportunity to use approximations for the sinusoidal term which will greatly simplify the analysis.

This objective can be achieved by the transformation $u = y + a$, which simply re-defines the y-axis so that the lamination is centred around a rather than zero. In addition, we will replace B with μH and define the lamination to be of width w.

Figure 3-6 and Equation 3-43 then become

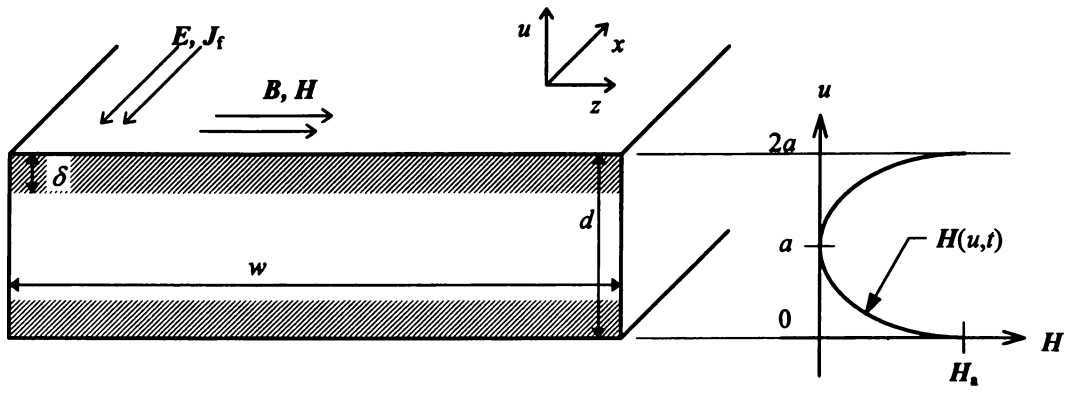

Figure 4-3 *Asymmetric Field Penetration Into Lamination*

$$\mu H_z(u,t) = \mu H_a\left[1 + \sum_{n=1}^{\infty}(-1)^n \frac{4}{(2n-1)\pi} e^{-\frac{(2n-1)^2 t}{\tau_m}} \cos\left(\frac{(2n-1)\pi}{2a}(u-a)\right)\right]$$

Now

$$\begin{aligned}\cos\left(\frac{\pi}{2a}(u-a)\right) &= \cos\left(\frac{\pi}{2a}u\right)\cos\left(\frac{\pi}{a}\right) + \sin\left(\frac{\pi}{2a}u\right)\sin\left(\frac{\pi}{2}\right)\\ &= \cos\left(\frac{\pi}{2a}u\right)\cdot 0 + \sin\left(\frac{\pi}{2a}u\right)\cdot 1\\ &= \sin\left(\frac{\pi}{2a}u\right)\end{aligned}$$

$$\therefore H_z(u,t) = H_a\left[1 + \sum_{n=1}^{\infty}(-1)^n \frac{4}{(2n-1)\pi} e^{-\frac{(2n-1)^2 t}{\tau_m}} \sin\left(\frac{(2n-1)\pi}{2a}u\right)\right] \quad \textit{Equation 4-41}$$

In practical terms, restricting this equation to first order accuracy will not introduce significant error, except at very short times when other assumptions made in this analytical approach are also invalid. The magnetic field strength in the lamination is therefore approximated by

$$H = H_a\left[1 - \frac{4}{\pi} e^{\frac{-t}{\tau_m}} \sin\left(\frac{\pi}{2a}u\right)\right] \quad \textit{Equation 4-42}$$

4.4.2 APPROXIMATION FOR PERMEABILITY

The permeability curve of a magnetic material describes the relationship between the applied current and the flux produced in the material. At a point in the core, the permeability is a function of the local value of H. This is a non-linear empirical relationship, but for most applications can be taken as constant. Due to the high peak currents created by the capacitive discharge pulse, permeability is far from constant for the output transformer but we assume here that it can be adequately modelled by a simple function $\mu(H)$.

Two approximations are proposed, neither of which is an ideal match to the experimental curve. However, each approximation has different strengths, and so it is useful to consider them both.

4.4.2.1 Step Function Approximation

The first approximation for permeability is a *step function* defined by Equation 4-43 and illustrated in Figure 3-11.

$$\begin{aligned} \mu(H) &= \mu_s && \text{for } H < H_s \\ &= \mu_0 \approx 0 && \text{for } H > H_s \end{aligned} \qquad \textit{Equation 4-43}$$

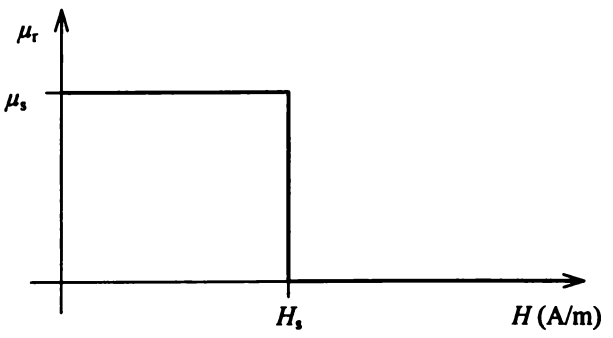

Figure 3-11 *Step Function Approximation For Permeability*

The high permeability value μ_s is not equivalent to the material's peak permeability, but is an average value over the assumed effective range of operation. Similarly, H_s is not defined

4.4.3 INDUCTANCE EQUATION

Referring to the geometry of the lamination given in Figure 4-3, consider an elemental area of the lamination, of width w, between u and $u + \mathrm{d}u$. In this region,

$$\mathrm{d}\Phi = B\mathrm{d}A \qquad \text{where} \quad \mathrm{d}A = w\mathrm{d}u \qquad \text{and} \quad B = \mu H$$

$$\Rightarrow \mathrm{d}\Phi = \mu H w \mathrm{d}u \qquad \textit{Equation 4-47}$$

For the calculation of inductance we will use the attenuation function for permeability. By substituting Equation 4-44 into Equation 4-47 we can therefore write

$$\frac{\mathrm{d}\Phi}{\mathrm{d}u} = \frac{\mu_i}{1+\frac{H}{H_k}} Hw \qquad \textit{Equation 4-48}$$

Once flux has been calculated, we can find the inductance. By combining Equations 2-37 and 4-46, we find that

$$L = \frac{N^2}{H_a \ell}\Phi \qquad \textit{Equation 4-49}$$

4.4.4 SMALL FIELD SOLUTION

Due to the time delay in the growth of magnetic field in the core, there is a small amount of time at the beginning of the pulse when $I << I_k$, and so by Equation 4-46, $H_a << H_k$. During this time, $\frac{H}{H_k} \approx 0$ and Equation 4-48 simplifies to

$$\frac{\mathrm{d}\Phi_1}{\mathrm{d}u} \approx \mu_i Hw \qquad \textit{Equation 4-50}$$

where Φ_1 is the flux found by considering the small magnetic field occurring in the short time immediately following the start of the pulse.

Substituting for H from Equation 4-42 gives

$$\frac{d\Phi_1}{du} = \mu_i w H_a \left(1 - \frac{4}{\pi} e^{\frac{-t}{\tau_m}} \sin\left(\frac{\pi u}{2a}\right)\right) \qquad \textit{Equation 4-51}$$

If u is small, we can approximate $\sin\left(\frac{\pi u}{2a}\right)$ by $\frac{\pi u}{2a}$. This is a valid simplification during the beginning of the pulse, as the magnetic field will not have penetrated far beyond the edge of the lamination. We will need to restrict u to less than a, but since the sinusoidal function is symmetrical, the flux appearing at the opposite edge of the lamination (where $u = 2a$) will simply double the result. Equation 4-51 then simplifies to

$$\frac{d\Phi_1}{du} \approx 2\mu_i w H_a \left(1 - \frac{4}{\pi} e^{\frac{-t}{\tau_m}} \frac{\pi u}{2a}\right)$$

$$= 2\mu_i w H_a \left(1 - \frac{2}{a} e^{\frac{-t}{\tau_m}} u\right) \qquad \textit{Equation 4-52}$$

The flux can then be found by integrating Equation 4-52.

$$\int d\Phi_1 = \int_0^a 2\mu_i w H_a \left(1 - \frac{2}{a} e^{\frac{-t}{\tau_m}} u\right) du$$

$$= 2\mu_i w H_a \int_0^a \left(1 - \frac{2}{a} e^{\frac{-t}{\tau_m}} u\right) du$$

$$= 2\mu_i w H_a \left([u]_0^a - \frac{2}{a} e^{\frac{-t}{\tau_m}} \left[\frac{1}{2} u^2\right]_0^a\right)$$

$$= 2\mu_i w H_a \left(a - a e^{\frac{-t}{\tau_m}}\right)$$

$$\Rightarrow \Phi_1 = 2wa\mu_i H_a \left(1 - e^{\frac{-t}{\tau_m}}\right) \qquad \textit{Equation 4-53}$$

As this solution applies only to small values of time, the Exponential Series can be used to simplify the result. The exponential term of Equation 4-53 is approximately equal to $1-\frac{t}{\tau_m}$, resulting in

$$\Phi_1 = 2wa\mu_i H_a \frac{t}{\tau_m} \qquad \textit{Equation 4-54}$$

Substituting Equation 4-54 into Equation 4-49 enables us to find an expression for the inductance at small fields. As this derivation considered only a single lamination, Equation 4-55 must be multiplied by the total number of laminations when applied to a transformer.

$$L_1 = \frac{2N^2 wa\mu_i}{\ell}\frac{t}{\tau_m} \qquad \textit{Equation 4-55}$$

4.4.5 LARGE FIELD SOLUTION

4.4.5.1 Inductance In Terms Of Magnetic Field Strength

Due to the low impedance of the circuit, the current I quickly rises to the level of I_k and greater (refer to the comments made in Footnote 11). We therefore consider the solution when $H \geq H_k$. For Φ_2, the flux at large magnetic fields, we have

$$\frac{d\Phi_2}{du} = \frac{\mu_i}{1+\frac{H}{H_k}} Hw \qquad \textit{Equation 4-48}$$

$$= \frac{\mu_i H_k}{H_k + H} Hw$$

$$= \frac{\mu_i w H_k}{1 + \frac{H_k}{H}}$$

Since $\frac{H_k}{H} \leq 1$, the Binomial Expansion may be used to simplify this expression.

$$\Rightarrow \frac{d\Phi_2}{du} \approx \mu_i w H_k \left(1 - \frac{H_k}{H}\right) \qquad \textit{Equation 4-56}$$

By substituting for H from Equation 4-42 we find that

$$d\Phi_2 = \mu_i w H_k \left(1 - \frac{H_k}{H_a\left(1 - \frac{4}{\pi} e^{\frac{-t}{\tau_m}} \sin\left(\frac{\pi u}{2a}\right)\right)}\right) du \qquad \textit{Equation 4-57}$$

Let us restrict u to $0 \leq u \leq a$, which again requires that the result be doubled to allow for flux penetrating from the opposite side of the lamination. Over time the magnetic field can be expected to fully penetrate the core, so we will approximate the sinusoidal term by[12] $\sin\left(\frac{\pi u}{2a}\right) \approx \frac{u}{a}$.

$$d\Phi_2 = 2\mu_i w H_k \left(1 - \frac{H_k}{H_a\left(1 - \frac{4u}{\pi a} e^{\frac{-t}{\tau_m}}\right)}\right) du \qquad \textit{Equation 4-58}$$

[12] This approximation differs from that used for the small field solution. If the field is small, we can assume that u is also small, thus $\sin\left(\frac{\pi u}{2a}\right) \approx \frac{\pi u}{2a}$ is a good approximation. Across the entire range of $0 \leq u \leq a$ however, $\sin\left(\frac{\pi u}{2a}\right) \approx \frac{u}{a}$ provides a better approximation.

As time t is not small, $\frac{4u}{\pi a} e^{\frac{-t}{\tau_m}}$ will be less than one, allowing us to again make use of the Binomial Expansion.

$$\Rightarrow d\Phi_2 \approx 2\mu_i w H_k \left(1 - \frac{H_k}{H_a}\left(1 + \frac{4u}{\pi a} e^{\frac{-t}{\tau_m}}\right)\right) du \qquad \textit{Equation 4-59}$$

Equation 4-59 can then be integrated to find the large field solution for the inductance.

$$\begin{aligned}
\int d\Phi_2 &= \int_0^a 2\mu_i w H_k \left(1 - \frac{H_k}{H_a}\left(1 + \frac{4u}{\pi a} e^{\frac{-t}{\tau_m}}\right)\right) du \\
&= 2\mu_i w H_k \left(\int_0^a du - \frac{H_k}{H_a}\left(\int_0^a du + \frac{4}{\pi a} e^{\frac{-t}{\tau_m}} \int_0^a u\, du\right)\right) \\
&= 2\mu_i w H_k \left(a - \frac{H_k}{H_a}\left(a + \frac{4}{\pi a} e^{\frac{-t}{\tau_m}} \cdot \frac{1}{2} a^2\right)\right)
\end{aligned}$$

$$\Rightarrow \Phi_2 = 2wa\mu_i H_k \left(1 - \frac{H_k}{H_a}\left(1 + \frac{2}{\pi} e^{\frac{-t}{\tau_m}}\right)\right) \qquad \textit{Equation 4-60}$$

As t increases, $e^{\frac{-t}{\tau}} \rightarrow 0$ and we will therefore simplify Equation 4-60 to

$$\Phi_2 = 2wa\mu_i H_k \left(1 - \frac{H_k}{H_a}\right) \qquad \textit{Equation 4-61}$$

By substituting Equation 4-61 into Equation 4-49, we obtain a large field expression for inductance. Again, this expression has been derived for a single lamination, and must be multiplied by the total number of laminations when applied to a transformer.

$$L_2 = \frac{2N^2 wa\mu_i}{\ell} \frac{H_k}{H_a}\left(1 - \frac{H_k}{H_a}\right) \qquad \textit{Equation 4-62}$$

4.4.5.2 Inductance In Terms Of Time

This expression for inductance in Equation 4-62 can be written in terms of time t as follows. From Equations 4-45 and 4-46 we can write

$$\frac{H_k}{H_a} = \frac{NI_k}{\ell}\frac{\ell}{NI_m} = \frac{I_k}{I_m} \qquad \textit{Equation 4-63}$$

I_m is given by Equation 4-24, and if we make the approximation that $\sin \omega t \approx \omega t$ we find that

$$\frac{H_k}{H} = \frac{\omega C_s V_0 e^{\frac{-t_k}{\tau_a}} \omega t_k}{\omega C_s V_0 e^{\frac{-t}{\tau_a}} \omega t} = \frac{t_k}{t} e^{\frac{(t-t_k)}{\tau_a}} \qquad \textit{Equation 4-64}$$

where t_k is the time taken for the magnetic field strength to reach the knee point. Substituting Equation 4-64 into Equation 4-62 results in an equation for inductance as a function of time.

$$L_2 = \frac{2N^2 wa\mu_i}{\ell}\frac{t_k}{t} e^{\frac{(t-t_k)}{\tau_a}}\left(1 - \frac{t_k}{t} e^{\frac{(t-t_k)}{\tau_a}}\right) \qquad \textit{Equation 4-65}$$

Since L_2 is the large field expression, t will be large in comparison to t_k, and we can make use of the simplifications $\frac{t_k}{t} << 1$ and $e^{\frac{(t-t_k)}{\tau_a}} \approx 1 + \frac{t - t_k}{\tau_a}$. Equation 4-65 is then simplified to

$$L_2 \approx \frac{2N^2 wa\mu_i}{\ell}\frac{t_k}{t}\left(1 + \frac{t - t_k}{\tau_a}\right)$$

$$L_2 = \frac{2N^2 wa\mu_i}{\ell}\frac{t_k}{t}\left(\frac{t + \tau_a - t_k}{\tau_a}\right) \qquad \textit{Equation 4-66}$$

If we also assume that $t << \tau_a$, we arrive at

$$L_2 \approx \frac{2N^2 wa\mu_i}{\ell} \frac{t_k}{t} \qquad \textit{Equation 4-67}$$

The maximum inductance can easily be found at $\frac{dL_2}{dH_a} = 0$. Differentiating Equation 4-62 gives

$$\begin{aligned} 0 &= \frac{dL_2}{dH_a} \\ &= \frac{2N^2 wa\mu_i}{\ell} \frac{d}{dH_a}\left(\frac{H_k}{H_a} - \frac{H_k^2}{H_a^2}\right) \\ &= -\frac{H_k}{H_a^2} + \frac{2H_k^2}{H_a^3} \end{aligned}$$

$$\Rightarrow H_a = 2H_k \qquad \textit{Equation 4-68}$$

$$\therefore L_{max} = \frac{2N^2 wa\mu_i}{\ell}\left(\frac{H_k}{2H_k} - \frac{H_k^2}{4H_k^2}\right)$$

$$\Rightarrow L_{max} = \frac{N^2 wa\mu_i}{2\ell} \qquad \textit{Equation 4-69}$$

4.4.6 Inductance Variation With Time

We now have enough information to fully describe the inductance as a function of time. It is convenient to define the expressions for inductance in terms of the time-independent, constant-permeability inductance L_0.

$$L_0 = \mu_i \frac{N^2 A}{\ell} \qquad \textit{Equation 2-34}$$

where from Figure 4-3, $A = wd = 2wa$

$$\Rightarrow L_0 = \mu_i \frac{2N^2 wa}{\ell} \qquad \textit{Equation 4-70}$$

The expression when time is small becomes

$$L_1 = L_0 \frac{t}{\tau_m} \qquad \textit{Equation 4-55}$$

For times much greater than t_k we have

$$L_2 = L_0 \frac{t_k}{t} \qquad \textit{Equation 4-67}$$

The maximum inductance is found to be

$$L_{max} = \frac{L_0}{4} \qquad \textit{Equation 4-69}$$

By substituting Equation 4-69 into Equation 4-67 we can also find the time t_{max} at which the inductance is maximum

$$L_{max} = L_0 \frac{t_k}{t_{max}} = \frac{L_0}{4}$$

$$\Rightarrow t_{max} = 4t_k \qquad \textit{Equation 4-71}$$

There is no explicit relationship between $t_k \approx \frac{kH_k L_m}{V_0}$, which is related to saturation, and $\tau_m = \mu\sigma\left(\frac{2a}{\pi}\right)^2$, which is a function of the magnetic and electrical properties of the core.

The short-time and long-time expressions for inductance define the limits of behaviour. The real curve lies in between these extremes and will progress from the short-time solution, through the maximum point and converge on the long-time solution. The curve of Figure 4-5 is an approximation based on the above equations.

In Section 4.3 it is shown that the power delivered to the load is increased when the inductance is maximised. The equations presented here may be used to illustrate the impact on inductance of varying the equivalent circuit parameters of material properties. For example, Figure 4-5 shows how the inductance changes if the core is changed to a material with half the time constant τ_m.

To illustrate this result, we will calculate the inductance curve as a function of time for the output transformer described in Figure 5-1.

$$L_0 = \mu_i \frac{2N^2 wa}{\ell}$$ ***Equation 4-72***

where $\mu_i = 11\,000 \times \mu_0$

$N = 50$

$w = 24.2$ mm

$a = 0.25$ mm (per lamination, × 50 laminations)

$\ell = 152$ mm

$\Rightarrow L_0 = 138$ mH

For the initial time period,

$$L_1 = L_0 \frac{t}{\tau_m}$$ ***Equation 4-55***

where

$$\tau_m = \mu\sigma\left(\frac{2a}{\pi}\right)^2$$ ***Equation 3-36***

where $\mu = 0.006$ H/m

$\sigma = 2.2 \times 10^6$ S/m

$a = 0.25$ mm

$\Rightarrow \tau_m = 3.34 \times 10^{-4}$

As time becomes large

$$L_2 = L_0 \frac{t_k}{t}$$ ***Equation 4-67***

where

$$t_k \approx \frac{kH_k L_m}{V_0}$$ *Equation 4-73*

where $k \approx 1$

$H_k = 120$ A/m

$L_m = 300$ μH (the expected average value from Chapter 3.3)

$V_0 = 600$ V

$\Rightarrow t_k = 6.0 \times 10^{-5}$

and from Equations 4-69 and 4-71 we have

$L_{max} = 35$ mH

$t_{max} = 240$ μs

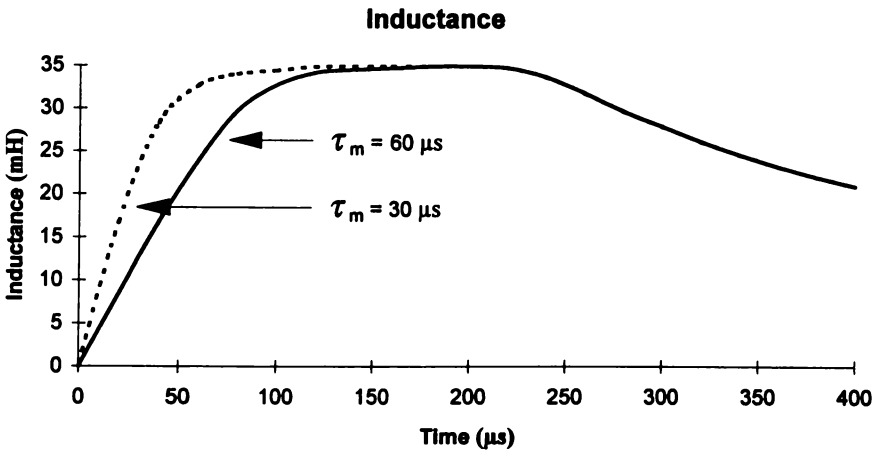

Figure 4-5 *Variation Of Inductance With Time*

The shape of the inductance curve is easily explained by considering pulse magnetisation. As the magnetic field penetrates the core, the magnetised area and hence the inductance grows in relation to the magnetic time constant. Once the edge of the core begins to saturate, the magnetised area reaches a maximum and stays almost constant as the band of high permeability moves towards the centre. Once this band reaches the centre, the effective area begins to drop as saturation also approaches the centre, and the inductance falls away. Reducing τ_m is therefore one way of increasing the effective inductance.

The graph of Figure 4-5 shows a higher maximum inductance than would be expected, especially considering that the effective inductance calculated in Chapter 3.3 is $5 \times 10^{-3} L_0$. Experience tells us that the inductance is much less than L_0, but perhaps it is not as small as $5 \times 10^{-3} L_0$.

Figure 4-5 also indicates that the core does not saturate until about 240 μs after the beginning of the pulse. The entire core is not considered to be saturated until the saturated side of the high-μ band has travelled to the centre of the lamination, and there is effectively no region in the core which has a high permeability. The time until saturation occurs can be found from Equation 3-43 by setting B to the level of saturation, $B = 2.0$ T, and solving for the time t.[13] This results in $t \approx 310$ μs, which is in general agreement with the analytical result. Experimental and simulation results indicate that the core saturates during the pulse for $R_{load} > 320\ \Omega$, which is also in general agreement with the result of Figure 4-5.

4.5 HIGH PERMEABILITY BAND

In Chapter 3.3 the concept of a region of high permeability was developed on the basis of the diffusion of the magnetic field into the core material. We now investigate this effect on the basis of the analytical model and non-linear permeability discussed in this chapter.

In order to display the correct characteristics of a high permeability band, both penetration time and saturation must be taken into account. Equation 4-42 accounts for penetration time, while the non-linear permeability approximations discussed in Section 4.4.2 introduce saturation into the calculations.

Prior to magnetisation, the magnetic domains are randomly oriented and the net magnetic field strength, and hence flux, is zero. As the magnetic field moves into the material, the domains begin to align resulting in a large increase in flux. Once saturated, the domains are

[13] Results were found using Mathcad 7

fully aligned and the magnetic field strength and flux are very high.[14] If the magnetic field strength H continues to increase, the flux will also increase but at a rate much slower than that prior to saturation. As permeability is proportional to the rate of increase of flux, permeability will fall as the rate of increase in flux falls.

The capacitive discharge current rises to a peak and then begins falling, inducing a voltage of the opposite polarity in the output coil. As the magnetic field strength H is proportional to the current I, H rises and falls with the current.

As illustrated by the material data in Figure 4-4, the permeability begins at an initial value and rises to a peak, then begins dropping towards saturation as H continues to rise. When the current I and hence the magnetic field strength H falls, the permeability returns to its peak value before falling again to the initial value.

A residual magnetism remains at the completion of the pulse, the value of which depends on the material and shape of the core. It is generally low for those output transformers which have an inherent air gap. The effects of high permeability caused by the decreasing portion of the current pulse, and the residual magnetism are not examined in this thesis.

The magnetic field strength H is approximated by Equation 4-42.

$$H = H_s\left[1-\frac{4}{\pi}e^{\frac{-t}{\tau_m}}\sin\left(\frac{\pi}{2a}u\right)\right] \qquad \textit{Equation 4-42}$$

This may be further simplified by considering u and t to be small (say $u < a$, and $t < \tau_m$), allowing us to write $\sin\left(\frac{\pi u}{2a}\right) \approx \frac{\pi u}{2a}$ and $e^{\frac{-t}{\tau_m}} \approx 1 - \frac{t}{\tau_m}$.

$$\Rightarrow H \approx H_s\left[1 - \frac{2u}{a}\left(1 - \frac{t}{\tau_m}\right)\right] \qquad \textit{Equation 4-74}$$

---

[14] Output voltage is low however, since induced voltage is determined by the rate of change of flux, $V = -N\frac{d\Phi}{dt}$, and the change in flux is small when permeability is small.

While the use of these approximations may adversely affect the numerical accuracy of the results, they allow the behaviour of the circuit to be analysed in a way that is easily grasped, and greatly assist in understanding the flux penetration into the core.

4.5.1 STEP FUNCTION APPROXIMATION

The step function of Equation 4-43 shown in Figure 3-11 will be used first to estimate the progression of the high-permeability region through the lamination.

$$\begin{aligned} \mu(H) &= \mu_s && \text{for } H < H_s \\ &= \mu_0 \approx 0 && \text{for } H > H_s \end{aligned} \qquad \textit{Equation 4-43}$$

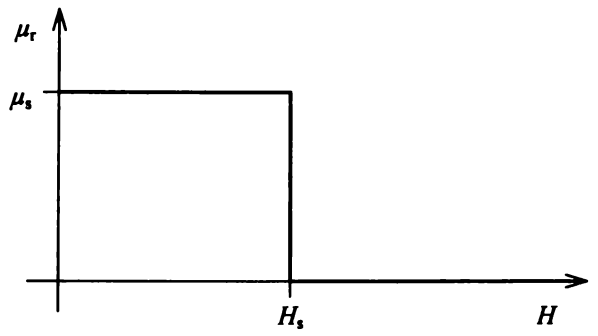

Figure 3-11 *Step Function Approximation For Permeability*

The variation of flux with distance penetrated into the core can be found by substituting Equation 4-74 into Equation 4-47, which results in

$$d\Phi = w\mu H du$$

$$\Rightarrow \frac{d\Phi}{w du} = \mu H_a \left[1 - \frac{2u}{a}\left(1 - \frac{t}{\tau_m} \right) \right] \qquad \textit{Equation 4-75}$$

Introducing Equation 4-43 for permeability and noting that $\frac{d\Phi}{wdu} = B$ gives

$$B = \mu_s H_a\left[1 - \frac{2u}{a}\left(1 - \frac{t}{\tau_m}\right)\right] \quad \text{for } H < H_s$$
$$= 0 \quad \text{for } H > H_s \qquad \textit{Equation 4-76}$$

Equation 4-76 can be used to plot the magnetic flux density B with respect to distance u at any specified time. The step point can be found by setting H to H_s and u to u_s in Equation 4-74.

$$H_s = H_a\left[1 - \frac{2u_s}{a}\left(1 - \frac{t}{\tau_m}\right)\right]$$

$$\Leftrightarrow \frac{2u_s}{a}\left(1 - \frac{t}{\tau_m}\right) = 1 - \frac{H_s}{H_a}$$

$$\Rightarrow u_s = \frac{a\left(1 - \frac{H_s}{H_a}\right)}{2\left(1 - \frac{t}{\tau_m}\right)} \qquad \textit{Equation 4-77}$$

To evaluate this equation we must assume that the current is constant, which results in a constant value for the applied field H_a. This applied field should be large enough to drive the core well into saturation, and we will assume that $H_a = 2 \cdot H_s$. Equation 4-77 can then be used to find the position in the core, at a particular time t, where the permeability changes suddenly from μ_s to 0.

Figure 4-6 illustrates the use of Equations 4-76 and 4-77 to determine the band of magnetic flux density B at various values of t.

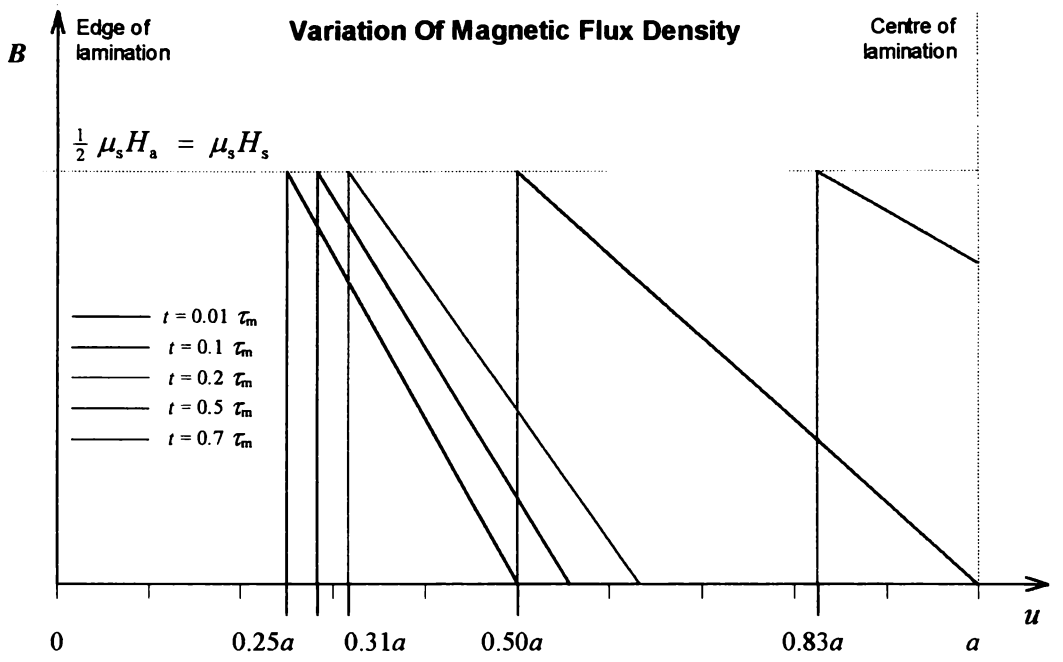

Figure 4-6 *Magnetic Field Penetration - Step Model*

This approximation clearly illustrates the effect of the magnetic field moving into the core. It is not expected, however, that B should drop to zero once the core saturates. The magnetic flux density should equal $B = \mu_0(H + M_s)$ once the core has saturated, that is, the curve should remain almost constant in comparison to the rapid increase of magnetic flux density when $\mu = \mu_s$. This deficiency caused by the step model is improved by use of the attenuation function as illustrated in Section 4.5.2.

4.5.2 ATTENUATION FUNCTION APPROXIMATION

We now use the second approximation for permeability to investigate the band of magnetisation in the core material.

$$\mu(H) = \frac{\mu_i}{1 + \frac{H}{H_k}} \qquad \textit{Equation 4-44}$$

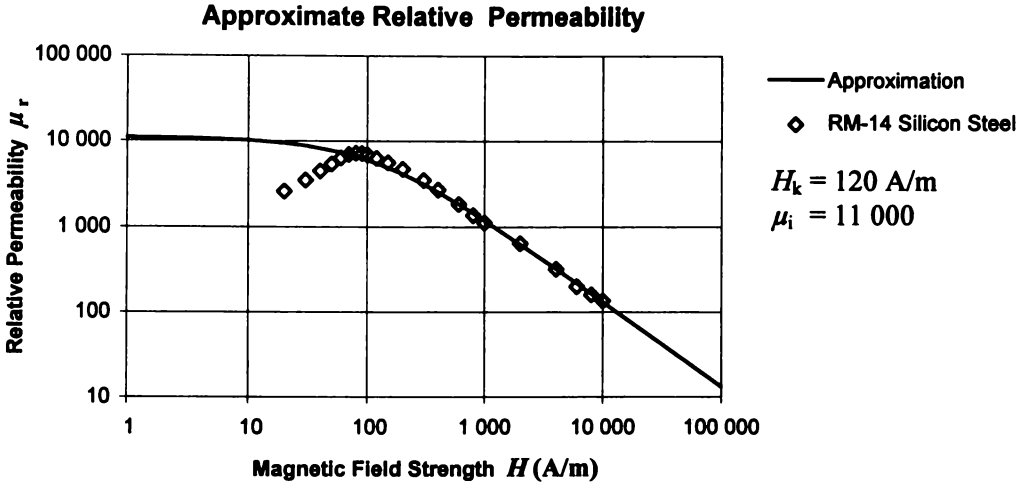

Figure 4-4 *Attenuation Function Approximation For Permeability*

Although the function chosen to model permeability does not correctly represent low magnetic field strength behaviour, this deficiency will not greatly impact the calculations. The impedance of the electric fence energiser discharge circuit is purposely kept very small, which allows the current to very quickly rise above I_k, the level of the current at the knee point of the permeability curve. The magnetic field will take time to penetrate to an arbitrary point in the core, but due to the large value of the driving magnetic field, once magnetised that point will almost instantly reach its peak value and begin to fall. The attenuation function approximation for permeability therefore appears to be a very suitable approximation.

Although the peak of the permeability data shown in Figure 4-4 occurs at around 100 A/m, it is immediately evident from considering the *B-H* loop (see for example Figure 2-3) that this is not the saturation point. For the RM-14 silicon steel whose permeability curve is plotted

in Figure 4-4, saturation is specified at 2.0 T, which corresponds to approximately 60 kA/m and a relative permeability of 22.

Using the attenuation approximation for the permeability then, we can find an expression for the magnetic flux density $B = \frac{d\Phi}{w du}$ by substituting Equations 4-44 and 4-74 into Equation 4-47.

$$\begin{aligned}\frac{d\Phi}{w du} &= \mu H \\ &= \frac{\mu_i}{1+\frac{H}{H_k}} H_a \left[1 - \frac{2u}{a}\left(1 - \frac{t}{\tau_m}\right)\right]\end{aligned}$$

$$\Rightarrow B = \mu_i H_a \frac{1 - \frac{2u}{a}\left(1 - \frac{t}{\tau_m}\right)}{1 + \frac{H_a}{H_k}\left(1 - \frac{2u}{a}\left(1 - \frac{t}{\tau_m}\right)\right)} \qquad \textit{Equation 4-78}$$

Figure 4-7 illustrates the penetration of the magnetic field into the lamination using Equation 4-78. As H_k is smaller than the value for H_s in the step function, and the permeability falls gradually, a larger value of H_a than that used with the step function is required to ensure that the core is driven hard into saturation.[15] Figure 4-7 therefore uses a value of $H_a = 10 \cdot H_k$.

[15] Refer to Footnote 11, where we note that $I_k \sim 0.36$ A and $I_{peak} \sim 300$ A.

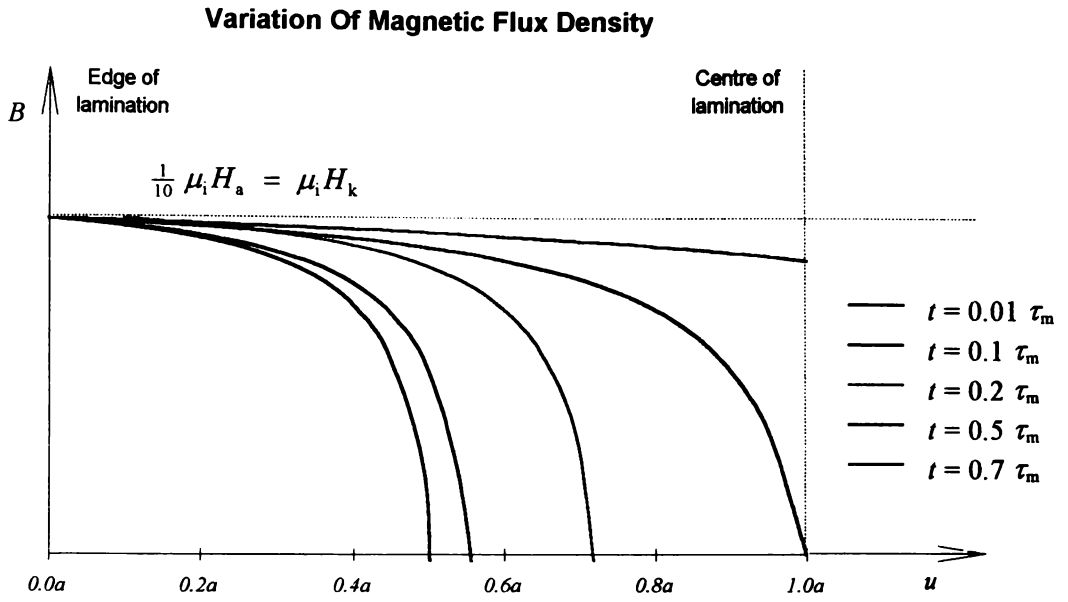

Figure 4-7 *Magnetic Field Penetration - Attenuation Model*

When t is large in relation to the time constant τ_m, the magnetic field strength H will be much greater than H_k, and Equation 4-44 may be simplified to

$$\mu(H) = \frac{\mu_i}{1 + \frac{H}{H_k}}$$

$$\approx \frac{\mu_i H_k}{H} \qquad \textit{Equation 4-79}$$

From Equation 4-47 then, we find that

$$\frac{d\Phi}{w\,du} = \mu H$$

$$= \frac{\mu_i H_k}{H} H$$

$$\Rightarrow B = \mu_i H_k \qquad \textit{Equation 4-80}$$

which is a constant. As noted in Footnote 14, a constant magnetic flux density implies a constant flux and since $V = -N\frac{d\Phi}{dt}$, the output voltage of the transformer will be zero when the core is saturated.

4.6 REMARKS

In discussing magnetisation, Maxwell wrote

> "*The scientific value of a theory of this kind, in which we make so many assumptions, and introduce so many adjustable constants, cannot be estimated merely by its numerical agreement with certain sets of experiments. If it has any value it is because it enables us to form a mental image of what takes place in a piece of iron during magnetisation.*" [*Maxwell* 1892 Vol. II p. 90].

There seems to be a preoccupation these days with the numerical accuracy of a model, especially if used in an electrical circuit simulator. In many cases, the accuracy of the model is critical. However, as Maxwell pointed out, a simplified analytical model may have great value if it allows us to better understand the behaviour of the device. The accurate numerical model and the simplified analytical model are complementary - each has its place in design work.

The equations presented in this chapter have continued to shed light on the behaviour of the output transformer, and have also provided useful information regarding the relationship between the transformer and the capacitive discharge circuit.

Chapter Five ELECTRICAL CIRCUIT MODEL

The primary motivation for developing an electrical circuit model of the pulse transformer is to facilitate simulation. The design of a magnetic component is not a closed process that leads to a unique solution, but is rather an open ended process which combines science with experience. Simulation is therefore particularly useful in transformer design, as multiple design iterations can be quickly tested, reducing dependence upon costly and time consuming prototypes. The output transformer design process in particular will benefit from the use of a reliable simulation model, as this process lacks the design rules and experience which normally guide the engineer.

The benefits of an electrical circuit model are not limited to simulation. A well chosen model may preserve the correspondence between physical geometry and electrical equivalent circuit, and so provide much insight into the relationship between the physical design and electrical behaviour.

In this chapter, an electrical equivalent model of the output transformer is developed using the inductor-reluctance method, with the modelling technique demonstrated using as an example a typical electric fence output transformer. Methods are then presented by which all of the parameters required by the model can be calculated from the specification and geometry of the transformer. This chapter has drawn in particular on the following sources: *Hamill* [1993]; *Severns and Bloom* [1985]; *Severns* [1996, 1997]; *Hayt and Kemmerly* [1971]; and *Harrison* [1992].

5.1 INTRODUCTION

At the turn of the century, transformer inductive modelling was developed to assist with the analysis of fault conditions in power distribution networks. In the 1930s, wide band telephony required the modelling of resistive and capacitive effects. During the time of WWII, pulse transformers for radar emphasised the need for transient models, and very extensive modelling of magnetics was undertaken in the 1950s for mag-amps and other non-linear devices. Since the 1980s, the upsurge of computer simulation has driven new interest in modelling.

Models are representations of the real world which are used, often unconsciously, to assist in understanding a physical reality. In electronics, ideal components are used in theory and simulation to represent observed circuit behaviour. While in most cases the observed behaviour is close to ideal, parasitic elements are an unavoidable property of real components and will cause the part's operation to deviate from that of an ideal component. For example, besides capacitance a real capacitor comprises equivalent series resistance (ESR), equivalent series inductance (ESL), leakage resistance and dielectric absorption [*Duncan* 1991]. These higher order effects become more significant as frequency increases, for example during rapid transients.

A model is not only useful for simulating the performance of a device. A well chosen model can assist in component design and optimisation, and in understanding the circuit's operation. It may even be useful for synthesising a specialised device. The *accuracy* of a model corresponds to how well it represents the true behaviour of a system, but its *usefulness* is related to how well it helps one to understand and analyse the system.

The desired characteristics of a model are that it:

- accurately represents the component;
- is no more complicated than necessary;
- has element values which are readily obtainable from measurement, computation, or finite element analysis;
- relates directly to reality with a minimum of abstraction;
- is compatible with software;
- can be used to design and optimise the component before it is fabricated.

5.1.1 TRANSFORMER MODELLING

Magnetic behaviour is far from ideal and is difficult to represent using discrete components. An example of this is the observed failure to achieve complete power transfer from one winding of a transformer to another. Leakage inductance is essentially a concept created to represent part of this effect, and although it displays the correct circuit behaviour, it is far from being equivalent to the physical process. Non-linear magnetics are in general very poorly modelled.

The purpose of a transformer model is to represent the transformer, a device which combines both magnetic and electric systems, in a form that can be readily understood and manipulated. Magnetic systems are difficult to conceptualise, and because of the electronics engineers' familiarity with electrical circuits, it is natural to think of a magnetic circuit in terms of its electrical analogue. The challenge then is to convert the magnetic circuit into an electrical circuit, which can then be implemented on software such as SPICE which simulates electric circuit behaviour.

There are many different ways to model a transformer for simulation purposes. The method chosen will depend on the particular application, the required accuracy, the acceptable degree of complexity, and in some cases the relative values of the model elements. In some applications a very simple model will suffice - in others, a much more complex model is needed to accurately recreate the behaviour of the physical device.

The simplest model which gives acceptable results should be chosen. Even though most transformers have frequency dependent characteristics, single frequency models are usually adequate [*Severns* 1992]. Of the many types of transformer model available, the *coupled-inductor* model is often chosen although it has the disadvantage of requiring accurate determination of the coupling co-efficient. This method links two coils through mutual inductance. *Inductor-reluctance* models have the form of the familiar transformer equivalent circuit and include an ideal transformer. A comprehensive review of various modelling techniques may be found in *Severns* [1992, 1996].

Software is available which directly simulates the magnetic field and physical geometry of a transformer. These products generally rely on a finite element approach, and although improving rapidly, are still very expensive and difficult to use.

Electrical circuit simulators have, however, become well established in the field of electronics design for prototyping, analysing and optimising circuits. Such is their appeal that a diverse range of systems including acoustic, mechanical and magnetic have been simulated by electrical equivalent circuits.

5.1.2 SPICE

Analogue circuit simulators are predominantly derived from SPICE, a public domain program developed by *Nagel* [1975]. Although originally designed to simulate integrated circuits, SPICE is a general purpose program that has become the standard for electronic circuit simulation. It can perform various analyses, including operating (or quiescent) point calculation, frequency domain simulation, transient (or time-based) simulation, and statistical, sensitivity and worst case analyses. SPICE contains models for both passive and active circuit elements.[1]

SPICE requires the circuit devices and commands to be defined by a standard syntax. The simulation algorithm is then carried out, as summarised by the following steps [*Nichols et. al.* 1994].

Step 1. A coupled set of non-linear first-order differential equations is formulated to represent the behaviour of the circuit.

Step 2. Time derivatives in the differential equations are replaced by finite difference approximations which discretise time.

Step 3. An initial estimate of the solution is made (known as the DC bias point).

Step 4. The time is advanced by the pre-defined time step.

---

[1] The time domain simulation of coupled inductors or transformers on SPICE2 is difficult and the program frequently fails to converge. This weakness in SPICE2 is well known [*Pei and Lauritzen* 1986] and is not related to the inclusion of non-linear elements. Later versions of SPICE do not appear to have addressed this weakness. PSpice 4.05 used during the course of this research is based on SPICE2.

Step 5. The non-linear equations are solved by the Newton-Raphson technique, which takes a linear approximation of the set of circuit equations.

Step 6. The equation set is re-linearised and solved again. This step is repeated to refine the solution estimate until a pre-defined precision is reached.

Step 7. The result is tested to ensure that it is an adequate solution, within the defined tolerance, to the differential equation set at that time point.

Step 8. The time is advanced to the next point, and a prediction made of the solution at the new point. The procedure is repeated from Step 5, using the prediction as the initial estimate of the solution for the Newton-Raphson process.

If Step 7 fails, or Step 5 does not converge, the time step is reduced and the procedure continued.

5.1.3 Magnetic Core Models

Magnetic materials contain a large number of non-linear effects, which poses a major modelling challenge. Despite a considerable amount of research into this subject, the best transformer models still require a significant compromise between accuracy and simplicity.

If the operating conditions are limited such that the transformer can be assumed to operate in the linear region of the *B-H* loop, a "black box" approach using a simple or even linear function to relate *B* and *H* may be sufficient. In this case, the form of the model bears little resemblance to the actual transformer - it is simply intended to produce the correct output for a given input. This approach provides no understanding of the transformer's behaviour, and its use is best restricted to cases where the transformer is a minor and essentially ideal component in the circuit.

A network synthesis approach may be taken to account for higher order effects. *R*, *C* and *L* components are added to the basic transformer equivalent circuit, to account for non-linearities introduced by the magnetic core and parasitic elements inherent in the

transformer. Other attempts to model the non-linear core have included the use of polynomial dependent sources and look-up tables.

The Jiles-Atherton model is a phenomenological approach presented by *Jiles and Atherton* [1986] which relates the hysteresis loop back to the actual processes occurring in magnetic material, and provides the best description to date of ferromagnetic hysteresis. The incorporation of this model into a circuit simulator is difficult [*Williams* 1994] and is the source of many convergence problems.

5.1.4 JILES-ATHERTON BASED MODEL

The model presented by *Harrison* [1992] is the only reference found to a previous attempt to simulate the electric fence output transformer. The focus of this work was the development of a theoretically sound model of the magnetic core, and the final implementation also modelled remanent induction, winding resistance, core loss, parasitic capacitance and path inductance, in addition to the circuitry required to create the capacitive discharge pulse. The modelling of magnetic skin effect was investigated but not successfully implemented.

The length of any air gap present in the magnetic path has a significant impact on magnetic parameters such as effective permeability and remanent flux density. *Harrison* [1992] developed an experimental method which found an accurate value for the air gap length by comparing changes in inductance. By analysing simulation results, the major loss component in the circuit was identified as being series resistance in the primary discharge path. This was confirmed experimentally.

Both E-I core and I core transformers were successfully simulated, optimised and designed with the aid of this model.

The energiser discharge, a transient application with rapid switching of an SCR releasing a high-current flow from a storage capacitor, is a difficult application for the SPICE algorithm to successfully simulate. The Jiles-Atherton non-linear magnetic core model is also known to cause convergence errors when implemented in SPICE [*Prigozy* 1994], and is disregarded by almost all design engineers for this reason. Only two SPICE simulators currently use the Jiles-Atherton approach - MicroSim's *PSpice* and Spectrum's *MicroCap*.

Another criticism of the Jiles-Atherton implementation concerns the difficulty of obtaining values for the parameters of interdomain coupling, thermal energy, domain anisotropy and domain flexing, which are required by the model. These parameter values are not available from manufacturers, nor can they be derived from published data, and therefore must be found using a curve fitting approach.

The geometry of the transformer, a key consideration in any design, is not directly modelled by *Harrison* [1992], and consequently the model provides no information about the physical implementation of the transformer.

5.1.5 PHYSICAL MODEL

The inductor-reluctance method is chosen for the development of the output transformer model primarily because it is a physical model, that is, there is direct equivalence between the model and the real transformer. Approximations are still required, but are based on a sound knowledge of the application and operation of the output transformer. The model presented in this thesis is developed entirely from the physical geometry of the transformer.

Severns explains the benefits of a physical model as follows.

> "*Models which are derived directly from the structure of the magnetic component ... are referred to as physical models. This class of models has several advantages. Because they follow the actual physical structure of the component they maintain an intuitive feeling related to the behaviour of the component. This is very helpful in avoiding mistakes and providing guidance in tweaking a model when it doesn't quite do the job. This technique is also very helpful in determining the distribution of parasitic inductances in complex multi layer structures such as those found in high voltage transformers. Having determined the proper distribution of the inductances makes it much easier to properly assign locations and values for parasitic capacitances which are of particular importance in high voltage applications.*" [*Severns* 1992 p. 22].

The principle behind a physical model is to define a magnetic circuit and convert it to an electric circuit by Equation 2-36.

$$V = -N\frac{d\Phi}{dt} = -L\frac{dI}{dt} \qquad \textit{Equation 2-36}$$

Under specified conditions, a synthesised model may provide results which more closely match the measured performance than the model developed here, but the benefits of the chosen approach greatly outweigh its limitations. This thesis improves on the previous model presented by *Harrison* [1992] in the following areas:

- the model is a direct representation of the physical transformer. Geometry is reflected in the model, and changes to the model have physical significance and can be directly related to changes in the transformer design;

- the model is general in the sense that the equivalent parameters are not specific to any particular energiser or fence operating conditions. Hence the model is valid for a wide range of operating conditions;

- the internal behaviour of the transformer is represented by equivalent parameters which may be analysed and varied in the simulation, thus providing greater understanding of output transformer behaviour;

- the model is completely defined by the geometry, winding arrangement and specification of the transformer, and a design may therefore be simulated and optimised without the need to build a prototype or take measurements on a physical sample;

- the model is independent of the simulator. As saturation is a major factor in output transformers, the non-linear magnetic core model has been a key consideration in the past when selecting simulation software. The model presented here provides the flexibility of using a complex representation of the magnetic core, or a simplified model, or even a linear approximation should operating conditions allow;

- the model is valid for any core arrangement, including I-cores and other incomplete cores shapes.

It is important that the output transformer model never be considered independently of the surrounding circuit. Parasitic elements in the circuit can have a significant influence on the output performance [*Harrison* 1992]. It would not be unusual for the resistance of the discharge path to have a greater impact on the results than the transformer winding resistance.

5.2 MODEL DEVELOPMENT

Figure 5-1 contains all of the information required to derive the output transformer model and calculate all parameter values for the transformer shown.

To illustrate the modelling process, a complete model will be derived with all parameter values calculated for one particular design. Once understood, the principles can easily be applied to any output transformer.

Calculations for parasitic elements such as coil capacitance and leakage inductance can only be as accurate as the representation on which the calculations are based. For example, in order to calculate the secondary coil capacitance the coil is assumed to be perfectly layer wound, although in practice this would never be the case. It would be impractical if not impossible to calculate the capacitance based on a randomly wound coil, and measurement is therefore likely to yield a more accurate value than calculation. A model based on measured values may therefore produce more accurate results [*Glasoe and Lebacqz* 1948 p. 53]. However, the calculated values are more useful in that they allow the model to be created before the transformer has been built, and they are valid for various operating conditions. Measured values are strictly only applicable to the transformer and operating conditions under which they were measured.

Measured values may however be substituted for calculated values where they are available.

5.2.1 TRANSFORMER SPECIFICATION

The key to a successful model is to carefully define the layout and winding arrangement, shown here in Figure 5-1a, as this is the basis from which the electrical equivalent model is developed. The physical structure of the transformer is drawn with lamination and bobbin dimensions accurately defined. In this example, the coils are encapsulated with epoxy resin to provide greater dielectric strength and mechanical stability.

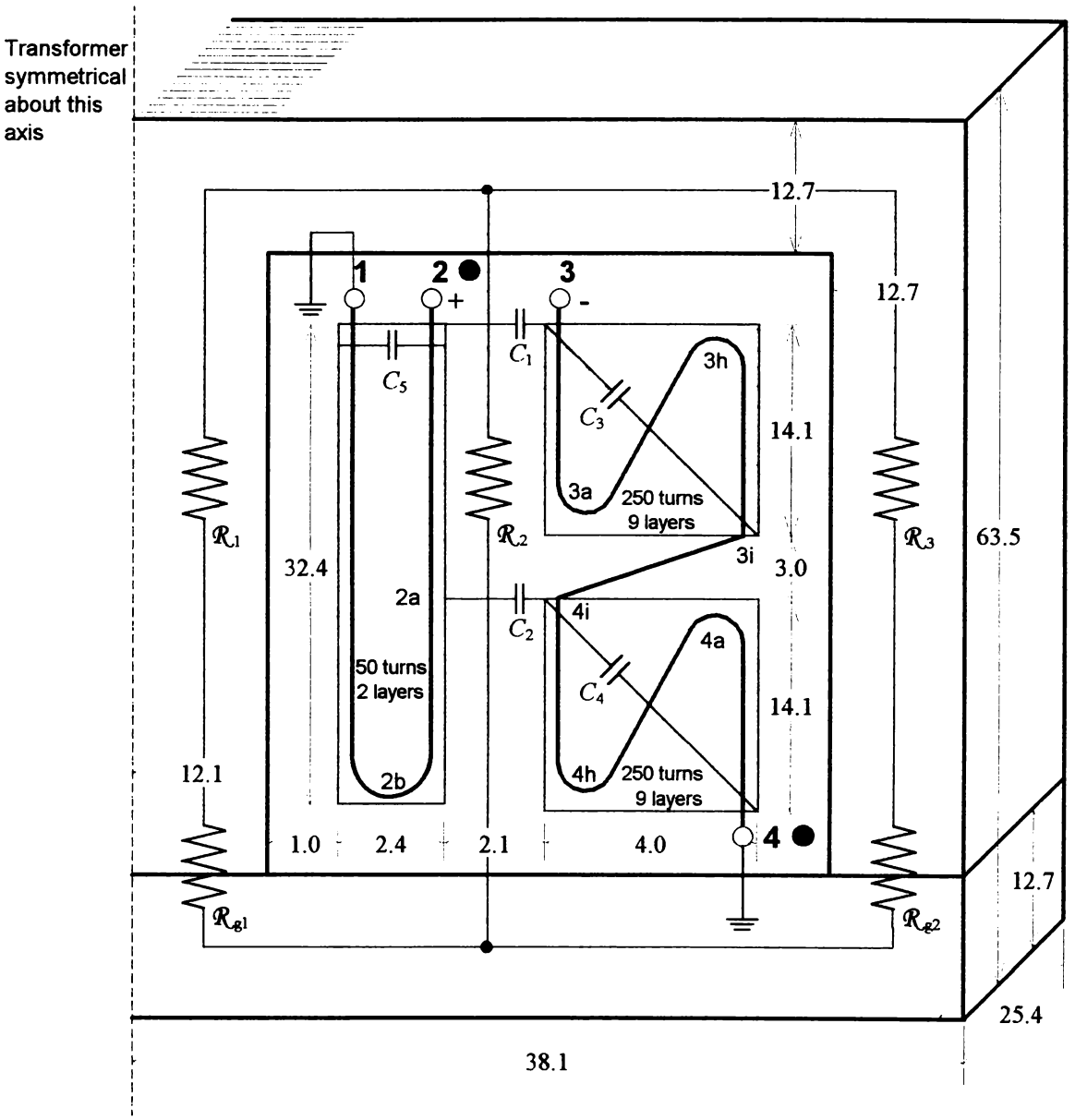

Figure 5-1a *Transformer Layout* (dimensions in mm)

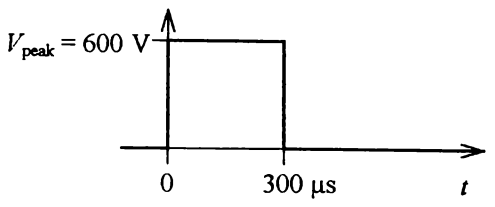

Figure 5-1b *Idealised Primary Pulse*

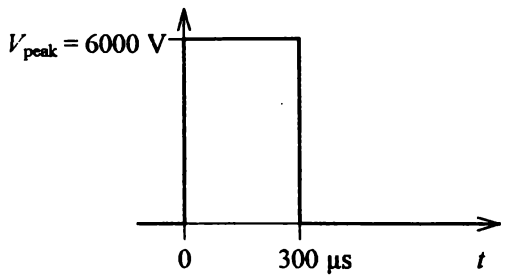

Figure 5-1c *Idealised Secondary Pulse*

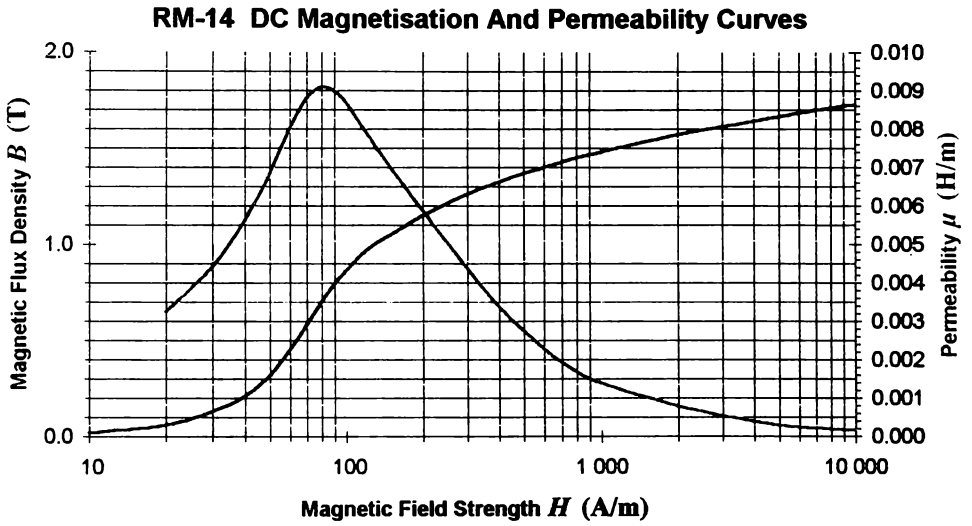

Figure 5-1d *Magnetic Material Characteristics*

Engineering Data

Primary Wire	Size: 1.12 mm	Outer Ø: 1.217 mm	Resistance: 17.98 x 10^{-3} Ω/m
Secondary Wire	Size: 0.40 mm	Outer Ø: 0.462 mm	Resistance: 141.76 x 10^{-3} Ω/m
Lamination	Size: #43A	Grade: RM-14	Resistivity: 45 x 10^{-8} Ω·m
Bobbin	Material: Pocan B 4235		Dielectric Constant: 3.9
Encapsulant	Material: Araldite Epoxy Resin		Dielectric Constant: 3.9

Figure 5-1e *Material Data*

A representation of the two concentrically wound coils is superimposed on top of the physical layout, and it is important that this accurately defines winding directions, wire positions and voltage potentials. The wires exit the transformer at the terminals labelled 1 and 2 (primary coil) and 3 and 4 (secondary coil). The dot notation is used to indicate polarity, and since this transformer is configured for a negative output pulse, terminal 3 will be negative with respect to the grounded terminal 4.

Windings are the sources in a magnetic circuit, creating the flux which flows primarily through the core material. Each distinct section of the magnetic circuit is assigned a reluctance, labelled here as $\mathcal{R}_1$ and $\mathcal{R}_3$. As leakage is a significant factor in pulse transformers, the leakage path identified by $\mathcal{R}_2$ is included. The primary and secondary coils are layer-wound, so there will be no other significant leakage paths.

The transformer core is assembled from separate stacks of E and I laminations butted against each other. This design results in a significant air gap between the two stacks of laminations. Although the air gap length is very small in comparison with the total magnetic path length, the reluctance of the gap can prove to be significant since the permeability of air is much less than the permeability of the lamination. The air gaps are indicated by $\mathcal{R}_{g1}$ and $\mathcal{R}_{g2}$.

When the capacitive discharge occurs, the pulses represented by Figures 5-1b and 5-1c pass through the windings. At its peak, the voltage potentials caused by the pulse are significant between the layers of each coil, and between the coils. A distributed parasitic capacitance must be modelled by a single lumped equivalent capacitor, which stores the same amount of energy as that stored by the distributed capacitance.

When voltage is present across terminals 1 and 2, the potential difference between the two layers of the primary coil will reduce with distance from the terminals becoming zero at point 2b. The potential difference will be greatest at the terminals, and so the primary coil capacitance C_5 is placed at this point. Capacitance between adjacent layers of the two coils will also be greatest at the point of greatest potential, as shown by the placement of C_1 and C_2. Inter-winding capacitance within each of the sections of the secondary coil is represented by C_3 and C_4 connected from the start to the finish of each section. The placement of these capacitors illustrates the importance of drawing an accurate physical layout.

Parasitic capacitance would also exist between the coils and the core. Calculations following the methods presented in Section 5.2.3 resulted in values of 11 pF for the primary to core capacitance and 9 pF for the secondary to core capacitance - negligibly small in comparison with C_1 - C_5. The capacitance that exists between adjacent turns and layers of the same coil is also negligible in comparison with the inter-coil capacitance [*Glasoe and Lebacqz* 1948 p. 520]. These additional parasitic capacitances will therefore not be included in the model.

5.2.2 INDUCTOR-RELUCTANCE METHOD

The output transformer model uses the inductor-reluctance method to convert the complex, distributed magnetic circuit into an inductance model consisting of a network of inductors and transformers. This can then be connected directly into the surrounding electrical circuit. Inductor-reluctance modelling consists of four steps [*Hamill* 1993].

Step 1. The magnetic circuit of the transformer is represented by a reluctance model, which is drawn in terms of magnetic voltages F_m and magnetic resistances $\mathcal{R}$.

Step 2. The dual of the reluctance model is formed by applying the laws of electrical voltage-current duality converted to its magnetic circuit equivalent[2]:

- network loops become nodes;
- network nodes become loops;
- each mmf F_m [A] becomes a flux source with the same numerical value $\Phi = F_m^*$ [Wb];
- each reluctance, $\mathcal{R}$ [H^{-1}] is replaced by a permeance of the same numerical value $\mathcal{P} = \mathcal{R}^*$ [H].

Step 3. One winding is chosen as the reference winding, having N_{ref} turns. The current source associated with each winding of N_i turns is replaced by an ideal transformer of ratio $N_{ref}:N_i$ feeding a pair of terminals. Each permeance $\mathcal{P}$ [H] is scaled by N_{ref}^2.

Step 4. Each permeance is replaced by an inductance $L = N_{ref}^2 \mathcal{P}$ [H] (Equation 2-35).

The magnetic circuit of Figure 5-1a, drawn in terms of magnetic voltages F_m and magnetic resistances $\mathcal{R}$, is shown in Figure 5-2. To allow parasitic capacitance to be added as shown in Figure 5-1a, the sources must be divided equally to create the necessary nodes.

---

[2] Magnetic circuit duality is discussed in more detail in Appendix 1.

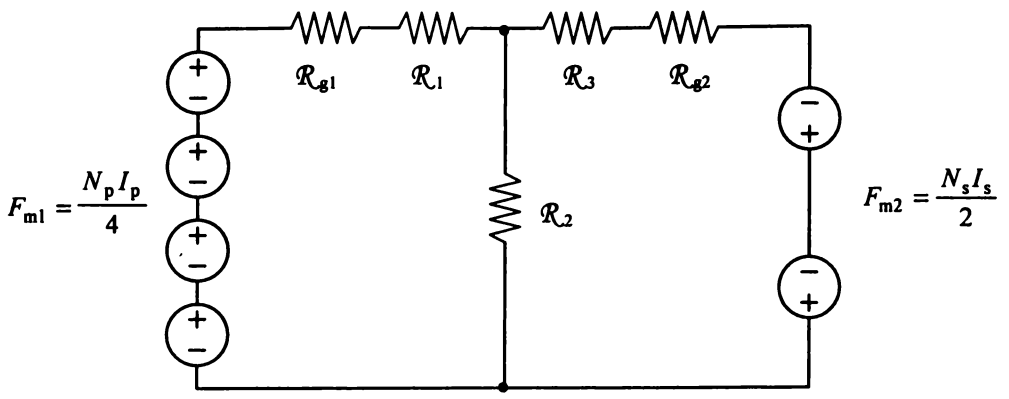

Figure 5-2 *Magnetic Circuit*

Following the principles of duality, the dual of this circuit is drawn as in Figure 5-3.

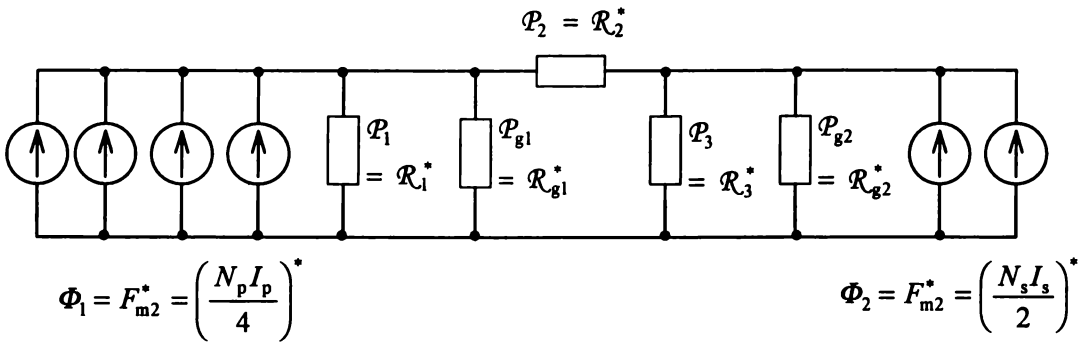

Figure 5-3 *Magnetic Circuit Dual*

The circuit is next scaled to render it in a more usable form. The transformer's primary winding will be chosen as the reference winding, and the associated current sources are replaced by ideal transformers with a turns ratio of $(N_p/4):N_p$. The secondary current sources are replaced by ideal transformers with a turns ratio of $N_p:(N_s/2)$. The permeances can be replaced directly by inductors.

With this scaling, the circuit has the form of Figure 5-4.

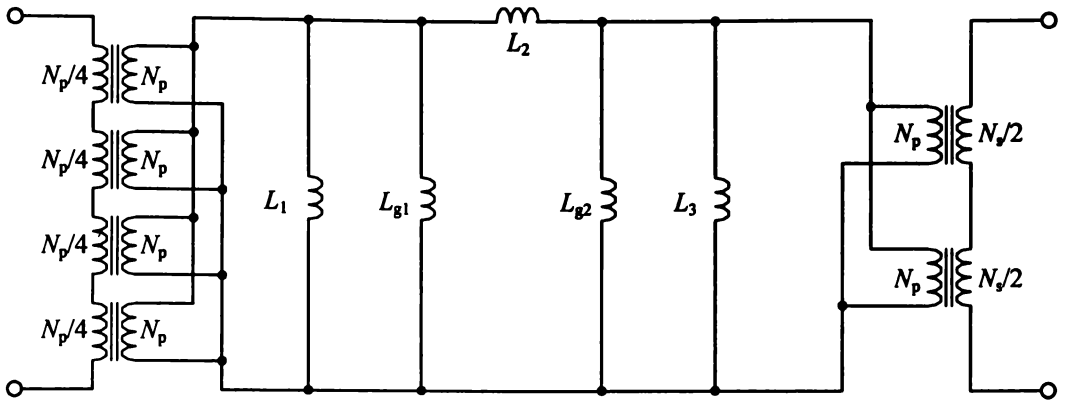

Figure 5-4 *Magnetic Circuit Model*

This circuit can be further simplified by reflecting inductance to the primary side of the transformer, noting that as the turns ratio is equal to unity, the inductance does not change in magnitude when reflected across the transformer. The diagram is then simplified by making use of the identities [*Severns* 1996] shown in Figure 5-5.

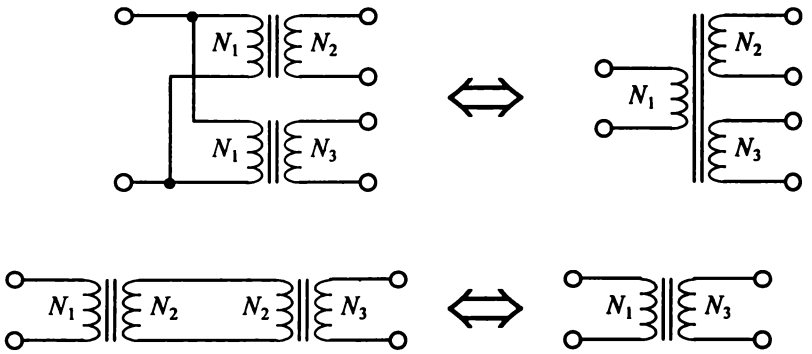

Figure 5-5 *Transformer Identities*

The inductance model of the output transformer is then drawn as

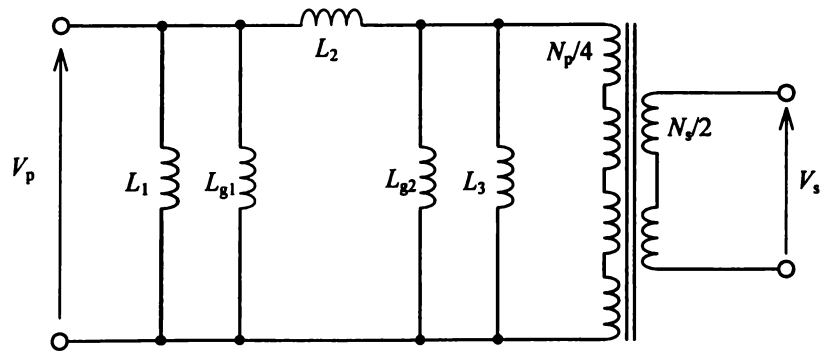

Figure 5-6 *Simplified Magnetic Circuit Model*

Referring to Figure 5-1a, the remainder of the equivalent circuit of the output transformer can be added. The lumped parasitic capacitances are placed between the appropriate nodes of the model. A non-linear magnetic core is indicated for L_1 and L_3, which represent the magnetic flux path through the laminations. Resistors representing coil resistance are added to the primary and secondary, positioned so that they conduct the correct amount of current. A constant resistance whose value is the DC resistance of the coil is of sufficient accuracy for this application.[3]

Although "*representing the losses remains somewhat of an art*" [*Dugan et. al.* 1989], in this application a simple resistance placed across the magnetising inductance has been found to be satisfactory [*Harrison* 1992 p. 108, *Glasoe and Lebacqz* 1948 p. 510]. The dominant frequencies of the output pulse occur at around 1 kHz, and the waveform consists of a single pulse once per second. The total core loss is therefore much less than is usual for transformers, and has been shown to be an order of magnitude less than the winding losses [*Harrison* 1992 pp. 162-164]. In the interests of circuit simplicity, a simple equivalent core loss resistance will be used.[4]

The energiser output transformer model is now complete and is shown in Figure 5-7.

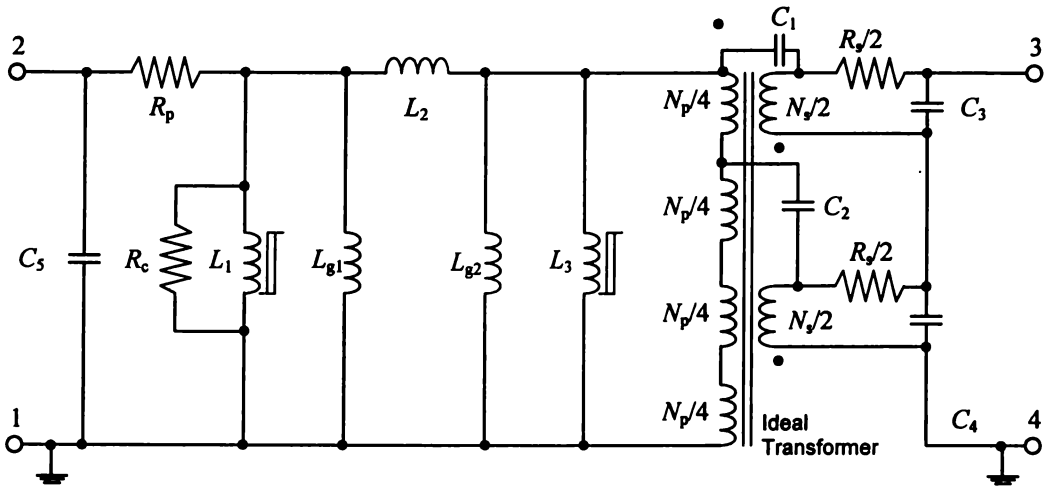

Figure 5-7 *Output Transformer Model*

[3] This conclusion is reached by *Harrison* [1992 pp. 130 - 131] during his investigation of winding resistance, and is discussed in more detail in Section 5.2.3.

[4] *Glasoe and Lebacqz* [1948] also use an equivalent resistance to represent core losses in high-power pulse transformers, and go so far as to suggest that under some conditions even this resistance may not be required.

5.2.3 Calculation Of Parameter Values

The model of Figure 5-7 requires the following parameters values.

- L_1 Central flux path inductance
- L_2 Leakage flux path inductance
- L_3 Outer flux path inductance
- L_{g1}, L_{g2} Air gap inductance
- C_1, C_2 Primary-secondary capacitance
- C_3, C_4 Secondary coil capacitance
- C_5 Primary coil capacitance
- R_p Primary winding resistance
- R_s Secondary winding resistance
- R_c Equivalent core loss resistance
- N_p Primary turns
- N_s Secondary turns

This section describes how all of these values may be calculated from the transformer specification. N_p and N_s are of course specified.

5.2.3.1 L_1 Central Flux Path Inductance

Inductance is calculated from

$$L = \frac{\mu N^2 A}{\ell} \qquad \textit{Equation 2-34}$$

From the transformer geometry and magnetic core data of Figure 5-1, the following values apply to L_1.

N_p	$= 50$	reference winding chosen for the inductance model
μ_1	≈ 0.006 H/m	at 1.2 T, an average value assuming no saturation[5]
A_1	$= (12.1 \text{ mm} \times 2) \times 25.4 \text{ mm}$	area of magnetic core centre limb
	$= 6.15 \times 10^{-4} \text{ m}^2$	
ℓ_1	$= 50.8 \times 10^{-3}$ m	average path length of centre limb only

$\Rightarrow \quad L_1 = 182$ mH

5.2.3.2 L_2 Leakage Flux Path Inductance

Leakage flux is that flux produced by one coil which does not link the other. For a layer-wound shell-form transformer, this flux travels almost entirely through the space between the primary and secondary.

In considering the reluctance model of Figure 5-1, $\mathcal{R}_2$ is simply an alternative path for the flux to travel, and the amount of leakage flux that follows this path will be proportional to its reluctance. Although less well defined than $\mathcal{R}_1$ or $\mathcal{R}_2$, its value can nevertheless be found from the geometry of the transformer, and may therefore be calculated by Equation 2-34.

---

[5] The effect of pulse magnetisation is neglected here, but is discussed in Section 5.3.

The separation of the coils is estimated as being the distance between the centres of the adjacent layers of the primary and secondary windings. This is therefore the thickness of the bobbin plus half the thickness of the primary plus secondary wires. We therefore have the following values.

$N_p = 50$

$\mu_0 = 4\pi \times 10^{-7}$ H/m

$A_2 \approx (35.6 \text{ mm})^2 - (29.88 \text{ mm})^2$ area between windings

$= 3.75 \times 10^{-4} \text{ m}^2$

$\ell_2 = 38.1 \times 10^{-3}$ m path length in air only between the coils

$\Rightarrow \quad L_2 = 32$ μH[6]

5.2.3.3 L_3 Outer Flux Path Inductance

As this flux path is through magnetic material, the reluctance is well defined and the permeability is the same as for L_1. From Figure 5-1,

where $N_p = 50$

$\mu_3 \approx 0.006$ H/m at 1.2 T[5]

$A_3 = 2 \times (12.7 \text{ mm} \times 25.4 \text{ mm})$ twice area of single outer limb

$= 6.45 \times 10^{-4} \text{ m}^2$

$\ell_3 = 102.2 \times 10^{-3}$ m effective path length of core less central limb

$\Rightarrow L_3 = 95$ mH

---

[6] *Dauhajre and Middlebrook* [1986] derive the following expression for effective leakage inductance by a consideration of magnetic energy.

$$L_2 = \frac{1}{3}\mu_0 N_p^2 \frac{h}{b} mlt$$

where h = build height of coils

b = coil width

mlt = mean length per turn = $2\pi\left(r_0 + \frac{h}{2}\right)$

r_0 = radius of inner coil

Although not all of the assumptions made in this derivation are valid for the output transformer, evaluation of this expression yielded a result very similar to that obtained by considering the reluctance of the leakage path.

With $N_p = 50$, $b = 32.4$ mm, $h = 8.5$ mm and $r_0 = 13.1$ mm, we find that $L_2 = 30$ μH.

5.2.3.4 L_{g1} Centre Limb Air Gap

The gap length is difficult to measure accurately, and must be estimated for the chosen design if the transformer has not been built. Typical figures are sometimes available from the manufacturer. Toroidal cores of powdered iron or ferrite material do not have an external air gap, but have a distributed gap inherent in the core material, the effect of which is taken into account by the low value of effective permeability.

The design of the example under consideration uses two stacks of laminations which are butt joined - that is, they are simply placed next to each other as opposed to being interleaved or welded, which are common techniques used to reduce the air gap of a laminated core. Butted laminations have a relatively large air gap, and we will use here the figure of 7×10^{-5} m for the total air gap found by *Harrison* [1992 p. 134]. This may be used as a typical value for the air gap length of butt joined lamination stacks.

The effect of flux fringing at the edges of the air gap can be taken into account with a correction factor [*Klontz, Novotny and Severns* 1997 §1.11]. However, since the faces of the gap are large compared to the gap length, in this example the correction factor is less than 1 %. The uncertainty in the value of gap length itself is much greater than this, so fringing is not significant here and will be ignored.

It is interesting to note that, despite the air gap length being only 0.02 % of the total magnetic path length, the inductance L_{g1} of the gap (which is inversely proportional to reluctance) is almost 20 % of the entire path inductance. The gap is therefore a significant factor in the design.[7]

[7] As calculated in Chapter 3.3 and noted in Section 5.3, the effects of pulse magnetisation result in values for L_1 and L_2 being much less than those calculated here. As a result, the air gap is less significant in the output transformer design than in most steady-state transformers, a result well-known in practice.

We then have for the centre limb air gap:

where $N_p = 50$

$A_1 \approx (12.1 \text{ mm} \times 2) \times 25.4 \text{ mm} = 6.15 \times 10^{-4} \text{ m}^2$ area of core centre limb

$\ell_{g1} = 3.5 \times 10^{-5}$ m half the quoted air gap length

$\Rightarrow L_{g1} = 55$ mH

5.2.3.5 L_{g2} Outer Leg Air Gap

The comments made regarding the centre limb air gap also apply to the outer leg air gap. The only difference in parameter values is a slightly different area.

$N_p = 50$

$A_3 \approx 2 \times (12.7 \text{ mm} \times 25.4 \text{ mm}) = 6.45 \times 10^{-4} \text{ m}^2$ twice area of single outer limb

$\ell_{g2} = 3.5 \times 10^{-5}$ m half the quoted air gap length

$\Rightarrow L_{g2} = 58$ mH

5.2.3.6 C_1 Primary - Secondary Capacitance

Parasitic capacitance in transformers accounts for energy stored in the electric field which exists between any conductors that have a potential difference. The stored energy is proportional to the square of the voltage, and so parasitic capacitance will be greatest where there exists the largest potential difference.

Energy storage occurs in both static and dynamic volumetric fields. Parasitic capacitance is therefore difficult to model because of the non-uniform electric fields involved, and the fact that the fields are a function of the configuration in which the transformer is used. The traditional approach has been to either ignore or estimate transformer parasitics using static field equations.

Although a static capacitance can be calculated from the geometry of the transformer, a more accurate equivalent value is obtained by taking into account the dynamic non-uniform field that results from the pulse discharge [*Collins* 1990].[8] An outline of the steps follows.

Step 1. Calculate the static volumetric capacitance C_s from Equation 5-1 by considering the primary and secondary coils as a parallel plate configuration as shown in Figure 5-8.

$$C_s = \frac{\varepsilon_r \varepsilon_0 \ell_e x}{d} \qquad \textit{Equation 5-1}$$

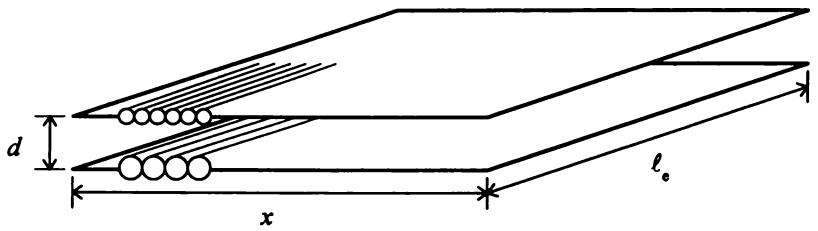

Figure 5-8 *Parallel Plate Capacitor*

Step 2. Determine the phase-voltage diagram $V(x)$ from the circuit configuration.

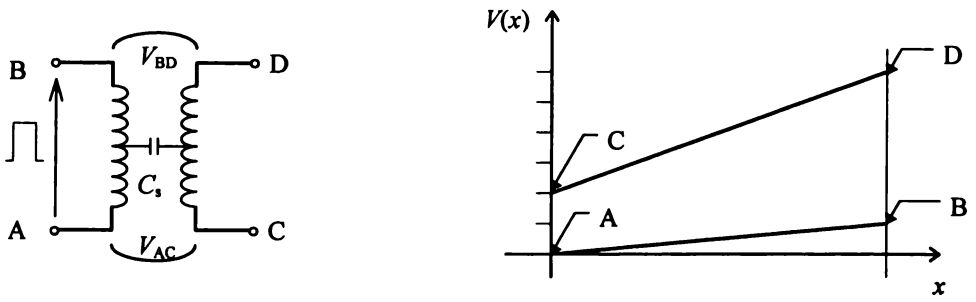

Figure 5-9 *Phase-Voltage Diagram*

Step 3. Determine the potential differences V_{AC} and V_{BD} from the phase-voltage diagram.

Step 4. Calculate the dynamic equivalent capacitance using Equation 5-2.

[8] The method of calculating this equivalent capacitance is discussed in greater detail in Appendix 2.

$$C_d = \frac{\left(V_{AC}^2 + V_{AC}V_{BD} + V_{BD}^2\right)}{3V_{peak}^2} C_s \qquad \textit{Equation 5-2}$$

Applying these steps to C_1, first the static capacitance is calculated.

where $\varepsilon_r = 3.9$ Pocan B 4235, the material used for the bobbin

$\varepsilon_0 = 8.85 \times 10^{-12}$ F/m

$\ell_e \approx 139$ mm ½ (outside diameter of primary winding + inside diameter of secondary winding)

$x = 14.1$ mm

$d = 2.1$ mm

$\Rightarrow \quad C_s = 32$ pF

Since succeeding layers of the coil effectively shield the preceding layers, we need only consider layers of the windings which are adjacent [*Collins* 1990 p. 1097]. The input pulse is approximated by the square pulse shown in Figure 5-1b.

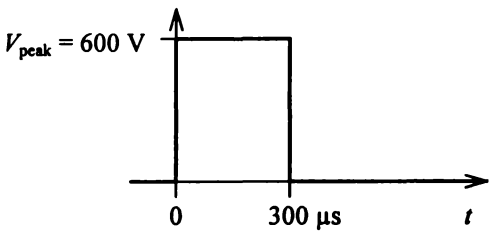

Figure 5-1b *Idealised Primary Pulse*

Referring to Figure 5-1a, the primary has a maximum voltage differential of 600 V, which is 300 V per layer. The peak output voltage will be taken as -6 kV, which over two sections and nine layers per section results in -330 V per layer. The phase-voltage diagram for C_1 can therefore be drawn as shown in Figure 5-10.

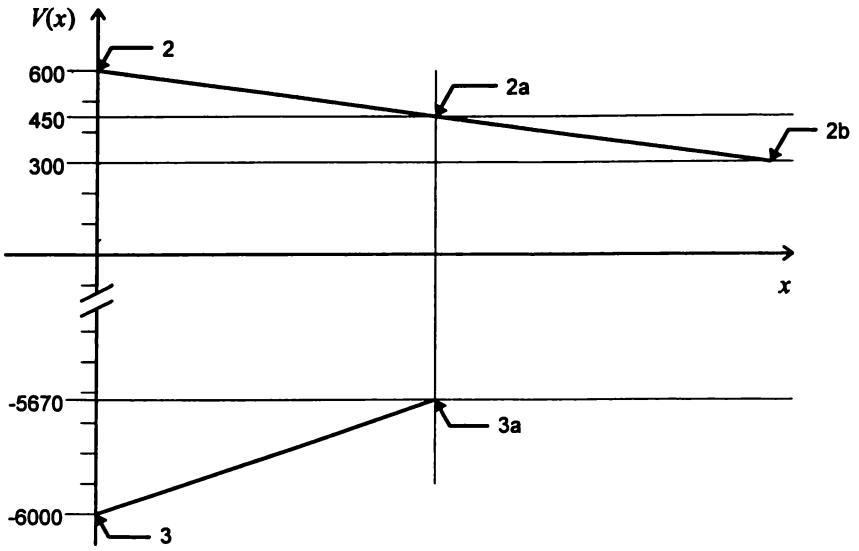

Figure 5-10 *Phase-Voltage Diagram For* C_1

From Figure 5-10 we find that V_{23} = 6600 V, and V_{2a3a} = 6120 V, and from these values we have

$$C_d = \frac{\left(V_{23}^2 + V_{23}V_{2a3a} + V_{2a3a}^2\right)}{3V_{peak}^2} C_s$$
$$= 112C_s$$

In other words, considering the effects of the dynamic non-uniform field results in a value for the parasitic capacitance which is 112 times the value of the static result calculated from the coil geometry. Given that there are very large potential differences between the primary and secondary, and especially between the terminals 2 and 3, this result is not surprising.

Since C_s = 32 pF we have

$$C_1 = 3.6 \text{ nF}$$

5.2.3.7 C_2 Primary - Secondary Capacitance

The geometry of the static capacitance for C_2 is the same as C_1, and hence the static capacitance C_s is 32 pF. We draw the phase-voltage diagram as

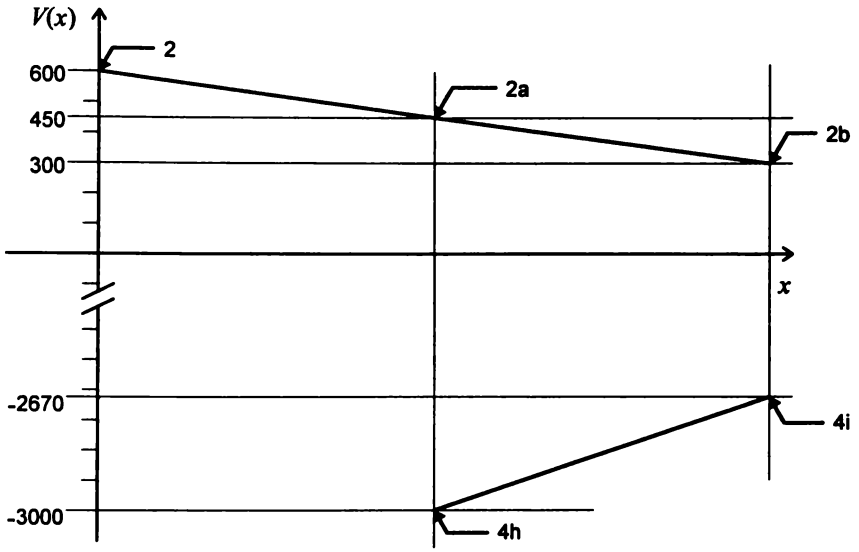

Figure 5-11 *Phase-Voltage Diagram For C_2*

From this diagram we see that $V_{2a4h} = 3450$ V, and $V_{2b4i} = 2970$ V. This leads to

$$C_d = 28.3C_s$$

Compared to C_1, the reduction in parasitic capacitance as a result of the lower potential differences is very noticeable. Since $C_s = 32$ pF we have

$$C_2 = 0.91 \text{ nF}$$

5.2.3.8 C_3 Secondary Coil Capacitance

The parasitic capacitance present in the secondary coil as a result of potential differences between the turns can also be calculated using the general method described in Appendix 2. The calculation assumes an ideal geometry and pulse shape which can never be realised in practice. However, this method allows us to determine a reasonable value from the

geometry. The interturn capacitance can be shown to be negligible in comparison with the interlayer capacitance [*Glasoe and Lebacqz* 1948 p. 520].

C_3 is the capacitance inherent in the section of the secondary coil indicated by 3 - 3i. An ideal representation of this half of the secondary coil is shown in Figure 5-12.

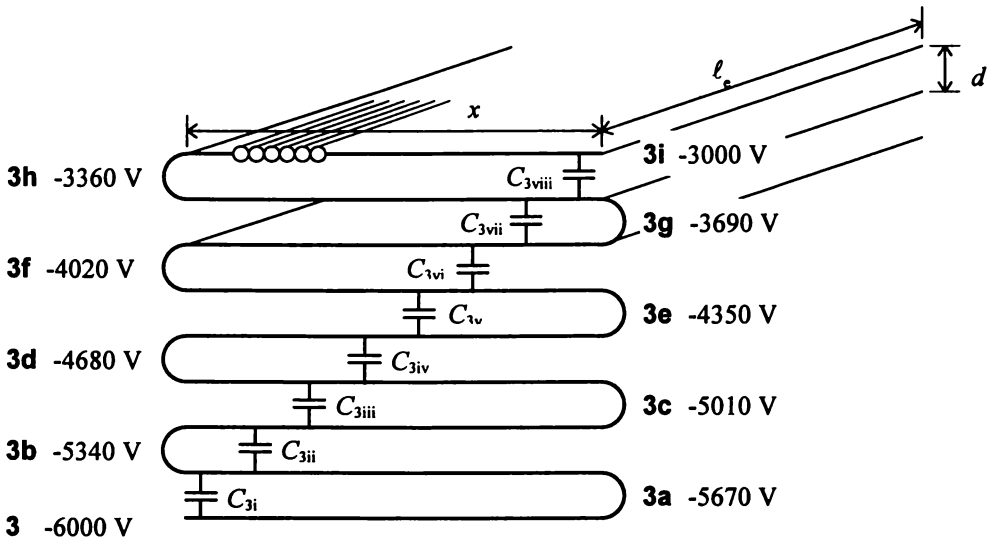

Figure 5-12 *Secondary Coil Capacitance*

As noted previously, each layer of the coil will effectively shield the next, so we need only calculate the capacitance between adjacent layers.

Consider first the capacitance C_{3i} between layers 3-3a and 3a-3b. The following values are applicable for the calculation of this static capacitance using Equation 5-1. To simplify later calculations, we have assumed here that ℓ_e is the mean length per turn for the entire coil, and thus is the same for all layers. The following values and resulting static capacitance therefore apply to all layers of the ideal coil.

$\varepsilon_r = 3.9$	Araldite epoxy resin, used to encapsulate the coil
$\ell_e \approx 173.6$ mm	coil mean length per turn
$x = 14.1$ mm	
$d = 0.46$ mm	distance between centres of the wires in adjacent layers

$\Rightarrow C_s = 184$ pF

The dynamic capacitance C_{3i} has the following phase-voltage diagram.

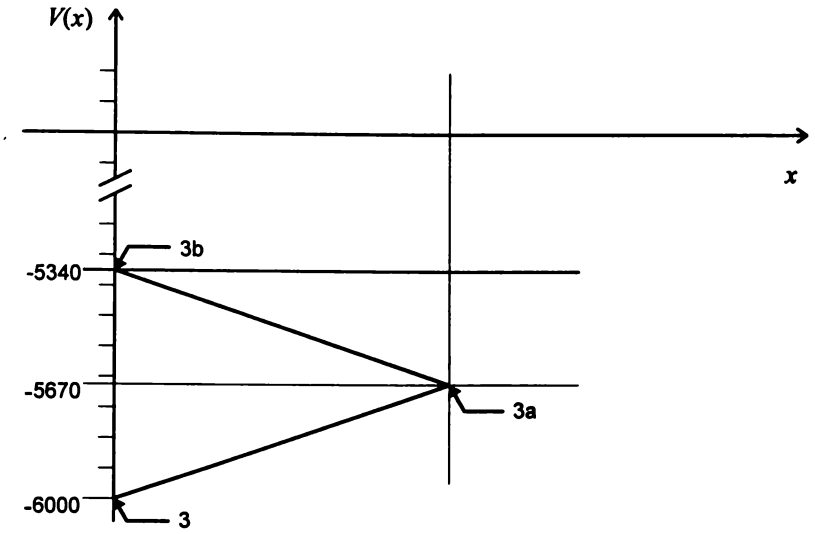

Figure 5-13 *Phase-Voltage Diagram For* C_{3i}

Here we have $V_{33a} = 660$ V, and $V_{3a} = 0$ V. We then find that $C_{3i} = 4.0 \times 10^{-3} C_s$, where $C_s = 184$ pF

$\Rightarrow \quad C_{3i} = 0.74$ pF

We next consider the capacitance C_{3ii} between layers 3a-3b and 3b-3c. $C_s = 184$ pF as found previously, but we also note from Figure 5-14 that the voltage differentials on the phase-voltage diagram are symmetrical to C_{3i}. As the capacitance is determined by the potential difference only, and not the magnitude of the voltage, the capacitance between each layer will be the same.

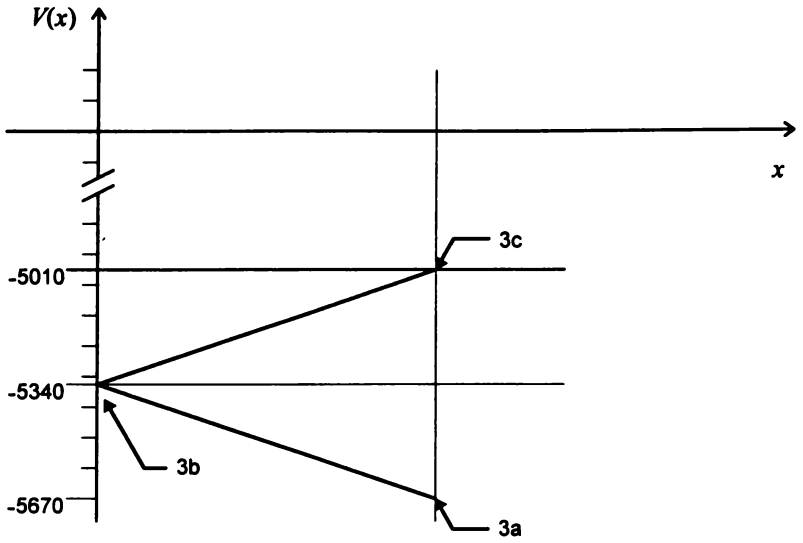

Figure 5-14 *Phase-Voltage Diagram For* C_{3ii}

Hence we have $C_{3i} = C_{3ii} = \ldots = C_{3viii} = 0.74$ pF, and the total coil capacitance is the sum of the capacitances between each layer [*Glasoe and Lebacqz* 1948 p. 520].

$$C_3 = \sum_{n=i}^{viii} C_{3n} = 5.9 \text{ pF}$$

5.2.3.9 C_4 Secondary Coil Capacitance

The geometry of both sections of the secondary coil is the same, and as the parasitic capacitance is determined by voltage differentials, the coil capacitance for both sections of the secondary will also be equal.

$\therefore \quad C_4 = 5.9$ pF

5.2.3.10 C_5 Primary Coil Capacitance

As the primary coil has only two layers, the calculation for this is simplified.

From Equation 5-1,

where $\varepsilon_r = 3.9$ Araldite epoxy resin, used to encapsulate the coil

$\ell_e \approx 127.6$ mm coil mean length per turn

$x = 32.4$ mm

$d = 1.2$ mm distance between centres of the wires in adjacent layers

$\Rightarrow \quad C_s = 119$ pF

As before, the primary voltage is assumed to be a 600 V square pulse, and the phase-voltage diagram of Figure 5-15 shows that $V_{12} = 600$ V, and $V_{2b} = 0$ V.

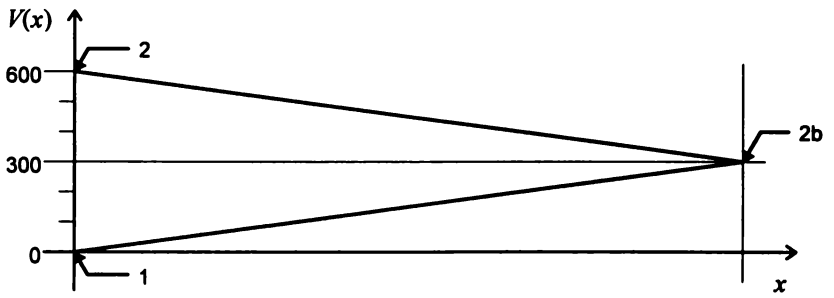

Figure 5-15 *Phase-Voltage Diagram For C_5*

This leads to

$$C_5 = 0.333 C_s = 39.7 \text{ pF}$$

5.2.3.11 R_p Primary Winding Resistance

The winding resistance of a coil is increased at high frequencies due to copper skin effect and proximity effect. The electric fence pulse has a frequency spectrum which falls to almost zero above 20 kHz and has a peak at around 1 kHz (see for example Figure 5-20).

Using Equation 2-46, the skin depth for copper wire at 20 kHz is calculated to be 0.47 mm, and at 1 kHz is 2.1mm. As the primary wire has a radius of 0.56 mm, the higher frequencies

of the pulse will be affected by the skin depth phenomenon. However, all frequencies below 13.5 kHz will be unaffected, and as this includes almost all of the pulse, skin effect will therefore be ignored.

Proximity effect will also be negligible in the primary winding, because the coil has very few turns and is wound on only two layers. We will assume then that the resistance of the primary wire is effectively the DC resistance.

DC winding resistance is easily calculated from the length of wire and specified resistivity. The mean length per turn (*mlt*) of the primary coil is 127.6 mm, which for 50 turns gives a total length of 6.38 m of wire. For 1.12 mm wire, the resistance per unit length is $17.98 \times 10^{-3}\ \Omega$/m. Therefore, we calculate a winding resistance of

$$R_p = 0.115\ \Omega$$

5.2.3.12 R_s Secondary Winding Resistance

Copper skin depth is less significant in the secondary coil than in the primary due to the smaller wire diameter. Proximity effect, however, becomes increasingly significant as the number of layers in the coil increase. With nine winding layers, the AC resistance of the secondary winding needs to be carefully considered.

As illustrated by Figure 5-20, the fundamental frequency of the output pulse is around 1 kHz, with few significant harmonics above 4 kHz and minimal amplitude above 20 kHz. The total copper loss is ideally found by summing the losses at each frequency. Since the amplitude of the harmonics falls off so rapidly with increasing frequency, 4 kHz will be taken as a representative value and the total secondary winding loss will be calculated at this frequency. This should be a conservative estimate.

Calculations for the effective AC resistance of a winding are usually based upon the original work by Dowell [*Dowell* 1966]. A number of references, including *Petkov* [1996] and *Severns* [1996], extend these ideas and relate them to practical design methods. In these references, an AC resistance coefficient K_r is defined as the ratio of the AC to DC resistance of a winding.

$$K_r = \frac{R_{ac}}{R_{dc}}$$ *Equation 5-3*

For the output transformer secondary coil with nine layers of 0.40 mm wire, K_r is calculated as 1.006 at 1 kHz, 1.09 at 4 kHz, and 3.26 at 20 kHz. Assuming the 4 kHz figure to be representative of the entire pulse, we can see that the alternating waveform results in a value for resistance which is 9 % greater than the DC value. For the purposes of this thesis, we will assume that the DC value is sufficiently accurate.[9]

For the secondary coil, *mlt* = 173.6 mm which results in a total length of 86.8 m for 500 turns. The resistance per unit length of 0.40 mm wire is 141.76 × 10^{-3} Ω/m, and therefore

$R_s = 12.30\ \Omega$

5.2.3.13 R_c Equivalent Core Loss Resistance

The equivalent core loss resistance introduces a loss into the model to account for hysteresis and eddy current losses. If the total losses are known, it is reasonably straightforward to calculate a value of resistance which will result in an equal amount of loss. For a pulsed application, core losses are difficult to quantify but are not required to high accuracy as they have less effect on the output performance than winding losses.

[9] The efficiency of the output transformer at 500 Ω is not very sensitive to the value of R_s. For example, a 100 % increase in R_s results in only a 4 % decrease in efficiency. At heavier loads however, R_s will become more significant and should be multiplied by K_r to provide a more accurate result.

The formula derived by *Glasoe and Lebacqz* [1948 p. 630] for pulse transformers will be used to provide an approximate calculation of the equivalent core loss resistance.

$$R_c = \frac{12 N_p^2 A \rho}{d^2 \ell_e} \qquad \textit{Equation 5-4}$$

where N_p	$= 50$	reference winding
A	$= 6.45 \times 10^{-4}$ m^2	cross-sectional area of core
ρ	$= 45 \times 10^{-8}$ Ω·m	resistivity of core material
d	$= 0.5 \times 10^{-3}$ m	lamination thickness
ℓ_e	$= 152.4 \times 10^{-3}$ m	mean magnetic path length

$\Rightarrow R_c = 229\ \Omega$

5.2.4 Comparison Of Parameter Values

Measured values have been obtained for many of these parameters [*Harrison* 1992], as summarised in Table 5-1. These values were found using resonant experimental techniques.

The measured value of magnetising inductance is the equivalent parallel inductance of the transformer measured under open circuit conditions, and includes the centre limb and outer limb inductances as well as the air gaps. This can be compared to the calculated values by neglecting L_2 and calculating the equivalent value of the four parallel inductors. This evaluates to 19 mH, which is in good agreement with the measured value.

Only a single lumped parasitic capacitance has been measured, and due to the complex nature of the parasitic capacitances it is not possible to combine the separate values which have been calculated into a single effective value. However, the largest of the multiple calculated capacitances is of the same magnitude as the measured value, which would indicate a reasonable match between calculation and experiment.

Most of the calculated values show close agreement with measurement. The critical parameter analysis of Section 5.4 demonstrates that any inaccuracies in these values have little impact on the overall accuracy of the model.

The primary objective has been to develop a complete model of the output transformer based solely on the specification of Figure 5-1. Although a number of simplifications and assumptions are required, the value of each parameter is calculated without requiring experimental information. This justifies a compromise in accuracy, but as shown by Table 5-1, the experimental results confirm that the methods of calculating parameter values as outlined in this chapter are more than adequate for the purposes of this model.

Parameter	Calculated Value	Measured Value	
L_1	182 mH	15 mH	Measured value is total effective magnetising inductance (including air gaps). Note: $L_1//L_3//L_{g1}//L_{g2}$ = 19 mH
L_3	95 mH		
L_{g1}	55 mH		
L_{g2}	58 mH		
L_2	32 µH	60 µH	
C_1	3.6 nF	2 nF	Measured value is total effective parasitic capacitance.
C_2	0.91 nF		
C_3	5.9 pF		
C_4	5.9 pF		
C_5	39.7 pF		
R_p	0.115 Ω	0.115 Ω	
R_s	12.30 Ω	12.3 Ω	
R_c	229 Ω	493 Ω	

Table 5-1 *Comparison Of Measured And Calculated Parameter Values*

5.3 IMPLEMENTATION

The following section describes the implementation of the electrical circuit model, and compares simulation results to measurements and to results from the previous output transformer model [*Harrison* 1992].

When considering the simulation, it is important to remember that the output transformer can never be considered in isolation from the remainder of the energiser circuit. The output pulse is influenced by every aspect of the discharge path, so the model of the discharge circuit, which may include the SCR, path resistance and storage capacitor parasitics, must be as accurate as the transformer model itself.

5.3.1 SIMULATOR

A key feature of the output transformer model developed in this thesis is its independence from the choice of simulator. Advanced features such as non-linear magnetic models, time dependent inductance, and SCR device models may be included if the simulator has these capabilities, but are not critical to the transformer model's performance.

The simulator chosen to implement the model in this thesis is PSpice version 4.05, from MicroSim Corporation.

When implementing the model, a great deal of time can be spent in adjusting parameters and refining the circuit to obtain an output that is identical to the measured result. The position taken in this thesis is that if the fundamental principles of the model are correct, an improvement in the accuracy of the result will provide little additional information about the transformer. While the results may look more impressive, time would be more profitably spent on using the model to understand the transformer and improve the design. The objective is to develop a model which will assist in understanding the transformer, and in applying theoretical concepts to practical design. Numerical accuracy is not the primary consideration, provided that the model does correctly represent the physical situation.

5.3.2 NON-LINEAR MAGNETIC CORE

Saturation plays a key role in the performance of an output transformer, and PSpice provides for saturating magnetic devices by offering a non-linear magnetic core model based on the Jiles-Atherton theory. The PSpice model does not take into account the magnetic field penetration time.

In the output transformer model of Figure 5-7, the magnetising inductances L_1 and L_3 are affected by saturation.[10] With these components defined using the PSpice non-linear core model, the simulated results can closely match the measured output. Figure 5-16 illustrates such a result, with saturation obvious by the sudden increase in current at 120 μs.

[10] In the case of an I-core transformer, only L_1 will be saturable.

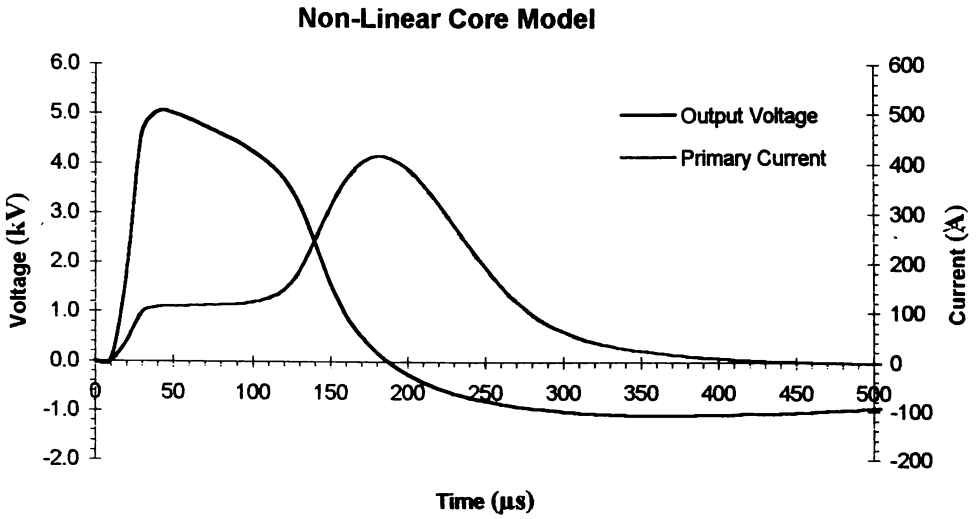

Figure 5-16 *Non-Linear Core Model Results - 500 Ω Load*

The non-linear core model allows the process of saturation to be investigated more easily than on a real transformer. Factors such as the pulse *B-H* loop can be displayed, and core losses can easily be calculated as functions of time.

The measured primary current pulses shown in Figure 5-17 illustrate the onset of saturation. At a load of 50 Ω, the core does not saturate. At 150 Ω, saturation is just beginning after 200 µs. At 500 Ω, the second current peak indicates that saturation has occurred, and the measured result confirms the accuracy of the simulation as shown in Figure 5-16. As the fence load reduces, the degree of saturation and hence the peak value of the current continues to increase.

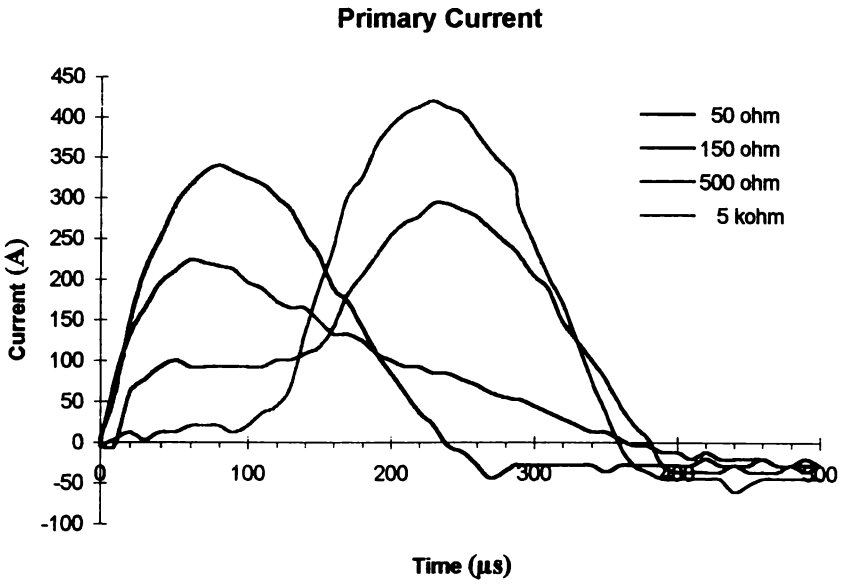

Figure 5-17 *Measured Primary Current Pulses*

Unfortunately, in order to successfully simulate the output transformer with a non-linear core, a number of features of the model had to be compromised. The load was reflected to the primary side of the transformer, and the parasitic capacitances C_1, C_2, C_3 and C_4 and secondary winding resistance R_s were disregarded. The equivalent parasitic capacitance C_5 was increased by a factor of ten to account for the significant primary-secondary capacitance of C_1.

In addition, the parameters used by the Jiles-Atherton model to describe the hysteresis characteristics of a magnetic material are very difficult to determine, and result in hysteresis curves which are not a good match of published figures [*Harrison* 1992, *Williams* 1994]. A number of the parameter values must be found by trial and error.

Although the waveforms shown in Figure 5-16 appear impressive, the equivalent circuit had to be severely compromised to achieve this, and the direct correspondence between the model and the physical transformer was lost. Should operating conditions change, the model would need to be re-optimised from measured waveforms, and so the advantage of being able to derive the model without requiring a physical sample would also be lost.

Difficulties were experienced with implementing the Jiles-Atherton non-linear core model that is built in to PSpice, as noted in a number of references [*Harrison* 1992, *Williams* 1994, *Chan et. al.* 1991]. In many cases, the circuit had to be substantially modified (for example, by removing the SCR) simply to allow the simulation to run.

While the existing output transformers do saturate, the non-linear core was not included in the final model presented here due to the difficulties and compromises which its use introduced. A non-linear core model could still be used if saturation was required for a particular situation, provided the inherent difficulties and compromises were taken into consideration.

Alternatively, a simulator using a different or simpler method of modelling non-linear magnetic devices could be investigated. A number of references discuss simplified magnetic core models including *Lee* [1993] and *Meares and Hymowitz* [1998].

5.3.3 LINEAR MAGNETISING INDUCTANCE

L_1 and L_3 represent the magnetic flux path through the transformer core. For the remainder of this chapter we consider a linear model in which the transformer core does not saturate, that is we assume that L_1 and L_3 are linear.

The calculated values for L_1 and L_3 found in Section 5.2.3 assume that the entire core area is available for magnetisation, and that the average relative permeability is approximately 5000. As discussed in Chapter 3, the time dependent nature of pulse magnetisation means that initially, only a very small area of the core is penetrated by the magnetic field. Once it has penetrated the core, the magnetic field strength quickly reaches the saturation value of the material. The effective core area is thus equivalent to the area of this thin band of high permeability moving into the lamination, and as inductance is proportional to core area, the effective inductance is considerably less than that calculated.

In Chapter 3.3.3, the ratio of the effective area to the total area of the core is estimated to be 5×10^{-3}. In the absence of a more accurate representation of pulse magnetisation, linear inductances will be specified for L_1 and L_3 with values calculated using this factor, resulting in

$$L_1 = 5 \times 10^{-3} \cdot 182 \times 10^{-3} = 0.9 \text{ mH} \qquad \textit{Equation 5-5}$$

$$L_3 = 5 \times 10^{-3} \cdot 95 \times 10^{-3} = 0.5 \text{ mH} \qquad \textit{Equation 5-6}$$

5.3.4 SPICE CIRCUIT FILE

The electrical circuit model shown in Figure 5-7, with values as calculated in Section 5.2.3 apart from the linear inductances L_1 and L_3 as noted Section 5.3.3, is easily implemented in SPICE. The output transformer model and additional discharge path components are shown in Figure 5-18, with discharge circuit and storage capacitor parasitic values taken from *Harrison* [1992].

The PSpice schematic shows the nodes numbered as required by SPICE notation. The actual PSpice circuit file is also given below. An explanation is not provided for SPICE notation and syntax - for further information about SPICE simulation or PSpice notation, refer to *MicroSim* [1991] or *Goody* [1995].

```
OUTPUT TRANSFORMER MODEL - March 98

*MODELS AND PARAMETERS
*---------------------

.PARAM  load=150ohm                    ;Fence load
.PARAM  cpa=1                          ;Critical Parameter Analysis
.MODEL  BYV96  D                       ;ideal BYV96 diode model
.LIB


*PULSE TRIGGER - SCR
*-------------------

Vgate     80     0      EXP(0V  5V  50ms 50us  50.12ms  100us)
Cgate     80     0       1uF
Xscr      72    80   0  BTW68
Ron       71    72      50mohm          ;SCR on resistance
Roff      70     0     500kohm          ;SCR off resistance
Cscr      70     0      10pF            ;to prevent false firing
Dscr       0    70     BYV96            ;to allow underswing
VIscr     70    71        0             ;ammeter (Current through SCR)

.Subckt  BTW68  Anode  Gate  Cathode
Xscr  Anode  Gate  Cathode  SCR  Params:
  +  Vdrm=1000     Vrrm=1000     Idrm=20uA
  +    Ih=20mA     dVdt=5000meg  Igt=50mA
  +   Vgt=1.5V      Vtm=2.1V     Itm=60A
  +   Ton=1us      Toff=500us
.ENDS   BTW68
```

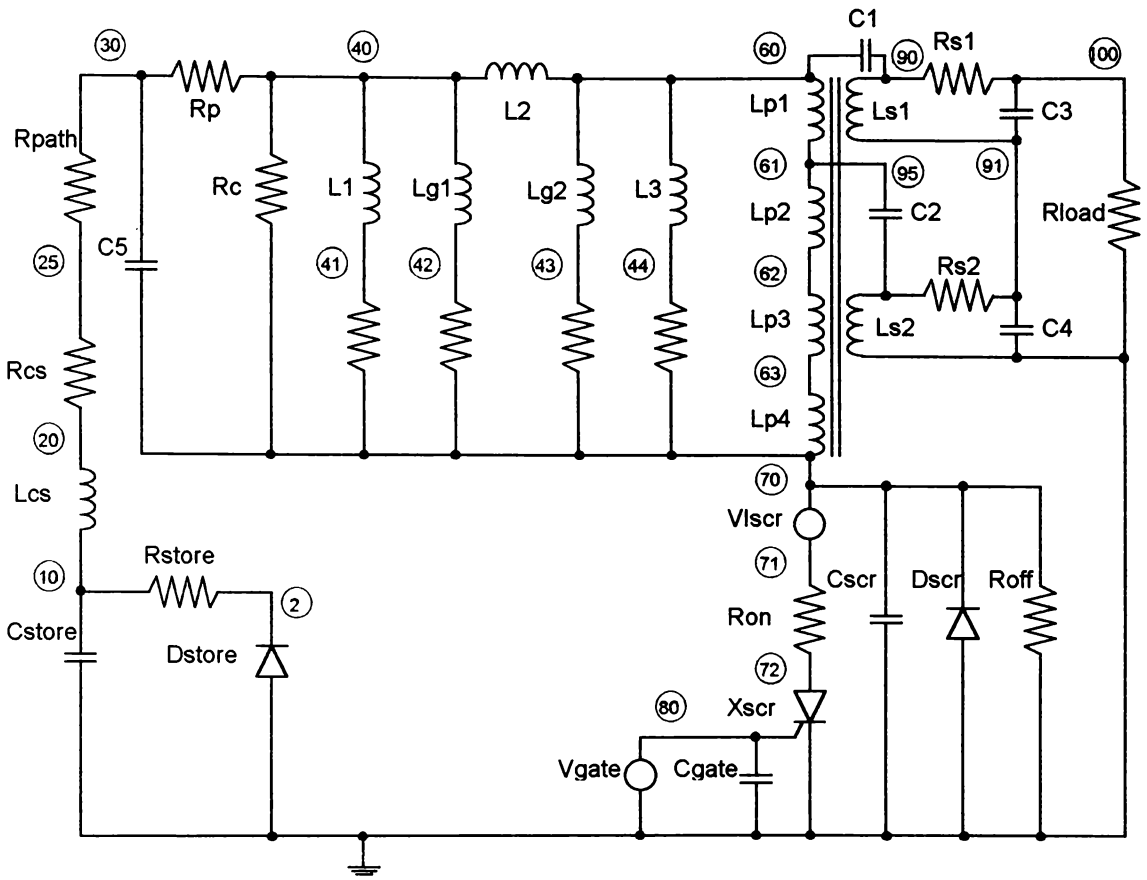

Figure 5-18 *PSpice Schematic*

```
*PULSE TRIGGER - SWITCH
*----------------------
*(May be used in the case of convergence problems)

*Vtrig1  81    0     SIN(0.5V  0.5V  250Hz  0  0  90deg)
*Vtrig2  82    0   PULSE(0V  1V  50ms  1us  999us  3ms  1s)
*Etrig   80    0   VALUE={V(81)*V(82)}
*Rtrig1  81    0       1ohm
*Rtrig2  82    0       1ohm
*Scr     70  0  80  0  Trigger

*Switch includes 0.27ohm path resistance
*.MODEL  Trigger  VSWITCH (Ron=0.27 Roff=10Meg Von=0.55 Voff=0.5)


*ENERGISER CIRCUIT
*-----------------

Cstore   10    0     84uF  IC=600V ;storage capacitor
Dstore    0    2    BYV96          ;to allow underswing
Rstore    2   10      10ohm
Lcs      10   20   0.88uH          ;storage cap parasitic
Rcs      20   25    0.15ohm        ; "       "     "
Rpath    25   30    0.27ohm

Rload   100    0  {load}           ;equivalent fence load
```

```
*IDEAL TRANSFORMER
*-----------------

Lp1       60    61      15mH
Lp2       61    62      15mH
Lp3       62    63      15mH
Lp4       63    70      15mH
Ls1       91    90        3H
Ls2        0    95        3H
Kideal   Lp1   Lp2   Lp3   Lp4   Ls1   Ls2   0.999999


*EQUIVALENT CIRCUIT
*------------------

L1        40    41     0.9mH          ;5m x 182mH
L2        40    60      32uH
L3        60    44     0.5mH          ;5m x 95mH
Lg1       40    42      55mH
Lg2       60    43      58mH

C1        60    90      3.6nF          ;parasitic capacitances
C2        61    95     0.91nF
C3       100    91      5.9pF
C4        91     0      5.9pF
C5        30    70     39.7pF

Rp        30    40    0.115ohm        ;primary winding R
Rs1       90   100     6.15ohm        ;secondary winding R
Rs2       95    91     6.15ohm
Rc        40    70      229ohm        ;equiv. core loss R

Rl1       41    70       1uohm        ;to prevent inductor loops
Rlg1      42    70       1uohm
Rlg2      43    70       1uohm
Rl3       44    70       1uohm


*ANALYSIS
*--------

.PROBE
.PRINT   TRAN   V(100)
*.FOUR   1kHz   V(100)   V(30)
.TRAN    2us    55ms    50ms    10us    UIC
.OPTIONS  itl4=25  itl5=0  abstol=1uA  chgtol=1nC
    +  vntol=0.1mV  reltol=0.45m  numdgt=5
*.STEP PARAM load LIST  10  20  100  200  1k  2k  10k  20k  50k
*.STEP  PARAM  cpa  LIST  2.0  1.1  1.0  0.9  0.1

.END
```

5.3.5 MODEL VERIFICATION

The parameters measured to compare the output performance of real electric fence energisers are the peak output voltage V_{peak} and the output energy E_{out} delivered to the load. Figure 5-19 compares the measured and simulated results for these two parameters with respect to the fence load. The model matches the trends shown by the real transformer, which is the most important requirement. Quantitatively, the results are satisfactory considering that, as explained in Sections 5.1.5 and 5.3.1, numerical accuracy has not been the focus of the model. The simulated output performance results shown in Figure 5-19 are similar enough to the measured values to confirm that the model is a valid representation of a real output transformer.

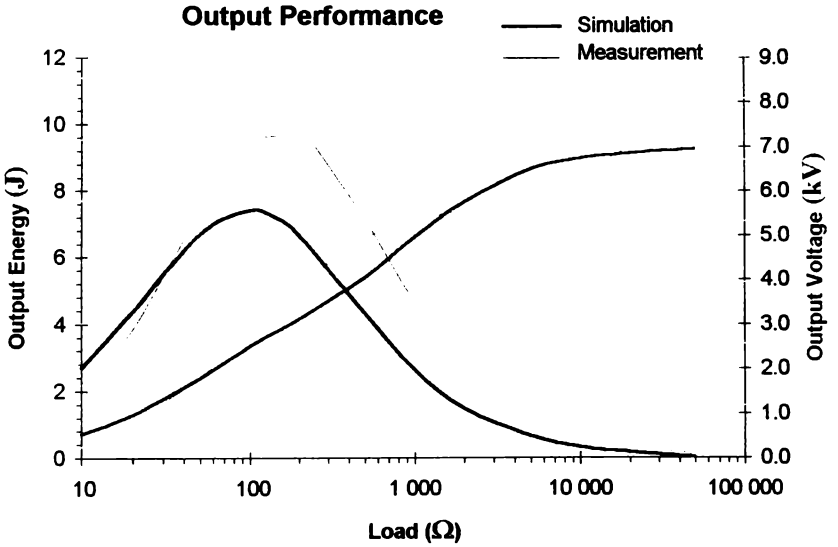

Figure 5-19 *Output Performance*

In addition to V_{peak} and E_{out}, other pulse parameters of interest in this application are the peak underswing voltage V_{min}, the peak primary discharge current I_{peak}, and the pulse width t_{pulse} to the first zero crossing. In Table 5-2, measured values for these parameters are compared with simulated results from the linear model developed in this thesis. Also included in the table for comparison are values from the non-linear core model developed by *Harrison* [1992].

	50 Ω Load			150 Ω Load		
	Measured	Linear Model	Non-Linear Model	Measured	Linear Model	Non-Linear Model
V_{peak} (kV)	1.81	1.79	1.78	3.38	2.87	3.30
V_{min} (kV)	0.03	0.46	0.02	0.42	1.12	0.45
E_{out} (J)	7.38	6.68	6.47	9.68	7.17	9.04
I_{peak} (A)	340	299	333	228	207	222
t_{pulse} (μs)	262	227	317	322	234	259
	500 Ω Load			5 kΩ Load		
	Measured	Linear Model	Non-Linear Model	Measured	Linear Model	Non-Linear Model
V_{peak} (kV)	4.92	4.04	4.89	8.04	6.49	5.88
V_{min} (kV)	1.88	1.84	1.41	3.16	2.32	2.07
E_{out} (J)	7.14	4.34	5.36	1.37	0.65	0.87
I_{peak} (A)	294	220	349	420	241	426
t_{pulse} (μs)	248	239	221	226	242	203

Table 5-2 *Pulse Parameter Comparison*

These results again confirm that the linear model performs in fundamentally the same fashion as the real transformer, with the notable exception of saturation. The impact of saturation is evident from the figures for peak discharge current. As shown by Figure 5-16, the current increases sharply after saturation occurs. The linear model of course cannot simulate this characteristic, whereas the non-linear model described in Section 5.3.2 and implemented by *Harrison* [1992] does account for saturation.

It is also interesting to examine the frequency spectrum of the output pulse. The simulation displays a good match to the measured frequency spectrum, with differences likely to be caused as much by deficiencies in the model of the discharge circuit or even inaccuracies in the experimental measurement, as by inadequacies of the transformer model. Figure 5-20 clearly shows that the fundamental frequency of the pulse is around 1 kHz, and that the pulse does not contain significant frequency components above 20 kHz.

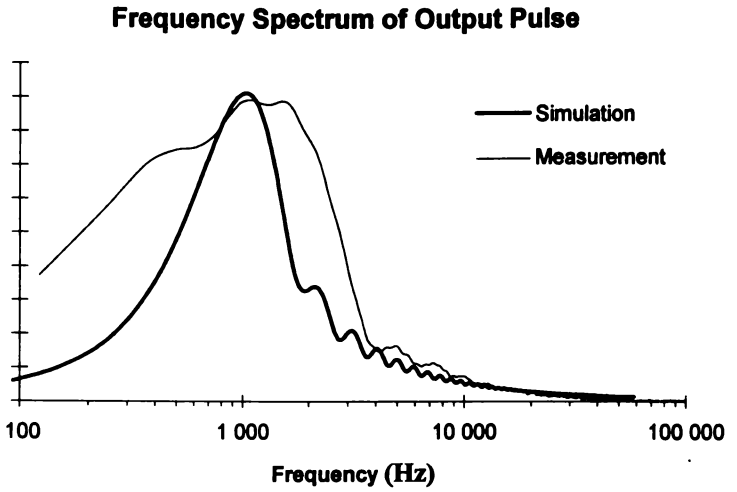

Figure 5-20 *Output Pulse Frequency Spectrum - 500 Ω Load*

Voltage waveforms are shown for comparison between simulation and measurement at fence loads of 150 Ω, 500 Ω and 5 kΩ. In Figure 5-22, the SCR turns off at 1100 μs in the simulation, causing the output voltage to return to zero. The measured waveform shows that this actually occurs at 400 μs. This limitation in the SCR model was not able to be corrected.

The high-frequency ringing which is particularly evident in the 5 kΩ simulation waveform is also present in the measured waveform, and becomes more apparent as the load tends towards open circuit.

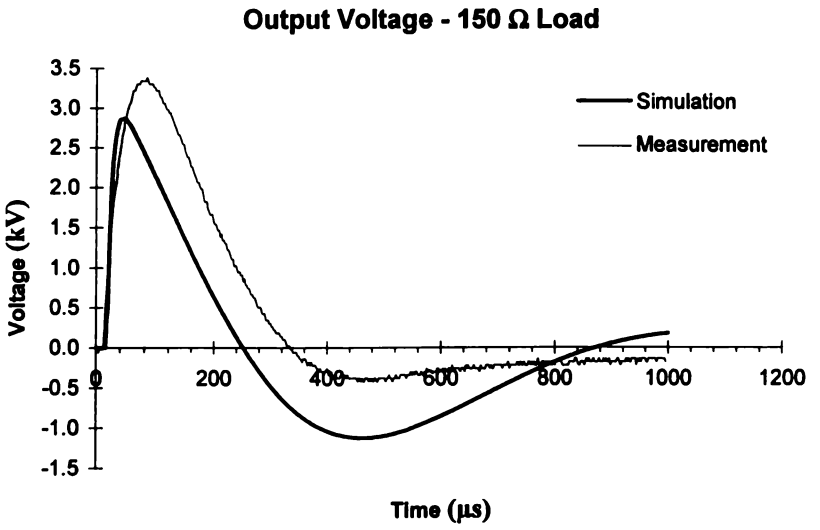

Figure 5-21 *Output Voltage Pulse - 150 Ω Load*

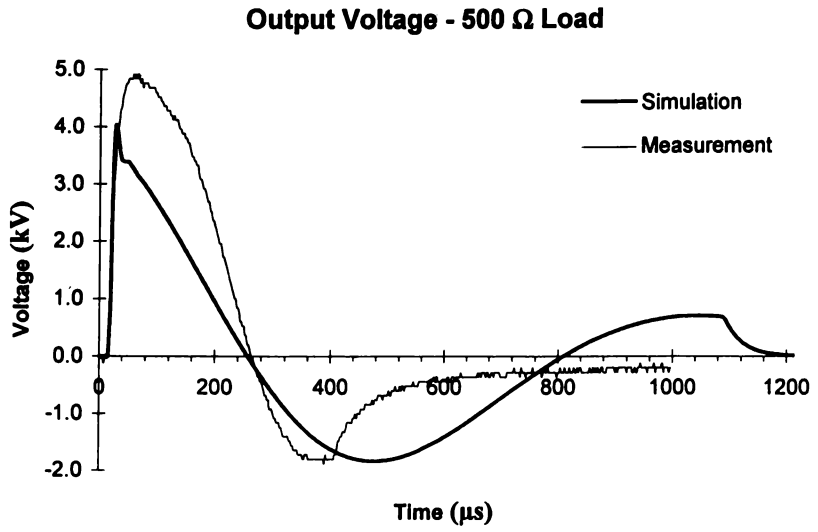

Figure 5-22 *Output Voltage Pulse - 500 Ω Load*

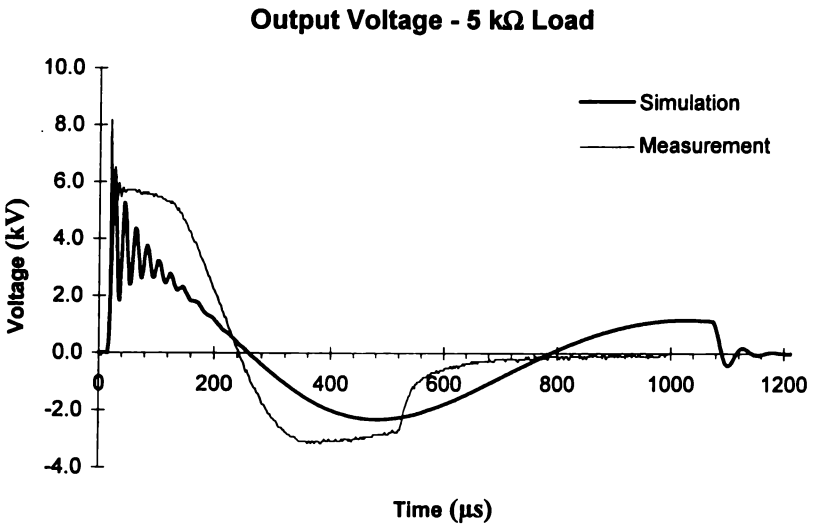

Figure 5-23 *Output Voltage Pulse - 5 kΩ Load*

5.4 CRITICAL PARAMETER ANALYSIS

The output transformer model allows the impact on performance of individual parameters to be easily investigated. This analysis would be exceedingly tedious, if not impossible, to do with physical transformers. In this analysis, each parameter of the model is varied individually, with the simulation run for values of 200 %, 110 %, 100 %, 90 % and 10 % of the nominal values. This *critical parameter analysis* identifies which parameters have a large effect on the transformer's performance, and which are insignificant. As there is a direct relationship between the model and the physical transformer, this quickly the highlights the areas of the transformer which should receive special attention during design.

While all of the parasitic parameters have been investigated, only those discussed below have a significant effect on the transformer's behaviour. This analysis indicates those parameters which need to be accurately determined to ensure that the model is accurate.

5.4.1 RINGING

Inductance L_2 representing the leakage flux, and inter-coil capacitance C_1 combine to create the high frequency ringing evident on the leading edge of the pulse. The magnitude of this ringing is greatly influenced by the values of L_2 and C_1, as illustrated by Figure 5-24. As C_2 is small in comparison to C_1, variation in the magnitude of C_2 has no effect on the output voltage pulse.

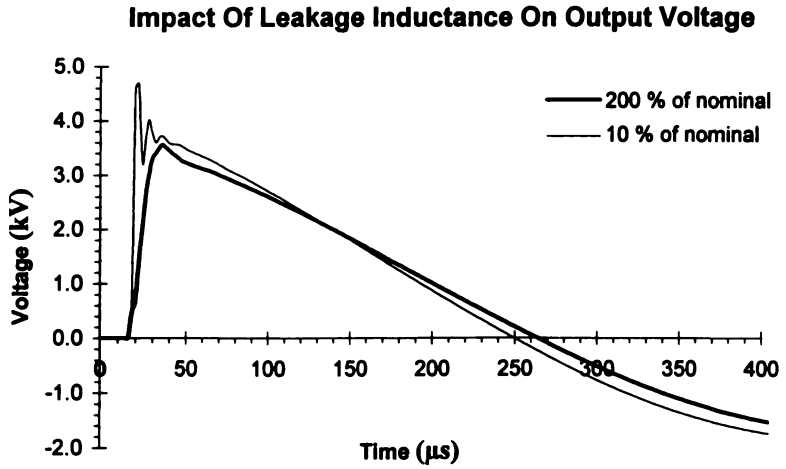

Figure 5-24 *Variation Of Leakage Inductance L_2 - 500 Ω Load*

From the values shown in Table 5-1, the measured value for L_2 is double the calculated value. Doubling the leakage inductance would dampen the ringing on the leading edge of the pulse, although not by a great amount. However, the measured pulses exhibit less ringing than the simulated pulses, so improving the accuracy of the calculation for L_2 would result in more realistic ringing in the model.

Variation in the values of the remaining parasitic capacitances C_3, C_4 and C_5 has no impact on the transformer's performance, and they could be omitted from the model with no loss of accuracy.

5.4.2 AIR GAP

The size of the air gap as represented by inductors L_{g1} and L_{g2} has virtually no effect on the output pulse, as a consequence of these values being large in comparison to the parallel magnetising inductances L_1 and L_3. In the current transformer design then, the length of the air gap is not critical - a result well known in practice.

The air gap will only become significant if the magnitude of L_{g1} and L_{g2} is of the order of L_1 and L_3. This may occur if the full core were able to be magnetised so that L_1 and L_3 were increased, or if the air gap became large enough so that L_{g1} and L_{g2} were of the order of L_1 and L_3.

As inductance is directly related to the path length by Equation 2-34, it is a simple matter to calculate the largest permissible air gap. For $L_{g1} \approx L_1 = 0.9$ mH, we must have $\ell_{g1} = 2.15 \times 10^{-3}$ m. Therefore, in the current design the total air gap length should not exceed 2 mm but is unlikely to have much impact on the performance for values smaller than this.

5.4.3 WINDING LOSS

Primary winding resistance has a minor influence on output voltage, but a major influence on output energy. The nominal value of R_p results in an output energy of 4.34 J delivered into a 500 Ω fence load. If the value of R_p is increased by 200 % of R_p, output energy reduces 9 % to 3.95 J, while for a value of 10 % of R_p, the output energy increases 9 % to 4.75 J. The significance of the primary copper loss as shown here verifies the result by *Harrison* [1992]. Table 5-1 shows that the calculated value for R_p exactly matches the measured value, which is a necessary requirement for an accurate model since this is a critical parameter.

The wire diameter is related to both the total coil area and the winding resistance, and winding resistance greatly affects the output energy of the transformer. It is therefore possible to use the model to relate the wire diameter to the output energy. As shown by Figure 5-25, there is an optimum point in the trade-off between maximum output energy and minimum coil area which corresponds to a wire size of 1 mm diameter.

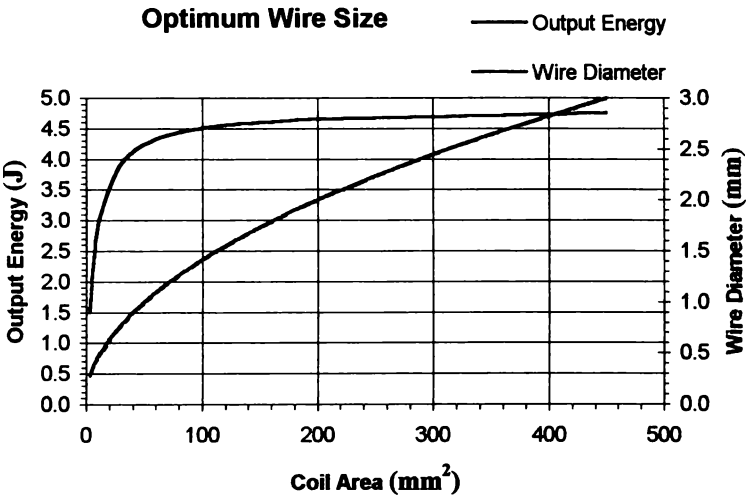

Figure 5-25 *Variation Of Coil Area - 500 Ω Load*

In this way, the model can be used to assist in choosing the optimum wire specification, although the choice of primary wire size is usually dictated by mechanical constraints such as the winding space available.

Secondary winding resistance also influences the efficiency, but to a lesser extent than the primary winding resistance when $R_{load} >> R_s$. For example, the peak output energy into a 500 Ω load decreases by just 4 % if the secondary winding resistance R_s is increased 100 %. As the load becomes heavier, the significance of the secondary winding loss increases.

5.4.4 CORE LOSS

The equivalent core loss resistance has negligible influence on the output voltage or energy, and therefore the accuracy of this parameter value in the model is not critical. This result justifies the use of the approximate formula used in calculating the value for core loss in Section 5.2.3. R_c will only become significant when its impedance is small in comparison to the magnetising inductance L_1 or leakage inductance L_{g1} $\left(Z_{R_c} \leq Z_{L_1 // L_{g1}}\right)$, that is if core losses are very large, or magnetising and leakage inductances L_1 and L_{g1} are large.

This can be seen from the equivalent circuit, where the relevant components only are shown in Figure 5-26.

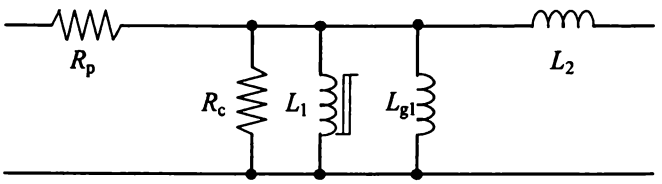

Figure 5-26 *Core Loss Equivalent Circuit*

For the transformer model, we have calculated that R_c = 229 Ω, L_1 = 0.9 mH and L_{g1} = 55 mH. As $L_1 \ll L_{g1}$, $Z_{L_1 // L_{g1}} \approx Z_{L_1}$. If the frequency is taken as 20 kHz, then the impedance of L_1 is about 100 Ω, and core loss will only become significant as R_c approaches this value. This is illustrated by Figure 5-27, which graphs the output energy predicted by the model as a function of the value of the equivalent core loss resistance.

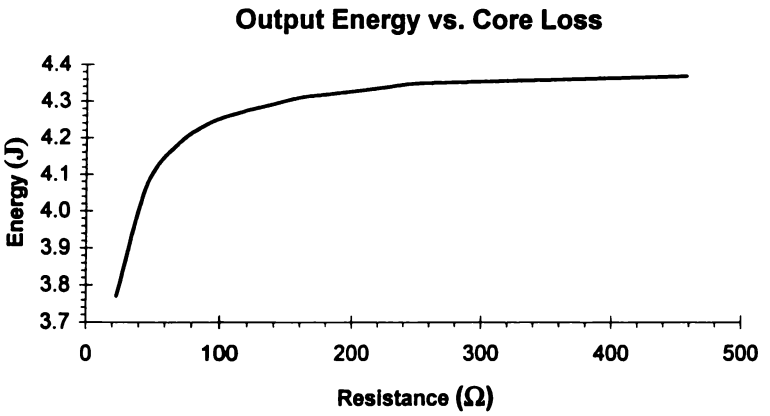

Figure 5-27 *Variation Of Core Loss Resistance R_c - 500 Ω Load*

There is a large difference between the measured and calculated values for R_c shown in Table 5-1. However, as illustrated by Figure 5-27, there is less than 1 % difference in output energy between the calculated value of 229 Ω and the measured value of 493 Ω. Therefore, the inaccuracy in the calculation for R_c has no effect on the accuracy of the model.

5.5 REMARKS

The success of this model does not depend on its numerical accuracy, but on its practical value.

The model presented in this chapter corresponds directly to the physical transformer, and may be developed before the transformer has been fabricated. Results have verified that the model displays satisfactory accuracy, despite difficulties with implementing the non-linear core model. The model is therefore expected to be a very useful tool in the design of output transformers, and has been demonstrated to be useful in optimising design parameters, such as choosing the optimum primary wire size and setting the maximum allowable air gap.

The inductor-reluctance method employed is flexible enough to allow modifications to suit particular applications. For example, it may be helpful to include the non-linear core model in certain cases, or to directly measure equivalent components if a prototype transformer is available, or to adjust parameter values to better match the measured output.

The model may be further improved by including the effect of pulse magnetisation as a function of time, and as already discussed, by including a non-linear saturating core model. It would also be worthwhile to put further effort into accurately modelling the energiser's primary discharge path, and integrating the transformer model into a simulation of the entire energiser circuit and fence system.

Chapter Six DISCUSSION

The scientists who laid the foundations of electromagnetism were well aware of the applied aspects of scientific research, even if their focus was entirely on the theoretical. Faraday wrote in 1831 that he had "*rather been desirous of discovering new facts and new relations dependent on magneto-electric induction, than of exalting the force of those already obtained; being assured that the latter would find their full development hereafter.*" [*Tyndall* 1870 p. 43].

While this thesis focuses on developing a theoretical description of the behaviour of the output transformer, the practical applications of the work have always been close at hand. This final chapter discusses some of the implications of the preceding work, outlines some practical results, and develops recommendations for the next step in the search for the perfect output transformer.

6.1 SUMMARY

This thesis focuses on developing a comprehensive understanding of the behaviour of the electric fence energiser output pulse transformer. The specific outcomes of this research are listed below, and have either contributed to our understanding of pulse transformer behaviour or have practical value in the design of output transformers.

1. The derivation of a solution to Maxwell's equations which describes the time and position dependent penetration of a magnetic field into a transformer lamination, under high current pulse conditions.

2. The formulation of a method for estimating the position of saturation in a lamination under high current pulse conditions.

3. The development of a quantitative estimate of the effective core area and pulse inductance of a lamination under high current pulse conditions.

4. The development of a simplified analytical model of an output transformer, giving transient solutions for magnetising current, primary winding current, output voltage, output power, efficiency, and inductance (including the spatial variation of inductance within a lamination).

5. The identification from the analytical model of the key parameters affecting output transformer performance: being the magnetising inductance and series discharge resistance.

6. The development of an electrical circuit model for the output transformer, which is based completely upon the transformer specification and maintains direct correspondence between electrical and physical parameters.

7. An overview of methods which allow the calculation of all of the parameter values required by the electrical circuit model.

8. An application of the electrical circuit model to practical results: investigating ringing on the leading edge of the pulse; the maximum allowable air-gap; the optimum primary wire size; and the significance of the core loss parameter.

6.2 REMARKS

6.2.1 'I' LAMINATIONS

The original motivation for conducting this research was the observation that output transformers with I lamination cores could perform as efficiently as those using E-I laminations. This unusual behaviour has been explained by the investigation into pulse magnetisation.

As we have discussed, the magnetic field created by the capacitive discharge pulse is established immediately in air but takes time to diffuse into a magnetic material, because of the eddy currents set up in the material. Due to the high strength of the applied field, saturation rapidly follows the penetration of magnetic field into the lamination, and only a small part of the core operates with the high permeability that is expected of magnetic materials. The average permeability is therefore much less than the peak permeability of the core material. In fact, the effective permeability of the I core is not much different to that of the E-I core (see for example Section 6.3.2). Air gaps in the E-I core will similarly have little effect. Any difference in performance between the two types of transformer would only be caused by differences in the total area of the core that is effectively magnetised, which is a function of the total volume of iron but is independent of the core geometry.

6.2.2 KEY REFERENCES

This research has placed us in a much stronger position to benefit from the work of *Früngel* [1965, 1976] and *Glasoe and Lebacqz* [1948]. In general, both references address topics which are substantially different to the output transformer. *Früngel* deals primarily with pulses of much greater power, while the radar pulse transformers discussed in *Glasoe and Lebacqz* are of much lower power - they are designed to avoid saturation and thus operate more like a steady state transformer than does the output transformer.

Although some of Früngel's comments quoted in Chapter 1.2.2 are incorrect as shown by the work in this thesis, his assertion that "*as long as during the short impulse duration there is sufficient core volume for magnetic field expansion or for orientation of sufficient magnetic domains, it is without consequence whether the magnetic circuit outside the coil field is closed or not*" [*Früngel* 1965 p. 213] is certainly consistent with the conclusions presented here.

Glasoe and Lebacqz [1948] contains a wealth of design information which, if treated carefully, could be applied to the output transformer. One example of this is Equation 5-4, the formula for equivalent core loss resistance which is used for the development of the electrical circuit model. Another example would be the condition for maximum power transfer,

$$R_{load} = \sqrt{\frac{L_{eq}}{C_{eq}}} \qquad \textit{Equation 6-1}$$

where L_{eq} is the equivalent leakage inductance and C_{eq} the equivalent parasitic capacitance. This produces a reasonable match to experimental results [*Harrison* 1992 p. 143], and could be used to alter the load at which the maximum output energy occurs.

6.3 APPLICATION

6.3.1 DESIGN RECOMMENDATIONS

It may at first appear that a small magnetic time constant τ_m (Equation 3-36) is desirable so that the magnetic field rapidly penetrates the lamination. However, a small magnetic time constant will also allow saturation to occur quickly, resulting in an overall reduction in the effectively magnetised area. It is therefore recommended that a core material with a large magnetic time constant be chosen. This implies a large conductivity, which will allow the creation of large eddy currents to oppose the penetration of the magnetic field. If the magnetic field penetrates slowly, thinner laminations could be used which would also be of benefit as there would be more boundaries from which the magnetic field would enter. This requirement implies that low quality sheet material be used, as suggested by *Früngel* [1965]. A high saturation point and low permeability will also be advantageous.

The analytical results highlight the requirements for a large magnetising inductance and small series resistance. The primary focus then during transformer design should be on finding a magnetic core material and geometry which gives the greatest effective core area under output pulse conditions. The transformer should also have a large winding area, and perhaps a circular cross-section to reduce winding loss and improve manufacturability.

Simply increasing the primary wire size however is unlikely to lead to an improvement in the performance of the energiser as a whole. While the primary discharge path resistance needs to be kept small, some impedance is required to prevent excessive peak currents and EMI emissions. At the instant the SCR is switched on, the inductance of the transformer is effectively zero and the circuit resistance plays a vital role in controlling the discharge. The identification of the primary winding resistance as a key loss element therefore leads to the recommendation that the discharge circuit as a whole be studied in much greater detail, with the objective of producing a gradual capacitive discharge with lower peak currents and less loss in the discharge circuit than is the case with current designs.

6.3.2 VOLUME - TIME FACTOR

The above recommendations are the first step in applying the theoretical work of this thesis to design. Einstein once said "*The skeptic will say, 'It may well be true that this system of equations is reasonable from a logical standpoint, but this does not prove that it corresponds to nature.' You are right, dear skeptic. Experience alone can decide on truth.*" [*Einstein* 1950]. The true test of this work is in its application. Although the accuracy of the theory was confirmed many times by comparison with experimental results, extended practical application is required.

One brief investigation is described as follows. Prior to this work there was no known relationship between the core size and power handling capability of an output transformer. This is due to two main factors:

- the core can be of many different geometries including I laminations and E-I laminations, and magnetic materials including silicon steel and iron powder;

- there is no clearly defined point to indicate when an output transformer has been over-extended. In general, output transformers are not limited by temperature rise regardless of how inefficiently they operate. The requirement then is usually an arbitrarily chosen efficiency. A smaller but more inefficient transformer can be compensated by greater stored energy, resulting in the same output energy.

This investigation uses the equations derived in Chapter 3, in particular Equation 3-43, to calculate a *Volume-Time Factor* (*V·t* Factor) which may be used to compare different core materials and geometries.

For each case, values for the magnetic flux density at magnetisation and saturation are chosen corresponding to 50 % of the peak permeability value. These values are taken from the magnetic characteristics of the core provided by the manufacturer. Equation 3-43 is used to find the time taken for the magnetic field at the centre of the lamination to reach saturation. A value for time between the onset of the pulse and saturation is chosen, and at this point in time Equation 3-43 is again used to solve for the position in the lamination where magnetisation and saturation occur - the difference between the two representing the

effective width of the high-μ band. The area of iron and the number of laminations into which the magnetic field penetrates are also taken into account.

An example of the Mathcad 7 worksheet used to calculate these values is given in Figure 6-1.

Multiplying the time to saturation, the width of the high-μ band, and the area available for magnetisation results in the figures shown in Table 6-1, which compares the Volume-Time Factor of various core types along with their experimentally measured efficiencies. Powdered iron cores may also be compared by considering each particle of iron to be a separate 'lamination'.

Core Type	Thickness	Relative *V·t* Factor	Efficiency
Strip wound E-core	0.25 mm	4.1	65 %
Strip wound C-core	0.2 mm	1.38	62 %
E-I lamination	0.5 mm	1.00	63 %
I lamination	0.5 mm	0.56	51 %
Iron Powder E core	50 µm	0.044	54 %
Metglas C-core	0.25 µm	0.039	46 %

Table 6-1 *Volume-Time Factor*

The trend shown by the *V·t Factor* is matched reasonably well by the measured efficiencies, although the differences between core types is much less pronounced in the efficiency figure than in the *V·t Factor*. This is a feature of output transformers which has been noted before - no matter what one does to them, they still perform fairly well.

While the *V·t* Factor is a very crude calculation, it does provide for the first time a method of theoretically comparing the merits of various core materials and geometries. Prior to this, trial and error was the only guide.

Core Material Comparison

RM-14 Silicon Steel E-I Laminations

Time to saturation (B_{sat} = 1.2T) at centre of lamination

$y := 0$ $\quad \tau := 3.34 \cdot 10^{-4}$ $\quad n := 1 .. 200$

$B_a := 2$ $\quad a := 0.25 \cdot 10^{-3}$

Trial solution: $t := 10^{-4}$

Given

$$1.2 = B_a \cdot \left[1 + \sum_n \left[(-1)^n \cdot \frac{4}{(2 \cdot n - 1) \cdot \pi} \cdot e^{\frac{-(2 \cdot n - 1)^2 \cdot t}{\tau}} \cdot \cos\left[\frac{(2 \cdot n - 1) \cdot \pi}{2 \cdot a} \cdot y \right] \right] \right]$$

find(t) =

Position of magnetisation point (B_{mag} = 0.15T) at t = 100μs

$t := 100 \cdot 10^{-6}$ $\quad \tau := 3.34 \cdot 10^{-4}$ $\quad n := 1 .. 1$

$B_a := 2$ $\quad a := 0.25 \cdot 10^{-3}$

Trial solution: $y := 10^{-5}$

Given

$$0.15 = B_a \cdot \left[1 + \sum_n \left[(-1)^n \cdot \frac{4}{(2 \cdot n - 1) \cdot \pi} \cdot e^{\frac{-(2 \cdot n - 1)^2 \cdot t}{\tau}} \cdot \cos\left[\frac{(2 \cdot n - 1) \cdot \pi}{2 \cdot a} \cdot y \right] \right] \right]$$

find(y) =

Position of saturation point (B_{sat} = 1.2T) at t = 100μs

$t := 100 \cdot 10^{-6}$ $\quad \tau := 3.34 \cdot 10^{-4}$ $\quad n := 1 .. 200$

$B_a := 2$ $\quad a := 0.25 \cdot 10^{-3}$

Trial solution: $y := 10^{-4}$

Given

$$1.2 = B_a \cdot \left[1 + \sum_n \left[(-1)^n \cdot \frac{4}{(2 \cdot n - 1) \cdot \pi} \cdot e^{\frac{-(2 \cdot n - 1)^2 \cdot t}{\tau}} \cdot \cos\left[\frac{(2 \cdot n - 1) \cdot \pi}{2 \cdot a} \cdot y \right] \right] \right]$$

find(y) =

Figure 6-1 *Calculation Of Volume-Time Factor - Mathcad Worksheet*

6.4 RECOMMENDATIONS

It is certainly not the case that the output transformer is now fully understood, and many questions remain unanswered. "*The universe is full of magical things, patiently waiting for our wits to grow sharper*" (Eden Phillpotts). The result of this work however is that the behaviour of the output transformer has been explained in detail which had previously been lacking. While it is tempting to continue extending and refining this theory, the foundation has clearly been laid and the following recommendations for further work point towards a different direction.

1. **Practical Application** It is recommended that the results of this thesis be applied to the design of an output transformer for a real application. As mentioned in Section 6.3.2, the true test of this work is in its application, and it is expected that at this stage, more insight would be gained from practical application than from continuing with the theoretical development. For a given application then, the theory would be applied to find the optimum core and winding characteristics, the electrical circuit model would be used to optimise the design, and the transformer would be built and compared with the predicted performance. A balance would need to be found between cost, size, efficiency, and manufacturability specific to that application.

2. **Discharge Circuit** It is recommended that priority be given to research of the discharge circuit. Continued investigation of the output transformer is less likely to achieve the design improvements that could be expected from an investigation of the discharge circuit.

3. **CAD Software** It is recommended that full use be made of the electrical circuit model. The potential for this model is far greater than simply being used to replace trial and error during the design of the output transformer. The lack of a robust model of the output transformer and capacitive discharge stage has traditionally prevented the complete energiser circuit from being simulated. The electrical circuit model developed in this thesis provides the opportunity for full simulation to be undertaken, giving access to the considerable capability of CAD software. Functionality of electrical circuit simulation software is constantly increasing, and the advanced capabilities of various packages include analogue/digital simulation, Monte Carlo (component tolerance) analysis, failure mode analysis, cross-probing and simulation from PCB layout, test system design, and worst case analysis.

Appendix One CIRCUIT DUALITY

Transformers are a combination of both magnetic and electric systems. Magnetic circuits are difficult to analyse, and because of the analogy between magnetic and electric quantities (Table 2-2), it is common to represent the complex, distributed magnetic circuit by a lumped electrical network with analogous behaviour. A common form of the equivalent circuit is derived using the inductor-reluctance method, which represents the magnetic circuit by inductors and ideal transformers.

Two circuits are *duals* if the mesh equations that characterise one of them have the same mathematical form as the nodal equations that characterise the other. They are said to be *exact duals* if each mesh equation of one circuit is numerically identical with the corresponding nodal equation of the other.

Although circuit duality is a technique primarily used with electric circuits, it is possible to adapt this to magnetic circuits for use in transformer modelling [*Hamill* 1993]. The principles of circuit duality are used to convert the reluctance model, which is a direct representation of the magnetic circuit, into an inductor model, which can be connected directly into the surrounding electrical network.

This appendix outlines the principles of duality which are relevant to the development of the output transformer model in Chapter 5. For a full discussion of circuit duality, refer to a circuit analysis text such as *Hayt and Kemmerly* [1971].

A1.1 DUALITY RELATIONSHIPS

Table A1-1 lists those duality relationships which are required for the inductor-reluctance model of the output transformer, with the analogous magnetic circuit quantities as defined by Table 2-2.

	Quantity		Dual Element
	Voltage source	(dual)⇒	Current source
	Magnetic voltage (mmf), F_m [A]	(dual)⇒	Magnetic current (flux), $\Phi = F_m^*$ [Wb]
	Resistance	(dual)⇒	Conductance
∴	Reluctance, $\mathcal{R}$[H^{-1}]	(dual)⇒	Permeance, $\mathcal{P} = \mathcal{R}^*$ [H]

Table A1-1 *Magnetic Dual Analogues*

A1.2 DUALITY PRINCIPLES

In order to convert a reluctance circuit model into an equivalent permeance circuit model, we form the dual of the magnetic circuit by the following steps.

Step 1. Each network loop is drawn as a node.

Step 2. Each node is drawn as a network loop.

Step 3. Each mmf F_m [A] is replaced by a flux source of the same numerical value $\Phi = F_m^*$ [Wb].

Step 4. Each reluctance $\mathcal{R}$ [H^{-1}] is replaced by a permeance of the same numerical value $\mathcal{P} = \mathcal{R}^*$ [H].

A1.3 CURRENT SOURCE DIRECTION

The direction of a current source in a dual circuit is determined by the following rule [*Hayt and Kemmerly* 1971 p. 134]:

- For a voltage source clockwise-sensed around a mesh, the current in the dual circuit flows into the enclosed node.

This is illustrated by Figure A1-1.

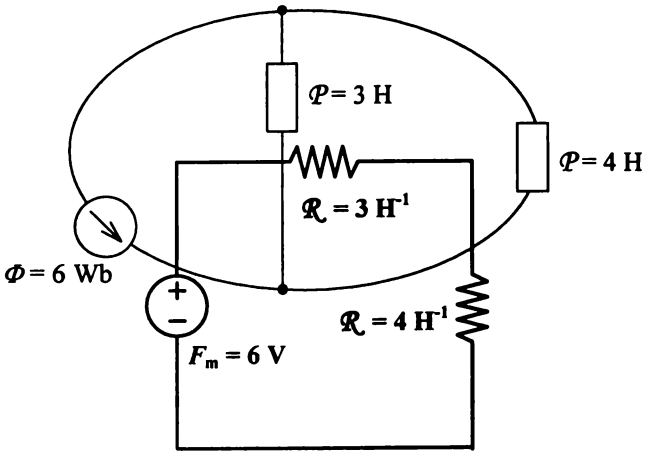

Figure A1-1 *Dual Circuit*

A1.4 INDUCTOR-RELUCTANCE MODEL

The procedure for creating an inductor-reluctance model of a transformer is as follows.

1. The magnetic circuit of the transformer is represented by a reluctance model, which is drawn in terms of magnetic voltages F_m and magnetic resistances $\mathcal{R}$. This reluctance model is drawn directly from the magnetic device's structure, with each distinct section of the magnetic circuit represented by a separate reluctance. Suitable approximations will often need to be made to represent the magnetic structure with discrete components, and to ensure that the circuit is not prohibitively complex.

2. The reluctance model is converted into an equivalent permeance model using the principles of duality outlined in Section A1.2.

3. One winding is chosen as the reference winding, having N_{ref} turns. The associated current source is replaced by a pair of terminals, and the current source associated with every other winding of N_i turns is replaced by an ideal transformer of ratio N_{ref}:N_i feeding a pair of terminals.

4. The circuit is scaled for the reference current source by multiplying impedances and dividing sources by N_{ref}.

5. The circuit is then scaled for the reference voltage by multiplying impedances and sources by N_{ref}.

6. Each permeance is replaced by an inductance of $L = N_{ref}^2 \mathcal{P}$ (Equation 2-35).

For further detail, and examples of inductor-reluctance modelling of transformers, refer to *Severns* [1996].

A1.5 NUMERICAL VALUE

When creating the circuit dual, the numerical value of the dual element remains the same as that of the original quantity. For example, a magnetic voltage source of $F_m = NI = 5$ A becomes in the dual circuit a magnetic current source Φ with a numerical value of 5. That is, $\Phi = |NI| = 5$ Wb.

When quantity equations rather than numerical values are used, care must be taken to distinguish between the numerical value of the dual and the original quantity. For this reason, a star (*) is used to indicate the numerical value of a quantity.

As an example, for a reluctance with the value $\mathcal{R} = \frac{\ell}{\mu A}$ the dual is a permeance with the value $\mathcal{P} = \left(\frac{\ell}{\mu A}\right)^*$, but since $\mathcal{P} = \frac{1}{\mathcal{R}}$ then in the dual circuit $\mathcal{R}^* = \frac{\mu A}{\ell}$.

Appendix Two CALCULATION OF DYNAMIC CAPACITANCE

Parasitic capacitance in transformers accounts for energy stored in the electric field which exists between any conductors that have a potential difference. Although a static capacitance can be calculated from the geometry of the transformer, a more accurate equivalent value for the parasitic capacitance is obtained by taking into account the dynamic non-uniform field that results from the pulse discharge.

Collins [1990] discusses a method of accounting for dynamic capacitance. His paper has been adapted to suit the specific application of an output transformer, a summary of which is given in this appendix. This method allows all of the output transformer parasitic capacitances to be calculated from the transformer specification, to sufficient accuracy as shown by the results in Chapter 5.3.5.

Collins [1990] should be referred to for more detail, and for discussion of the general method.

A2.1 STATIC CAPACITANCE

The numerical value of an equivalent capacitance which represents the dynamic parasitic capacitance of a transformer is found by considering the stored and transition energies of static and dynamic fields.

The following definitions will be used:

C_s = static volumetric capacitance

C_d = dynamic capacitance (an equivalent value for the time-varying, non-uniform field parasitic capacitance)

$\vec{W}_s$ = energy storage (a signed quantity equal in magnitude to capacitance energy storage)

W_d = energy dissipated per cycle

W_k = total transition energy

The static capacitance between windings, or layers of turns, can be found from the geometry of the transformer. As output transformer coils are usually wound on a square bobbin, the windings will be modelled as a flat plate capacitor as illustrated in Figure 5-8, with the static capacitance calculated using Equation 5-1.

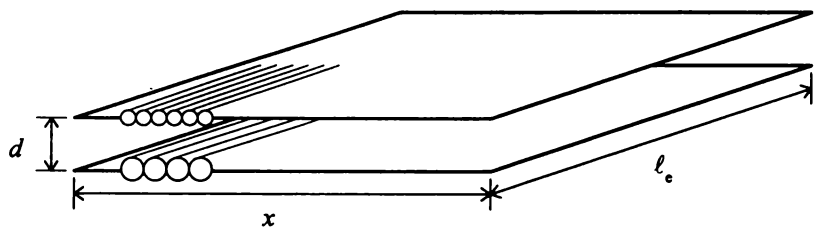

Figure 5-8 *Flat Plate Capacitor*

$$C_s = \frac{\varepsilon_r \varepsilon_0 \ell_e x}{d} \qquad \textit{Equation 5-1}$$

ε_r = relative permittivity (or dielectric constant) of the interwinding insulation, usually either the bobbin or epoxy resin

ε_0 = permittivity of free-space, 8.854×10^{-12} F/m

ℓ_e = effective (or average) length of turn [SI unit: m]

x = winding width [SI unit: m]

d = separation of windings [SI unit: m]

A2.2 ENERGY CONSIDERATIONS

The circuit configuration must be carefully drawn to show the polarity of all windings and the number of layers present in each coil, and the primary and secondary pulses must be approximated by square pulses. When the transformer is excited by a square ware, the potential between the windings is linear but non-uniform. This may be represented by a phase-voltage diagram, an example of which is shown below.

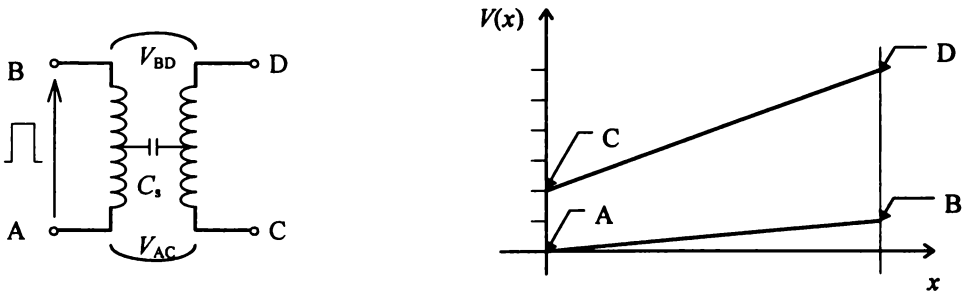

Figure A2-1 *Phase-Voltage Diagram*

If V_{AC} is the potential difference at one end of the winding, and V_{BD} is the potential difference at the other end, it can be shown that the total stored energy in the non-uniform field is given by

$$\vec{W}_s = \frac{C_s}{2}\frac{\left(V_{AC}^2 + V_{AC}V_{BD} + V_{BD}^2\right)}{3} \qquad \textit{Equation A2-1}$$

A graph of $\vec{W}_s$ will have the following form for an energiser pulse.

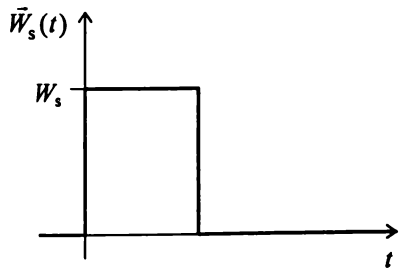

Figure A2-2 *Energy Storage*

Since $V = \sqrt{\frac{2E}{C}}$, we can translate the graph of the stored energy into a graph of the equivalent parasitic capacitor voltage, V_C.

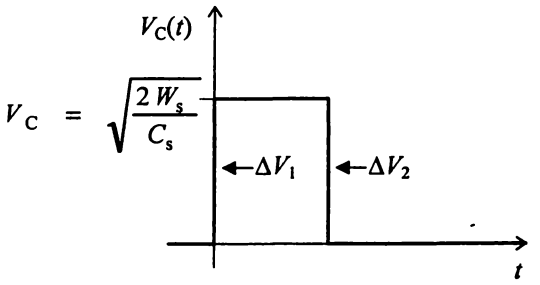

Figure A2-3 *Equivalent Parasitic Capacitor Voltage*

As shown by Figure A2-3, there are two transitions. The total transition energy is then calculated from

$$W_k = \Delta W_1 + \Delta W_2$$
$$= \tfrac{1}{2} C_s \Delta V_1^2 + \tfrac{1}{2} C_s \Delta V_2^2 \qquad \textit{Equation A2-2}$$

As the input pulse in this application does not have an offset voltage, and there are two transitions, using Equation A2-1 we can write directly that

$$W_k = 2 \times W_s$$
$$= \frac{\left(V_{AC}^2 + V_{AC} V_{BD} + V_{BD}^2\right)}{3} C_s \qquad \textit{Equation A2-3}$$

A2.3 COLLINS' POSTULATES

Collins makes two postulates:

1. that the energy dissipated per cycle, W_d in charging and discharging a capacitor with a square wave is equal to the total transition energy, W_k;

2. that the dynamic capacitance associated with the static non-uniform field capacitance, C_s may be represented in the small signal circuit model by C_d, a uniform field capacitor which is characterised by the same charge and discharge energy dissipation W_d per cycle.

A2.4 DYNAMIC CAPACITANCE

From the first postulate, we see that the energy dissipated per cycle has been found from a consideration of the potential difference between the windings. From the second postulate, we consider the effect of the primary pulse on the capacitor C_d. The voltage across this capacitor and the resultant stored energy is shown below.

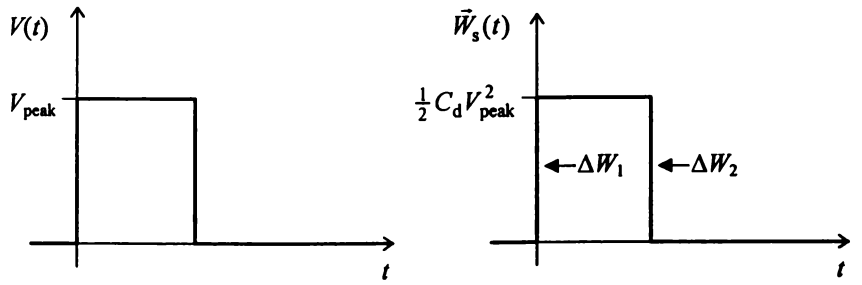

Figure A2-4 *Uniform Field Capacitance*

$$\begin{aligned} W_d &= \Delta W_1 + \Delta W_2 \\ &= \tfrac{1}{2} C_d V_{peak}^2 + \tfrac{1}{2} C_d V_{peak}^2 \\ &= C_d V_{peak}^2 \end{aligned}$$

Equation A2-4

Now since $W_d = W_k$ from Collins' first postulate, we can equate Equations A2-3 and A2-4 to give

$$C_d V_{peak}^2 = \frac{\left(V_{AC}^2 + V_{AC}V_{BD} + V_{BD}^2\right)}{3} C_s$$

$$\Leftrightarrow C_d = \frac{\left(V_{AC}^2 + V_{AC}V_{BD} + V_{BD}^2\right)}{3V_{peak}^2} C_s \qquad \textit{Equation 5-2}$$

BIBLIOGRAPHY

[*Albou* 1993] *PSpice Simulates Speedy SCR*, P. Albou, EDN (18 Feb. 1993), Vol. 38, pp. 147 - 148

[*Allied Signal* 1998] *Metglas Magnetic Alloy 2605SC*, Allied Signal, World Wide Web site http://www.alliedsignal.com/metglas/, downloaded 21 April 1998

[*Barnes* 1989] *The Electrified Fence As A Component Of A Physical Protection System*, B.W. Barnes, Proceedings - 1989 International Carnahan Conference on Security Technology (Oct. 1989), Zurich, pp. 237 - 241

[*Bartlett & Corle* 1985] *Measuring Maxwell's Displacement Current Inside A Capacitor*, D.F. Bartlett and T.R. Corle, Physical Review Letters (July 1985), Vol. 55 (1), pp. 59 - 62

[*Biegelmeier* 1987] *Effects Of Current Passing Through The Human Body And The Electrical Impedance Of The Human Body*, G. Biegelmeier, VDE-Verlag (1987), ETZ Report 20e, Berlin, 28 pp. A guide to *IEC 479* [1984]

[*Brockelsby et. al.* 1977] *Transmission Line Behaviour Of Electric Fence Lines*, W.K. Brockelsby, R.C.G. Niven and C.A. Standing, Gallagher Electronics Ltd. (1977), Hamilton NZ, 22 pp.

[*Carter* 1992] *Electromagnetism For Electronic Engineers*, R.G. Carter, 2nd Edition, Chapman & Hall (1992), London, 175 pp.

[*Castro* 1988] *Solving SPICE Problems*, R.D. Castro, IEE Proceedings - Part G (Aug. 1988), Vol. 135 (4), pp. 177 - 178

[*Chan et. al.* 1991] *Nonlinear Transformer Model For Circuit Simulation*, J.H. Chan, A. Vladimirescu, X.-C. Gao, P. Liebmann and J. Valainis, IEEE Transactions on Computer-Aided Design (April 1991), Vol. 10 (4), pp. 476 - 482

[*Chatterjee* 1995] *Hysteresis In Magnetic Systems*, B.K. Chatterjee, American Journal of Physics (July 1995), Vol. 63 (7), pp. 643 - 646

[*Clarke* 1995] *A Low-Cost Electric Fence Controller*, J. Clarke, Silicon Chip (July 1995), Vol. 8 (7), pp. 20 - 26

[*Collins* 1990] *An Accurate Method For Modeling Transformer Winding Capacitances*, J.A. Collins, Proceedings - IEEE IECON (Nov. 1990), Vol. 2, pp. 1094 - 1099

[*Collins* 1997] Discussion with John Collins, Cow Creek Enterprises, Oregon USA, 25 April, 1997

[*Dauhajre & Middlebrook* 1986] *Modeling And Estimation Of Leakage Phenomena In Magnetic Circuits*, A. Dauhajre and R.D. Middlebrook, Proceedings - IEEE Power Electronics Specialists Conference (1986), pp. 213 - 226

[*Dawson* 1982] *Electric Fence*, C. Dawson, Electronics Australia (Sept. 1982), Vol. 44 (9), pp. 80 - 85

[*Dawson* 1985] *Build This Electric Fence Controller*, C. Dawson, Electronics Australia (Dec. 1985), Vol. 47 (12), pp. 34 - 38

[*DeMaw* 1981] *Ferromagnetic-Core Design And Application Handbook*, M.F. DeMaw, Prentice-Hall (1981), Englewood Cliffs NJ USA, 256 pp.

[*Dowell* 1966] *Effects Of Eddy Currents In Transformer Windings*, P.L. Dowell, IEE Proceedings (Aug. 1966), Vol. 113 (8), pp. 1387 - 1394

[*Dugan et. al.* 1989] *Validated Techniques For Modelling Shell-Form EHV Transformers*, R.C. Dugan, R. Gabrick, J.C. Wright and K.W. Patten, IEEE Transactions on Power Delivery (1989), Vol. 4 (2), pp. 1070 - 1078

[*Duncan* 1991] *Sound Models For MicroCap*, B. Duncan, Electronics World + Wireless World (Oct. 1991), pp. 824 - 829

[*Einstein* 1950] Albert Einstein, quoted in Scientific American (April 1950), p. 17

[*Engelmann* 1985] *Static And Rotating Electromagnetic Devices*, R.H. Engelmann, Marcel Dekker (1985), New York, 524 pp.

[*Faraday* 1839] *Experimental Researches In Electricity*, M. Faraday, Reprinted by Dover Publications (1965), New York, Vol. I - 574 pp., Vol. II - 302 pp., Vol. III - 588 pp.
Originally published by: Vol. I - Taylor & Francis (1839), Vol. II - Richard & John Edward Taylor (1844), Vol. III - Taylor & Francis (1855)

[*Fink* 1975] *Electronics Engineers' Handbook*, D.G. Fink (ed.), McGraw-Hill (1975), New York

[*Früngel* 1965] *High Speed Pulse Technology*, F. Früngel, Vol. I, Academic Press (1965), New York, 620 pp.

[*Früngel* 1976] *High Speed Pulse Technology*, F. Früngel, Vol. III, Academic Press (1976), New York, 498 pp.

[*Gallagher* 1977] *History And Development Of Energisers*, Gallagher Electronics Ltd. (c. 1977), Hamilton NZ, 12 pp.

[*Gallagher* 1996] *Gallagher Power Fence Manual*, 10th Edition, Gallagher Group Ltd. (1996), Hamilton NZ, 42 pp.

[*Garikepati, Chang & Jiles* 1988] *Theory Of Ferromagnetic Hysteresis: Evaluation Of Stress From Hysteresis Curves*, P. Garikepati, T.T. Chang and D.C. Jiles, IEEE Transactions on Magnetics (Nov. 1988), Vol. 24 (6), pp. 2922 - 2924

[*Giacoletto* 1989] *Simple SCR And TRIAC PSPICE Computer Models*, L.J. Giacoletto, IEEE Transactions on Industrial Electronics (Aug. 1989), Vol. 36 (3), pp. 451 - 455

[*Glasoe & Lebacqz* 1948] *Pulse Generators*, G.N. Glasoe and J.V. Lebacqz (eds.), Massachusetts Institute of Technology Radiation Laboratory series - Vol. 5, McGraw-Hill (1948), New York, 741 pp. Part III: *Pulse Transformers*, W.H. Bostick

[*Goody* 1995] *PSpice For Windows: A Circuit Simulation Primer*, R.W. Goody, Prentice Hall (1995), Englewood Cliffs NJ USA, 372 pp.

[*Gray* 1972] *American Institute Of Physics Handbook*, D.E. Gray (ed.), 3rd Edition, McGraw-Hill (1972), New York

[*Grossner* 1967] *Transformers For Electronic Circuits*, N.R. Grossner, McGraw-Hill (1967), New York, 321 pp.

[*Hamill* 1993] *Lumped Equivalent Circuits Of Magnetic Components: The Gyrator-Capacitor Approach*, D.C. Hamill, IEEE Transactions on Power Delivery (April 1993), Vol. 8 (2), pp. 97 - 103

[*Hancock* 1991] *Electric Fences: Modelling The Electrical Characteristics And Behaviour Of Electric Fence Systems*, A.T. Hancock, Masters Thesis, University of Waikato (1991), 254 pp.

[*Harrison* 1992] *Modelling And Design Of Energiser Pulse Transformers*, C.B. Harrison, Masters Thesis, University of Waikato (1992), 225 pp.

[*Hayt & Kemmerly* 1971] *Engineering Circuit Analysis*, W.H. Hayt, Jr. and J.E. Kemmerly, 2nd Edition, McGraw-Hill (1971), Tokyo, 653 pp.

[*Hodgdon* 1988] *Mathematical Theory And Calculations Of Magnetic Hysteresis Curves*, M.L. Hodgdon, IEEE Transactions on Magnetics (Nov. 1988), Vol. 24 (6), pp. 3120 - 3122

[*Hultgren* 1989] *Cows And Electricity: Biological Interaction And Defects On Cow Behaviour, Health And Production Of Stray Voltage, Electric Cow-Trainers And High-Voltage Transmission Lines*, J. Hultgren, Swedish University of Agricultural Sciences (1989), Report 27, SKARA

[*IEC 479* 1984] *Effects Of Current Passing Through The Human Body*, IEC Report 479, 2nd Edition, Technical Committee 64 Working Group 4, IEC (1984), Geneva

[*Intusoft* 1996] *Solving Convergence Problems*, Intusoft, World Wide Web site http://www.intusoft.com, downloaded May 1996

[*Jiles & Atherton* 1986] *Theory Of Ferromagnetic Hysteresis*, D.C. Jiles and D.L. Atherton, Journal of Magnetism and Magnetic Materials (1986), Vol. 61, pp. 48 - 60

[*Jiles* 1994] *Frequency Dependence Of Hysteresis Curves In Conducting Magnetic Materials*, D.C. Jiles, Journal of Applied Physics (May 1994), Vol. 75 (10), p. 5511

[*Kehoe* 1996] *Magnetic Hysteresis In Line Pipe Steels*, I. Kehoe, Queen's University at Kingston, World Wide Web site http://physics.queensu.ca/atherton, downloaded 23 May 1996

[*Klontz, Novotny & Severns* 1997] How To Design Magnetic Components For Power Electronic Circuits, K. Klontz, D. Novotny and R. Severns, Seminar 4 - 6 June 1997, University of Wisconsin - Madison, Madison WI USA

[*Krolski* 1997] Discussion with Ken Krolski, Kentron Inc., Wisconsin USA, 6 - 7 May 1997

[*Landau & Lifshitz* 1960] *Electrodynamics Of Continuous Media*, L.D. Landau and E.M. Lifshitz, translated from Russian by J.B. Sykes and J.S. Bell, Course of Theoretical Physics series - Vol. 8, Pergamon Press (1960), Oxford, 417 pp.

[*Lawden* 1959] *Mathematics Of Engineering Systems (Linear And Non-Linear)*, D.F. Lawden, Methuen & Co. (1959), London, 404 pp.

[*Lee* 1993] *Computer-Aided Analysis And Design Of Switch-Mode Power Supplies*, Y.-S. Lee, Marcel Dekker (1993), New York, 522 pp.

[*Lerner & Trigg* 1991] *Encyclopedia Of Physics*, R.G. Lerner and G.L. Trigg (eds.), 2nd Edition, VCH Publishers (1991), New York

[*Lorrain & Corson* 1970] *Electromagnetic Fields And Waves*, P. Lorrain and D.R. Corson, 2nd Edition, W.H. Freeman and Co. (1970), New York, 706 pp.

[*Magnetics* 1991] *Powder Cores Catalogue*, Magnetics (1991), Butler PA USA

[*Maurer* 1975] *Steuerbare Kondensator-Zündanlage (Controllable Capacitive Ignition Circuit)*, F. Maurer, German, Funkschau (Nov. 1975), Vol. 47 (24), pp. 89 - 92

[*Maxwell* 1892] *A Treatise On Electricity And Magnetism*, J.C. Maxwell, 3rd Edition, Oxford University Press (1892), Oxford, Vol. I - 506 pp., Vol. II - 500 pp.

[*Mayergoyz* 1988] *Dynamic Preisach Models Of Hysteresis*, I.D. Mayergoyz, IEEE Transactions on Magnetics (Nov. 1988), Vol. 24 (6), pp. 2925 - 2927

[*McCutchan* 1980] *Electric Fence Design Principles*, J. McCutchan, Electrical Engineering Dept., University of Melbourne (1980), Melbourne, 460 pp.

[*McGraw-Hill* 1992] *McGraw-Hill Encyclopedia Of Science And Technology*, 7th Edition, McGraw-Hill (1992), New York

[*Meares & Hymowitz* 1998] *SPICE Models For Power Electronics*, L.G. Meares and C.E. Hymowitz, Intusoft, World Wide Web site http://www.intusoft.com/articles, downloaded 7 May 1998, 13 pp.

[*Micrometals* 1995] *Iron Powder Cores: Catalog 4*, Micrometals Inc. (1995), Issue H, Anaheim CA USA

[*MicroSim* 1991] *PSpice Circuit Analysis User's Guide*, Version 5.0, MicroSim Corporation (1991), Irvine CA USA, 572 pp.

[*Miller & Epstein* 1990] *Magnetism Without Metals*, J. Miller and A. Epstein, New Scientist (June 1990), Vol. 126 (1722), pp. 30 - 34

[*Nagel* 1975] *SPICE 2: A Computer Program To Simulate Semiconductor Circuits*, L.W. Nagel, Memo ERL-M520, Electronics Research Laboratory, University of California (May 1975), Berkeley CA USA

[*Nehmadi et. al.* 1990] *Experimental Result Study And Design Enhancement Of A Magnetic Pulse Compression Circuit By Using The PSpice Simulation Program*, M. Nehmadi, Y. Ifrah and I. Druckmann, Rev of Scientific Instruments (Dec. 1990), Vol. 61 (12), pp. 3807 -3811

[*Nichols et. al.* 1994] *Overview Of SPICE-Like Circuit Simulation Algorithms*, K.G. Nichols, T.J. Kazmierski, M. Zwolinski and A.D. Brown, IEE Proceedings - Circuits, Devices and Systems (Aug. 1994), Vol. 141 (4), pp. 242 - 249

[*Parker* 1994] *McGraw-Hill Dictionary Of Scientific And Technical Terms*, S.P. Parker (ed.), 5th Edition, McGraw-Hill (1994), New York, 2194 pp.

[*Pei & Lauritzen* 1986] *A Computer Model Of Magnetic Saturation And Hysteresis For Use On SPICE2*, D. Pei and P.O. Lauritzen, IEEE Transactions on Power Electronics (April 1986), Vol. PE-1 (2), pp. 101 - 110

[*Pernía, Nuño & Lopera* 1995] *1D/2D Transformer Electric Model For Simulation In Power Converters*, A.M. Pernía, F. Nuño and J.M. Lopera, Proceedings - IEEE Power Electronics Specialists Conference (1995). Vol. 2, pp. 1043 - 1049

[*Pescetti* 1989] *Mathematical Modelling Of Hysteresis*, D. Pescetti, Il Nuovo Cimento (Aug. 1989), Vol. 11D (8), pp. 1191 - 1216

[*Petkov* 1996] *Optimum Design Of A High-Power, High-Frequency Transformer*, R. Petkov, IEEE Transactions on Power Electronics (Jan. 1996), Vol. 11 (1), pp. 33 - 42

[*Petrie & Hymowitz* 1998] *A SPICE Model For Triacs*, A.F. Petrie and C.E. Hymowitz, Intusoft, World Wide Web site http://www.intusoft.com/articles, downloaded 7 May 1998, 5pp.

[*Philips* 1998] *Soft Ferrites: Data Handbook MA01*, Philips Components (1998), Eindhoven

[*Prigozy* 1993] *PSpice Computer Modeling Of Hysteresis Effects*, S. Prigozy, IEEE Transactions on Education (Feb. 1993), Vol. 36 (1), pp. 2 - 5

[*Prigozy* 1994] *PSpice Computer Modeling Of Power Transformers With Hysteresis Effects*, S. Prigozy, Computers in Education Journal (1994), Vol. 4 (2), pp. 68 - 76

[*Reitz, Milford & Christy* 1979] *Foundations Of Electromagnetic Theory*, J.R. Reitz, F.J. Milford and R.W. Christy, 3rd Edition, Addison-Wesley (1979), Reading MA USA, 534 pp.

[*Riley, Hobson & Bence* 1997] *Mathematical Methods For Physics And Engineering*, K.F. Riley, M.P. Hobson and S.J. Bence, Cambridge University Press (1997), Cambridge, 1008 pp.

[*Sadedin* 1984] *Geometry Of A Pulse Transformer For Electromagnetic Launching*, D.R. Sadedin, IEEE Transactions on Magnetics (March 1984), Vol. Mag-20 (2), pp. 381 - 384

[*Sandler* 1995] *Improved Spice Models Provide Accurate Nonlinear Magnetics Results*, S. Sandler and C Hymowitz, Power Conversion and Intelligent Motion (Sept. 1995), Vol. 21 (9), pp. 38 - 47

[*Saslow* 1991] *How A Superconductor Supports A Magnet, How Magnetically 'Soft' Iron Attracts A Magnet, And Eddy Currents For The Uninitiated*, W.M. Saslow, American Journal of Physics (Jan. 1991), Vol. 59 (1), pp. 16 - 25

[*Saslow* 1992] *Maxwell Theory Of Eddy Currents In Thin Conducting Sheets, And Applications To Electromagnetic Shielding And MAGLEV*, W.M. Saslow, American Journal of Physics (1992), Vol. 60 (8), pp. 693 - 711

[*Severns & Bloom* 1985] *Modern DC-To-DC Switchmode Power Converter Circuits*, R. Severns and G.E. Bloom, e/j Bloom Associates (1985), San Rafael CA USA, 342 pp.

[*Severns* 1992] *Transformer And Magnetic Component Modeling For SPICE Simulation*, R. Severns, Report prepared for Apple Computer (1992), 40 pp.

[*Severns* 1996] *Modelling Of Magnetic Components For Design And Simulation*, R. Severns, Seminar 21 - 22 Feb. 1996, University of Canterbury, Christchurch NZ

[*Severns* 1997] Discussion with Rudy Severns, Springtime Enterprises, Oregon USA, 22 - 24 April 1997

[*Shepherd, Morton & Spence* 1970] *Higher Electrical Engineering*, J. Shepherd, A.H. Morton and L.F. Spence, 2nd Edition, Pitman (1970), London, 877 pp.

[*Smythe* 1950] *Static And Dynamic Electricity*, W.R. Smythe, McGraw-Hill (1950), New York

[*Stafix* 1994] New Zealand Patent No. 250970/250037, Stafix Electric Fencing Ltd (1994)

[*Taylor* 1995] *Guide For The Use Of The International System Of Units*, B.N. Taylor, NIST Special Publication 811, 1995 Edition, US National Institute of Standards and Technology, 74 pp.

[*Tebble & Craik* 1969] *Magnetic Materials*, R.S. Tebble and D.J. Craik, John Wiley & Sons (1969), London, 726 pp.

[*Thomas and Finney* 1984] *Calculus And Analytical Geometry*, G.B. Thomas and R.L. Finney, 6th Edition, Addison-Wesley (1984), Reading MA USA, 1041 pp.

[*Tyndall* 1870] *Faraday As A Discoverer*, J. Tyndall, 2nd Edition, Longmans, Green & Co. (1870), London, 208 pp.

[*USC* 1998] *Introduction To Magnetism*, University of Southern California, World Wide Web site http://www.usc.edu/dept/materials_science/ MDA125/electrical/, downloaded 8 Jan. 1998

[*Wadsworth & Chanmugam* 1988] *Electrophysical Agents In Physiotherapy*, H Wadsworth and A.P.P. Chanmugam, Science Press (1988), Marrickville Aus., 396 pp.

[*Wells* 1920] *The Outline Of History*, H.G. Wells, Cassell & Co. (1920), London, 767 pp.

[*Wevill* 1981] *Inductive Discharge Car Ignition System*, K. Wevill., Practical Electronics (Oct. 1981), Vol. 17 (10), pp. 40 - 46

[*Williams* 1994] *A CAD Model Of Nonlinear Ferromagnetics For Circuit Simulation*, M.C. Williams, Masters Thesis, University of South Florida (1994), 109 pp.

[*Witulski* 1995] *Introduction To Modeling Of Transformers And Coupled Inductors*, A.F. Witulski, IEEE Transactions on Power Electronics (May 1995), Vol. 10 (3), pp. 349 - 357